UNIVERSITÀ DEGLI STUDI DI PADOVA

UNIVERSITÀ DEGLI STUDI DI PADOVA
DIPARTIMENTO DI SCIENZE CHIMICHE

CORSO DI LAUREA MAGISTRALE IN CHIMICA

TESI DI LAUREA MAGISTRALE

Synthesis and characterization of NOHC organometallic complexes

Relatrice: Prof. Cristina Tubaro

Correlatore: Prof. Dr. Thomas Strassner

Controrelatore: Prof. Paolo Maria Scrimin

LAUREANDA: Alice Benin

Anno Accademico 2021-2022

TABLE OF CONTENTS

LIST OF ABBREVIATIONS

CIE: Color coordinates, defined by an international commission (*CIE – Commission internationale de l'éclairage*)

COSY: Correlated Spectroscopy (2D-NMR)

DMF: dimethylformamide

EBL: electron blocking layer

EML: emission layer

ETL: electron transport layer

HBL: hole blocking layer

HMBC: Heteronuclear Multiple Bond Correlation Spectroscopy (2D-NMR)

HSQC: Heteronuclear Single Quantum Coherence Spectroscopy (2D-NMR)

HTL: hole transport layer

ILCT: intra-ligand charge transfer

LLCT: ligand-to-ligand charge transfer

M^C: coinage metal

MLCT: metal-to-ligand charge transfer

MMLCT: metal-metal-to-ligand charge transfer

NOESY: Nuclear Overhauser effect spectroscopy (2D-NMR)

NHC: N-heterocyclic carbenes

NOHC: N-oxyheterocyclic carbenes

PLQY: photoluminescence quantum yield

PMMA: polymethylmethacrylate

PQY: phosphorescent quantum yield

ABSTRACT

N-heterocyclic carbene ligands in transition metal complexes have been widely studied in the last decades. Surprisingly, *N*-oxy-heterocyclic carbene species (abbreviated NOHC) have not raised as much interest in scientific community. After the earliest researches on Ni(II), Pd(II), Rh(I), Ag(I) and Au(I) complexes with these types of ligands in 2007 and 2010, no new progresses have been reported until 2021.

In this master thesis, a collaboration between Università degli Studi di Padova and Technische Universität Dresden, we focused on the synthesis of Ag(I), Au(I) and Pt(II) NOHC complexes in order to explore different synthesis pathways for extended aromatic motifs and to evaluate the photoluminescence properties of the Pt(II) compounds.

The project can be summarized in these sections:

i) silver(I) and gold(I) complexes with symmetrically substituted N-O-heterocyclic carbene ligands;

ii) metal complexes with phenyl-substituted NOHC ligands;

iii) deoxygenation experiments in order to expand the type of NOHC ligands.

i) Silver(I) and gold(I) complexes with symmetrically substituted NOHC ligands.

Two bis-carbene silver(I) complexes and their gold(I) analogues, with the general formula $[ML_2]^+(PF_6)^-$ (L=NOHC ligand), have been synthesized. The Au(I) compounds were obtained through transmetalation from sensitive Ag(I) precursors. The symmetrically substituted benzyl-NOHC was already reported in the literature, whereas the 2-methylnaphtalenyl analogue was not. The proligand with the larger substituent contains small amounts of impurities (the monosubstituted compound) in both the proligand and complexes samples. That proved that for large aromatic substituents the synthesis via nucleophilic attack is not satisfactory.

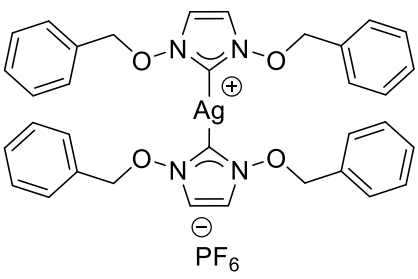

3

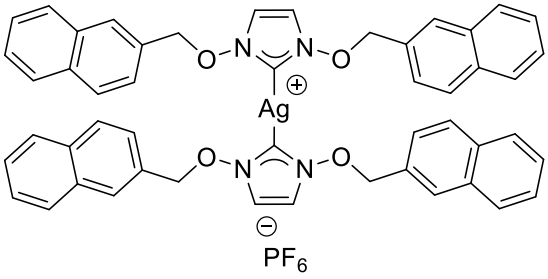

5

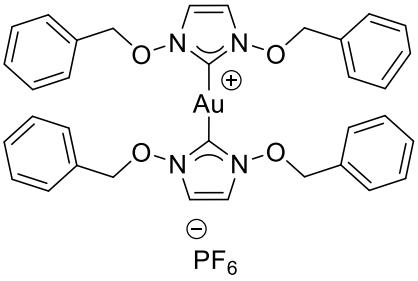

4

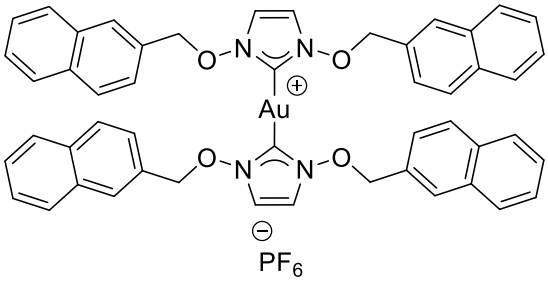

6

ii) Metal complexes with phenyl-substituted NOHC ligands.

Four Pt(II) cyclometalated complexes with a general formula [Pt(C^C*)(L^L)] (C^C*=cyclometalated NOHC ligand; L^L= β-diketonate ligand) have been obtained and fully characterized. Part of the structure of complex **13** was not defined by the obtained data.

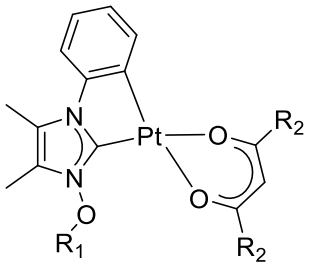

	R_1	R_2
11	Me	Me
12	Bn	Me
13	unknown	Mesityl
14	Bn	Mesityl

Single crystals of compounds **11** and **14** were analysed and the structure geometry have been confirmed as reported below.

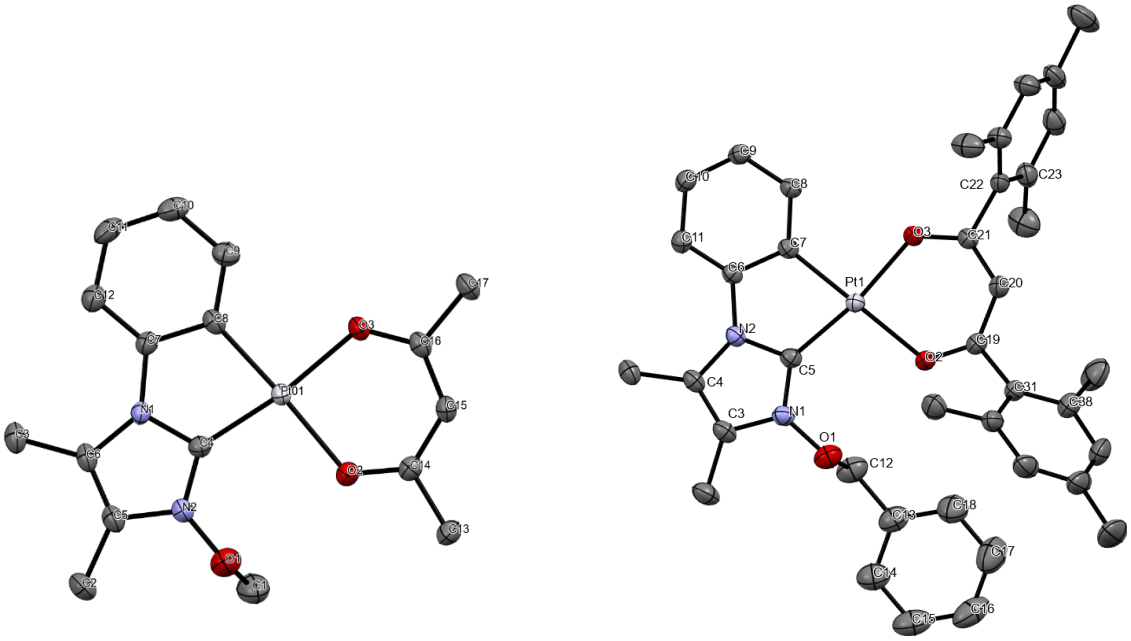

Photophysical characterization of the four compounds and comparison with results reported in the literature highlighted that the addition of an oxygen-bearing moiety on the nitrogen atom of the imidazole ring has a limited influence.

Compound	ϕ	λ_{em} (nm)	CIE coordinates (x;y)	τ_0 (μs)	k_r (x10^3 s^{-1})	k_{nr} (x10^3 s^{-1})
11	0.07	423; 449; 472	0.162; 0.128	28.1	35.6	473.1
12	0.04	424; 447; 475	0.169; 0.142	61.2	16.3	392.2
13	0.70	482	0.192; 0.319	1.5	659.9	282.8
14	0.17	482	0.198; 0.318	6.3	157.9	770.9

Cyclic voltammetries and quantum chemical calculations concerning the electron density distribution and the free energies of the ground singlet and the first excited triplet states confirmed the emission features and gave an estimation of the HOMO-LUMO gap.

The Au(I) complex **15** was synthesized both via weak base assisted metalation and through transmetalation route. Nonetheless, this last procedure affords a less impurities-containing product as demonstrated by ^{1}H NMR spectrum. The crystal structure of complex **15** was determined as well.

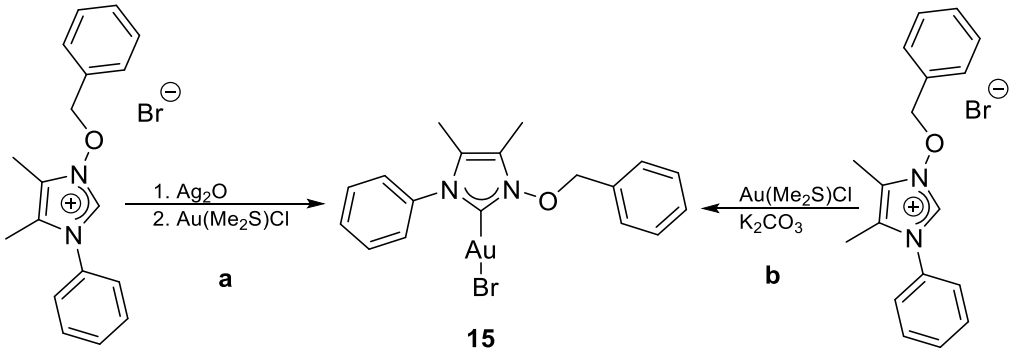

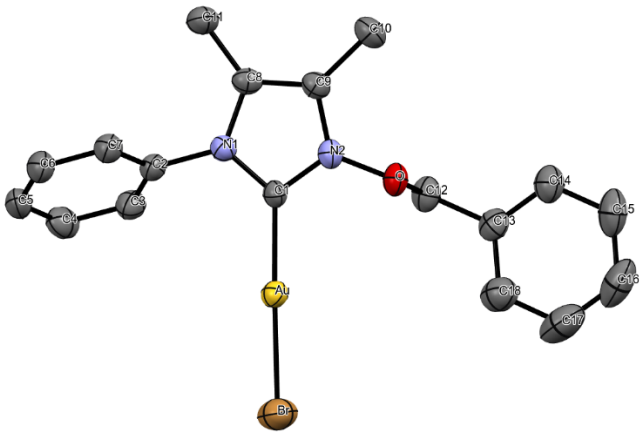

iii) Deoxygenation experiments.

To further modulate the properties of NOHC complexes, the cleavage of one of the N-O bonds could be considered as the synthesis of 1-hydroxyimidazole-3-oxide is easier and more efficient than the singly-oxygenated imidazolium rings.

Pd/C hydrogenation of 1-hydroxyimidazole-3-oxide proved to be unproductive as imidazole, the main side product, is barely separable from the mono-deoxygenated one.

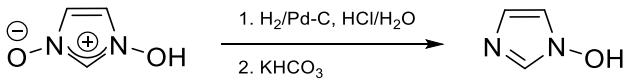

7 **16**

Raney-Nickel did not give the expected result as well, since no product was detected. A polymerization of the resulting compound can be hypothesized from the HRMS analysis.

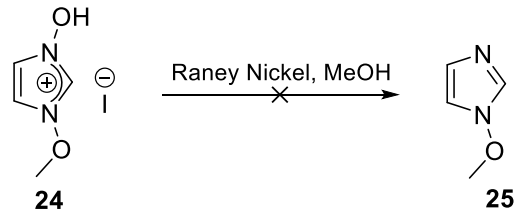

24 **25**

Chapter 1: INTRODUCTION

1.1 History of *N*-heterocyclic carbenes (NHCs)

N-heterocyclic carbenes are well-known to the literature since 1968, when their synthesis was discovered by Wanzlick and Öfele.[1,2] However, an important step in the research regarding these compounds was reached in 1998 when Arduengo published the proof of the crystallization of the first free carbene, 1,3-diadamatylimidazol-2-ylidene, isolated by deprotonation of 1,3-diadamantylimidazolium iodide.[3,4] Since then, these species themselves and their corresponding metal complexes have been widely studied.

The particular stability of these types of carbenes can be explained considering their electronic properties. Six electrons are located in the outer shell of the carbene carbon.

A general XCX carbene can be taken into account, where X can be either electron-withdrawing or electron-donating substituents. They can assume either a linear or a bent geometry. The orbitals of the central carbon atom participating in the linear geometry are the *p* orbitals, whereas a *p* and a σ orbitals are involved if the carbene has a bent geometry. The σ orbital is made of a combination of *s* and *p* orbitals and is therefore lower in energy than the *p* orbital.[5] Three electronic configurations of the carbene can be easily deducted from this simple orbital description (Figure 1). In particular, the non-bonding electrons in the sp^2-type conformation (bent geometry) can be either in a triplet $\sigma^1 p_\pi^1$, or in three possible singlet states: $\sigma^1 p_\pi^1$, σ^2 or p_π^2, but the σ^2 represents the most stable and common singlet configuration.[5] The band gap between the σ and the p_π orbitals determines the multiplicity of the carbene. In general, this gap is lower than 1.5 eV in case of a triplet carbene, whereas it is higher than 2 eV in case of a singlet carbene (Figure 1).[6]

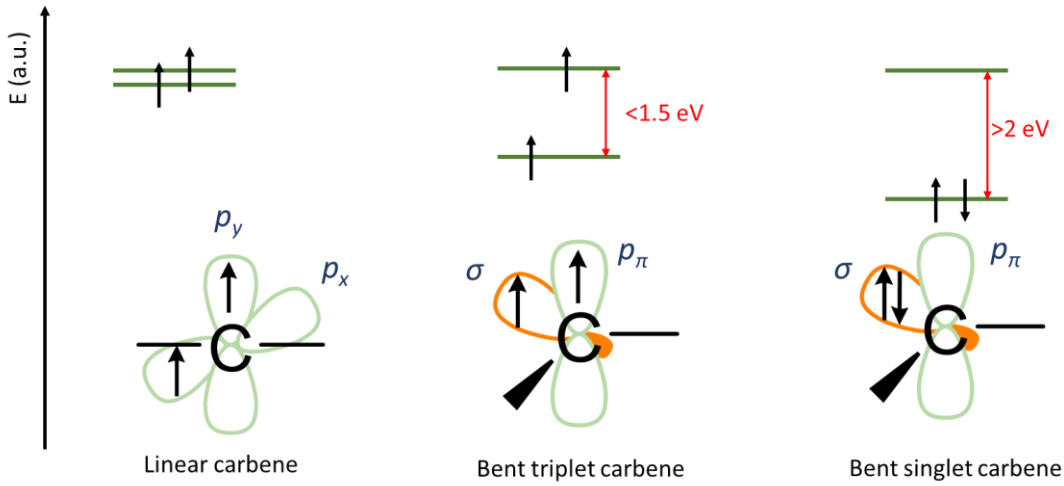

Figure 1. Energy levels of frontier orbitals and spin multiplicity of linear and bent, triplet and singlet carbenes.

The multiplicity of the substituted carbenes in their ground-state determines the reactivity of the species: singlet carbenes have one completely filled orbital and one completely vacant, hence they have an amphiphilic behaviour, instead triplet carbenes have two single-occupied orbitals and their reactivity resembles that of diradicals.[5,7,8]

The multiplicity of a carbene species is affected by the electronic properties of the substituents bound to the carbene carbon, because they directly influence the energy gap between the σ and p_π orbitals. The stronger the electron donation from these fragments, the larger the *s* character involved into one of the carbene carbon's σ orbitals. As a result, the angle between the three units decreases. All the explanations of this property in the literature involve the differential stabilization given to the σ and p_π orbitals by the orbitals of the connected moieties. A π-electron donation favours the singlet state because the superimposition to the vacant p_π orbital is favoured. In this case the hybridization of the carbene C is sp^2-like, the energy gap between σ and p_π orbitals is increased, therefore the species acquires a bent geometry with a smaller angle between the substituents and the C. This effect can be analysed also in terms of electronegativity: the withdrawal of electron density from the carbene C increases the positive charge on it and better stabilizes the 2*s* orbital with the respect to the 2*p* one.[5,7,9]

Examining the impact of the electron density on the molecular orbitals, we can have a more precise description of the carbene multiplicity. The inductive effect is realized through the superimposition between the 2s orbital of the carbene C atom and the combination of the

substituents' orbitals involved in the bonds. The σ-electron withdrawing moieties are lower in energy and better interact with the 2*s* orbitals of the carbene C. For this reason, the σ orbital has a higher s character, is lower in energy and the difference in energy with the p_π orbital - which does not experience this effect and remains unchanged - increases, favouring the singlet state.

On the other hand, the energy of electron donating substituents (i.e. the substituents with a lower electronegativity than carbon) is higher, therefore the σ orbital has a greater p character and a higher energy. This implies a lower energy difference between σ and p_π orbitals, hence the triplet state is favoured.

Concerning the mesomeric effect, the interaction between p or π orbitals of the substituents and p orbitals of the C centre should be taken into account. The p_x and p_y carbenic carbon's orbitals experience a loss of degeneracy acquiring electron density from π-electron donating substituents: increasing *s* character of σ favours the singlet state by enlarging the band gap. The opposite effect is registered when the C substituents are π-electron withdrawing. [5]

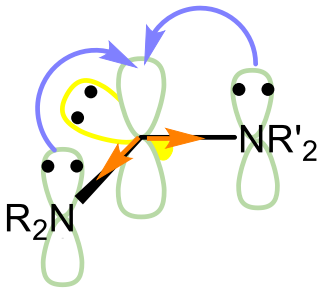

Figure 2. Representation of inductive (orange) and mesomeric (purple) effects on the carbenic C.

The nitrogen-based substituents in NHCs are σ-electron-withdrawing and π-electron-donating. The inductive effect is therefore responsible for the lowering of the σ orbital and the electron density provided by the mesomeric effect reduces the electronic unsaturation of the carbene C (Figure 2 and Figure 3). These combined effects increase the σ-p_π energy gap, favouring the singlet ground state multiplicity.[10]

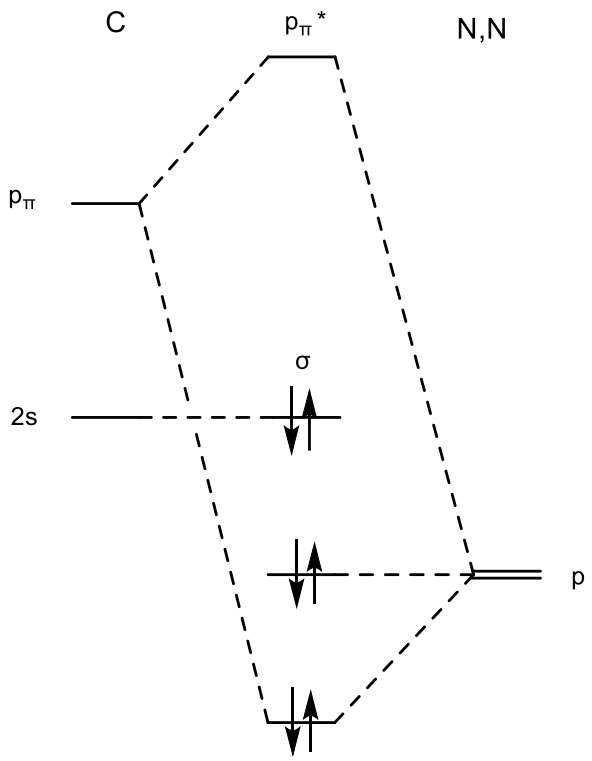

Figure 3. Qualitative MOs' diagram for di-nitrogen substituted carbene species.

In this thesis project the focus is on imidazole-2-ylidene derivatives (Figure 4) whose metal complexes have been widely studied both with alkaline, alkaline-earth metals and transition metals. The latter proved to be the most interesting with respect to the possible applications.[5]

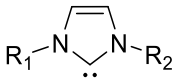

Figure 4. Generic structure of imidazole-2-ylidene.

Concerning the formation of a M-C bond, the carbene metal complexes are differentiated into two categories: Fischer-type and Schrock-type (Figure 5).

Generally, these two types of carbenes show these characteristics:

- Fischer carbenes are singlet carbenes, they usually have π-donor substituents such as -OMe or -NMe_2, hence the carbenic C behaves as an electrophilic species. The metal is usually a late transition metal in low oxidation state (e.g. Mo^0, Fe^0, Cr^0) and the ancillary ligands coordinated to this metal centres are good π-acceptors in order to withdraw some electron density from it. The formation of the M-$C_{carbene}$ bond does not

change the oxidation state of the central metal. The carbene can be considered as an L-type, 2-electrons donating ligand, as the π-back donation from the metal centre is limited. The nature of the Fischer carbene can be summarized as a σ-donor and weak π-acceptor ligand. The bond with the metal centre is defined by two opposite dative electron interactions.

- Schrock carbenes are triplet carbenes, they behave as nucleophilic ligands and their typical substituents are alkyl chains or hydrogen atoms. The metal centres are early transition metals in high oxidation states (e.g., Ta^{V}, W^{VI}); in the formation of the M-$C_{carbene}$ bond, the oxidation state of the metal is formally increased of two units. The carbene is conventionally a triplet X_2-type ligand and the bond can be described as two nonpolar covalent interactions.[10,11]

Fischer carbenes are also known to be carbene-transfer agents for the production of cyclopropanes. Schrock carbenes, instead, can act as metal ylides and transfer a methylene derivative to a carbonylic carbon.[10]

Figure 5. Schematic representation of the M-$C_{carbene}$ bond in Fischer (left) and Schrock (right) metal-carbene complexes.

NHCs are classified as Fischer-type carbenes even though the π back-donation from the M(d_π) orbital is considered negligible compared to the electron density donated to metal centre.[5]

1.2 Synthesis of NHC complexes

The two main approaches to obtain an imidazole-2-ylidene are i) deprotonation of an imidazolium salt and ii) reductive desulfurization of an imidazoline-2-thione (Scheme 1). The coordination of the carbene to the metal complex can be either performed in the same step as the NHC is produced or, if the compound is stable, in a second step (*vide infra*).

Generally, the synthesis of the imidazolium symmetrically N,N'-disubstituted ring is a one-step procedure starting from a 1,2-diketone, two equivalents of a primary amine and formaldehyde in presence of a Brønsted acid. The procedure for asymmetrically N,N'-disubstituted imidazolium unit requires instead two steps: in the first step the reaction of a 1,2-diketone, one equivalent of primary amine, formaldehyde and one equivalent of ammonium salt are reacted to form the imidazolium protonated at one of the two nitrogen atoms. In the second step a mild base like sodium bicarbonate deprotonates the unsubstituted nitrogen which nucleophilically attacks an alkyl or aryl halide (Scheme 1).[8]

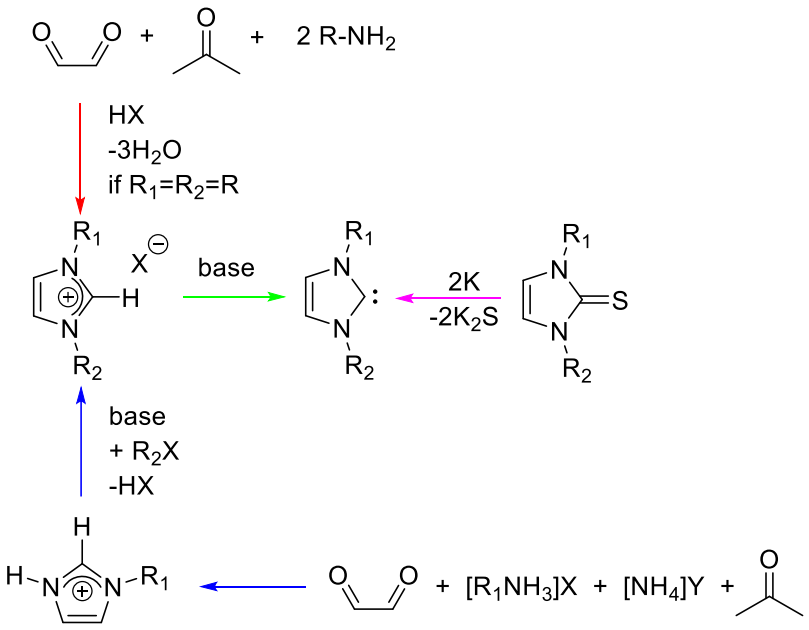

Scheme 1. Reaction's pathways for the synthesis of imidazole-2-ylidene. Red: one-step synthesis for symmetrically N,N'-disubstituted imidazolium salts; blue: two-step synthesis for asymmetrically disubstituted imidazolium salts; green: deprotonation of imidazolium salt; purple: de-sulfurization of imidazoline-2-thione.

The routes to obtain the imidazole-2-ylidene metal complex starting form imidazolium salts are:

- deprotonation of the C_2 position in the presence of a metal precursor (ML_n);
- formation of the Ag(I)-NHC complex and subsequent transmetalation of the carbene to a second metal centre.[12]

The latter method is usually carried out with Ag_2O but also with Ag_2CO_3, $AgNO_3$ and AgOAc (Scheme 2).

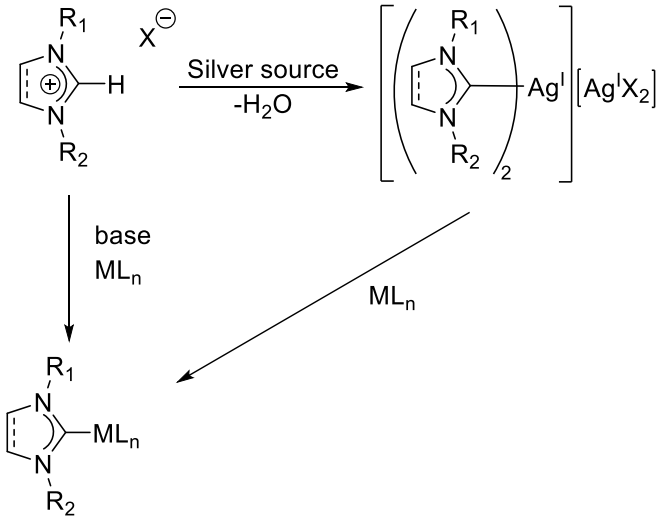

Scheme 2. Synthesis of NHC metal complexes starting from imidazolium or imidazolinium derivatives.

The imidazolium's counterions and substituents at the N atoms influence the type of the isolated NHC complex: a coordinating counterion, such as an halide, leads to a salt [NHC-Ag-NHC]$^{+}$[AgX_2]$^{-}$, which is in equilibrium with the neutral complex [NHC-Ag-X], instead a noncoordinating species, e.g. PF_6^{-}, gives only the charged bis-carbene complex [NHC-Ag-NHC]$^{+}X^{-}$ (Scheme 3).[8] The majority of examples dealing with the transmetalation procedure uses Ag_2O as a silver source; the protocol does not require an inert atmosphere nor the addition of a base and the deprotonation is usually selective at the C_2 position.[8,11,12]

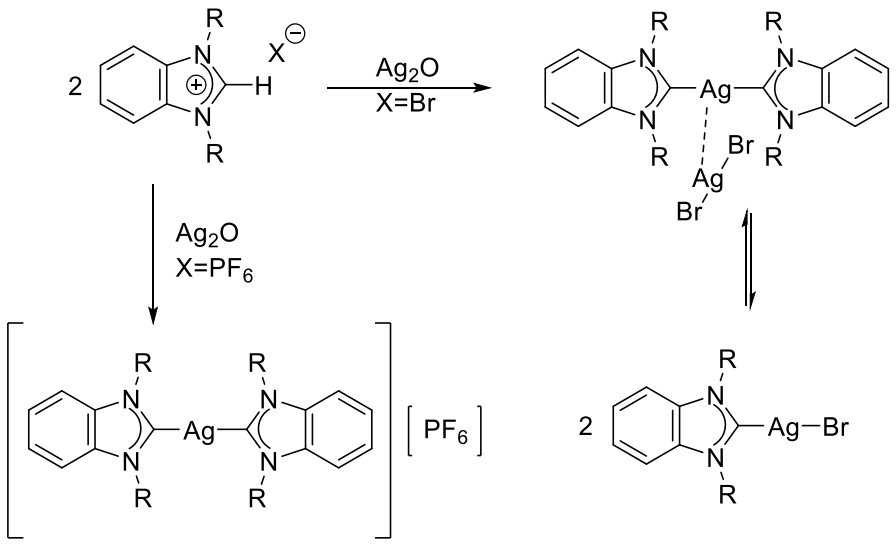

Scheme 3. Synthesis of Ag-NHC complexes with different counterions.

If the substituents at the nitrogen atoms are short alkyl chains, Ag···Ag and Ag···halide interactions can be established, thus producing different structures, as can be observed from the single crystal X-ray diffraction analysis.[12]

The transmetalation mechanism can either be monomolecular dissociative or bimolecular associative. The latter was evidenced in the Group 11 transmetalation compounds, the so-called coinage metals (M^C). M^C-NHC-M transition states have been confirmed in bis-carbene Cu(I) and Ag(I) compounds (Scheme 4).[13]

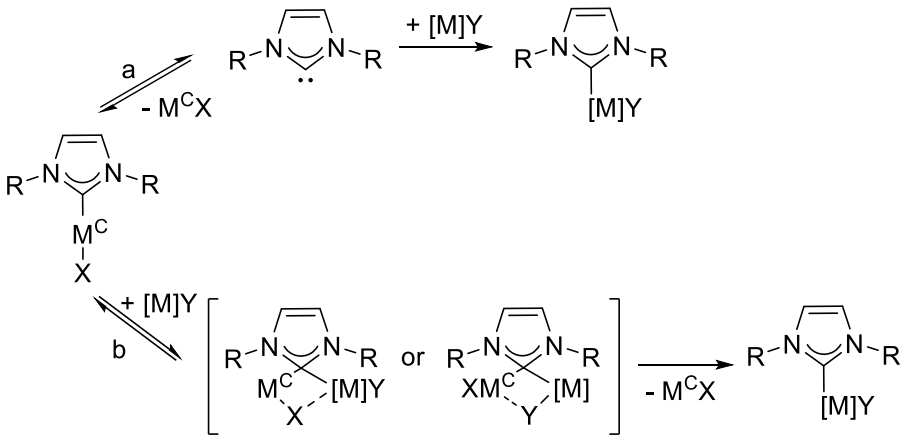

Scheme 4. Transmetalation mechanisms: a) monomolecular dissociative and b) bimolecular associative.

Ni(II), Pt(II), Pd(II), Cu(I), Cu(II), Co(I), Co(II), Au(I), Rh(I), Rh(III), Ir(I), Ir(III), Ru(II), Ru(III) and Ru(IV) NHC complexes have been synthesised via transmetalation from Ag(I) complexes.[12]

1.3 Applications of NHC complexes

The main application of NHC metal complexes is as homogeneous catalysts for different reactions. In particular palladium(II) complexes proved to be efficient in C-C coupling (Suzuki-Miyaura, Mizoroki-Heck), C-H activation, 1,2 addition of aldehydes and 1,4 addition of α,β-unsaturated compounds, Wacker oxidation reactions.[14,15]

Regarding copper, the reduction of cyclic enones and the hydrosilylation of ketones, esters and aldehydes and reduction of CO_2 into CO must be highlited.[14]

C-C cross-coupling, hydrogenation, Pauson-Khand cycloaddition and hydrofunctionalization can be catalysed by Co-NHC complexes;[16] instead Ni-NHCs can activate C-C, C-F and C-H bonds and promote cycloaddition, polymerization and C-C coupling reactions.[15]

Ru(II)-NHC carbene complexes and the study of the mechanism for the olefin metathesis process earned Grubbs, Schrock and Chauvin the Nobel Prize in Chemistry in 2005.

In particular, second generation Grubb's metathesis catalysts have a carbene as an olefine-exchange moiety and a N-heterocyclic carbene as a supporting ligand. These proved to be more efficient than the first generation ones, with a phosphine in place of the NHC ligand, as they better orient the incoming olefin (Figure 6).[17]

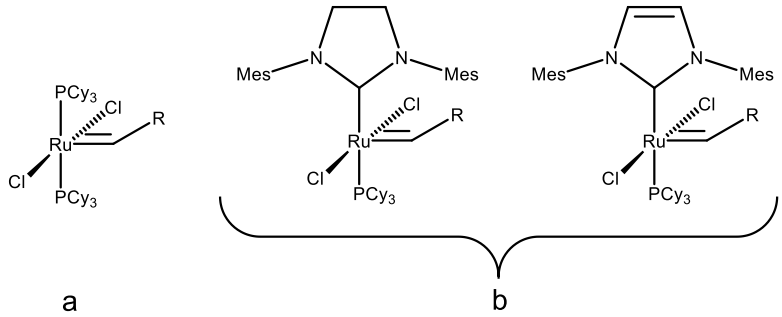

Figure 6. a) First generation and b) second generation Grubbs' catalysts.

Finally, NHC complexes with coinage metals exhibit highly chemotherapeutic efficiency and low toxicity towards humans' agents. Cu(I) and Au(I)-based NHC complexes prove antitumoral activity and Ag(I) analogous species have a remarkable antimicrobial activity.[18]

These features depend on the stability of the M^C-NHC bond which allows a slow release of the metal M^C in the cells, on the lipophilicity of the compounds which helps the cell penetration or on the generation of reactive oxygen species (ROS) as in the case of Cu(I)-NHC complexes.[19]

1.4 Photoluminescence properties of metal-carbene complexes

Particularly interesting for the aim of this thesis project are the luminescence properties of NHC metallic species.

Transition metal complexes feature a wide emission colour range in the visible part of the spectra due to the electronic transitions between molecular orbitals formed by the superimposition of d orbitals of the metal centres and ligands' molecular orbitals. The emission wavelength of these compounds can be finely tuned by adjusting the ligands' properties.

Exploiting the light emitted by these compounds when photo- or electro-excited is nowadays possible. Organic Light Emitting Diode (OLED) devices are used to create flexible, low-energy consumption and high-performance screens. The set-up of an OLED device can be summarized as a series of layers between the cathode and the anode (Figure 7). Holes are injected in transparent anode mainly consistent of indium-tin-oxide, namely a non-stoichiometric material based on SnO_2 and In_2O_3. They "move" in a hole transport layer (HTL) through electron hopping between nearest neighbours' HOMO electrons populating the vacant HOMO of the positively charged hole carrier species.[20]

Next to the cathode, where electrons are injected, the corresponding electron transport layer (ETL) enables the movement of the electrons toward the emission layer (EML) where electron and hole recombine forming an exciton and excite the emitter molecule through a charge transfer or the emitter traps one of the two charge carriers and becomes the site of the charges recombination.[20,21]

Hole-blocking layers (HBLs) and electron-blocking layers (EBLs) between EML and ETL and between HTL and EML respectively, can protect cathode and anode and make the transport more efficient minimizing ohmic losses.[20] A transparent glass on the ITO layer is generally added to protect the device.

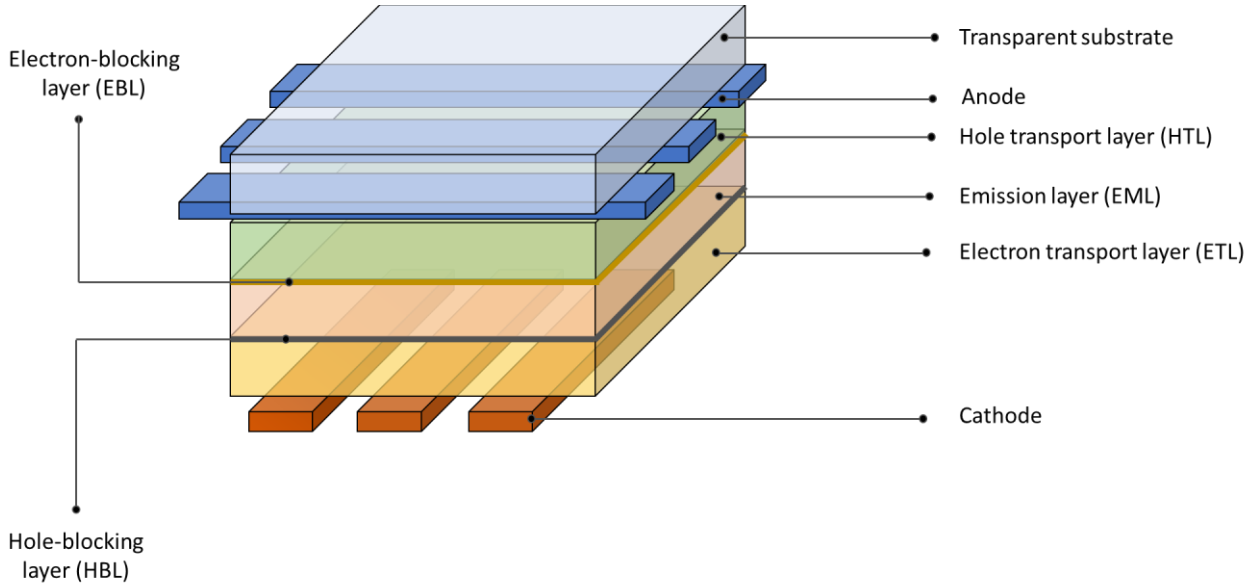

Figure 7. Simplified representation of an OLED device.

The emissive layer EML typically consists of host materials and light emissive dopants. To avoid quenching of the emitting light through the population of the triplet state by excitation energy transfer of the host material, this should lie at least 0.4 eV higher in energy than the triplet of the emitting complex.[20]

Metalorganic molecules serve as dopants for the EML due to the fine tunability of the emitted light and the possibility to tolerate high-energy transition states associated with the emission of deep blue light. Moreover, another advantage in the use of metal complexes is the exploitation of 75% of electron-to-photon conversion from the triplet state, which is dispersed in the form of heat in the case of organic molecules. Pure fluorescent emitter can only achieve quantum yields up to 25% according to spin-statistics.

Spin-orbit coupling (SOC) induced by the central metal mixes singlet and triplet states. After excitation, electrons populate the first excited singlet state and then - via intersystem crossing (ISC) - the lowest-lying triplet state. This effect is called *triplet harvesting*. Organic molecules do not experience a considerable ISC, because the mixing of singlet and triplet states is negligible and the triplet-to-singlet transition rates (k_r) are orders of magnitude smaller than the non-radiative relaxation rates ($\sum k_{nr}$).[20,22]

k_r is proportional to the spin-orbital interaction of the triplet state with the correspondent excited singlet (Equation 1).[20]

$$k_r \propto \left| \sum_{Sn} \frac{\langle \varphi_{Sn} | \hat{H}_{SO} | \varphi_{T1(i)} \rangle}{E_{T_1} - E_{Sn}} \right|^2 \quad \text{[Eq. 1]}$$

SOC is proportional to Z^4, where Z is the atomic number, hence the effect of singlet and triplet states mixing is massive for heavy metals.[20,23] For this reason, the population of the triplet state decays radiatively to the singlet ground state and the exciton to photon conversion reaches 100%, increasing the phosphorescent quantum yield (PQY).[20,21]

The group of *Tubaro*, as well as other groups in the literature, has intensively investigated the properties of dinuclear Au(I) NHC bis-carbene complexes which prove to have luminescence properties that make them available for OLED and bioimaging applications, considering the low toxicity of Au centres.[24] The synthesis of these complexes can follow two possible routes: i) transmetallation from a Ag complex precursor[18,24] and ii) base-assisted metalation with K_2CO_3 or NaOAc.[24–26]

The particular luminescence properties of Au(I) complexes should be analysed taking into account not only spin-orbit coupling, but also a relativistic contraction of 5d orbitals and aurophilic interaction which is explained further in this chapter.[27]

As reported for the compounds showed in Figure 8, the shorter the distance between two gold centres, the less energetic the light emitted after photoexcitation by the complex.[24]

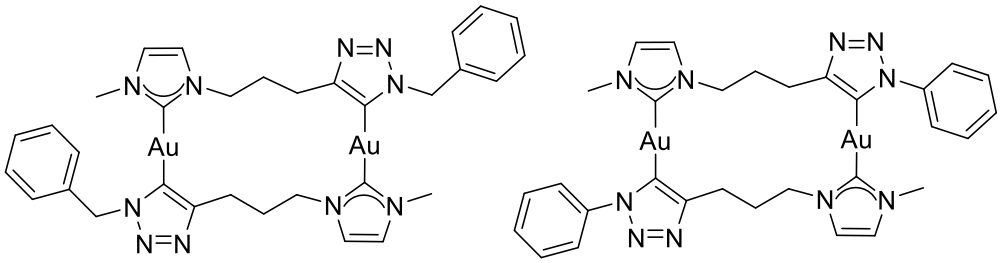

QY= 5 %
λ_{em} = 330 nm (λ_{exc}= 430 nm)
τ_0 = 1.21 μs
Au···Au distance = 3.348 Å

QY= 8 %
λ_{em} = 360 nm (λ_{exc}= 480 nm)
τ_0 = 0.23 μs
Au···Au distance = 3.068 Å

Figure 8. Dinuclear Au(I) complexes synthesized by Tubaro and co-workers. The reported τ is the average of the three values obtained from a three-component exponential decay.

Octahedral iridium(III) and square-planar platinum(II) NHC complexes proved to be efficient deep-blue emitters. The stability of these compounds is the main challenge because, to obtain an emission wavelength of about 460 nm, the excitation energy should be equal or greater than 2.70 eV, that is nearly the energy of a chemical bond. A good blue triplet emitter should fulfil these requirements: 1-2 μs decay time (τ_0) in order to keep the complex for a short time frame in an high-energy excited transition state; high PLQY; emission wavelength between 440 and 475 nm.[21]

NHCs excel as ligands for triplet emitter complexes because of their σ-donating ability having two main effects:

- the metal centred transition (MC d-d), which reduces the PQY, is not thermally accessible, and the non-radiative decay is hampered;
- the empty π* orbital is destabilized, producing an increase in the HOMO-LUMO gap which is responsible of an hypsochromic shift of the emitted wavelength.[23,28–30]

The intra-ligand charge transfer (ILCT π-π*) and the metal-to-ligand charge transfer (MLCT 5d-π*) are the main emissive pathways in Pt(II) square-planar complexes.[28]

The rigid square planar conformation of Pt(II) d^8 allows the maintenance of the geometry in the transition state enhancing the triplet emission. [28,31–34]

Strassner and *co-workers* report the photophysical properties of Pt(II) NHC complexes and their research is focused on the modification of the cyclometalated NHC to tune the emission wavelength and to increase the PLQY.[23,35]

The use of different diketonate ligands results in different PLQY: in particular changing from acetylacetonate to mesitylacetylacetonate the emitted light has a massive increase in PLQY as their steric hindrance is responsible of a more planar geometry in the excited triplet state, hence of a higher metal contribution to the decay emissive pathways which are more favourable than the non-radiative ones (Figure 9).[21,36]

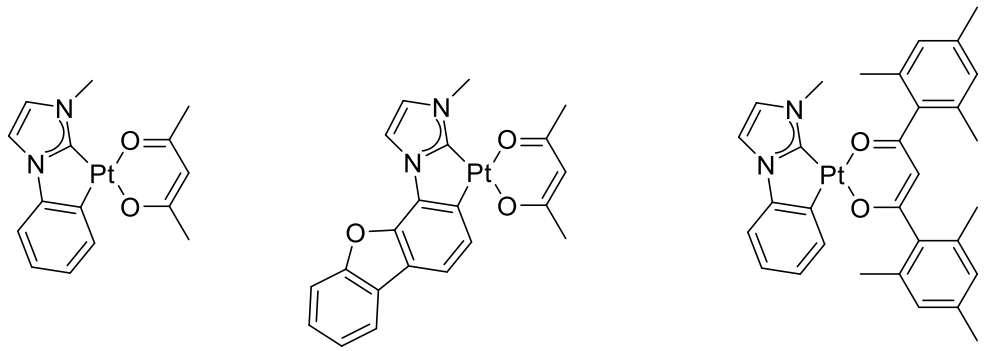

Figure 9. Quantum yields and emission wavelength of Pt(II) NHC complexes synthesized by Strassner and co-workers.[21]

1.5 Metallophilic interactions

The filled d_{z^2} and the vacant p_z orbitals along the z axis of the d^8 complexes, such as Pt(II) and Au(III) complexes, can interact in a so-called metallophilic interaction. Experimentally, this can be confirmed if the distance between two metal centres is smaller than the sum of their two Van der Waals radii. The close proximity can either be due to self-association or induced by one or more bridging ligands.[37]

In assembly-induced complexes, the proximity between the metallic centres is responsible of a superimposition of the d_{z^2} and the p_z orbitals, hence an increase in the energy of the HOMO and a decrease in the LUMO of the newly formed MOs can be observed (Figure 10). The weak

bonding interaction between the z-oriented orbitals determines a general decrease of the band gap and a bathochromic shift of the emitted light. The latter effect can be explained by the enhancement of the metal component in the frontier orbitals: this changes the excitation process from LC to metal-metal-to-ligand charge transfer (MMLCT), which is characterized by lower energy.[22,27,31,37–40]

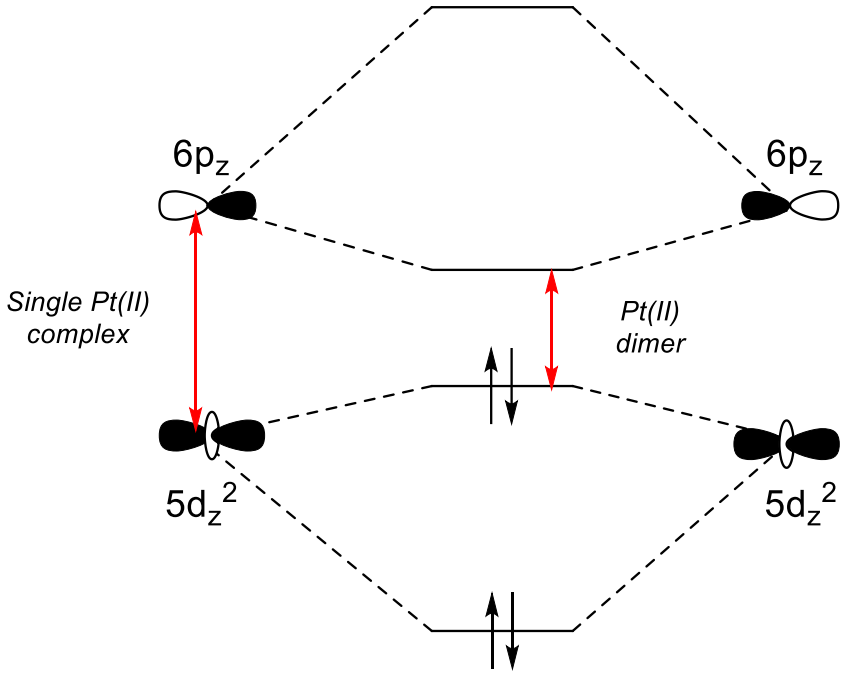

Figure 10. Qualitative MOs scheme for the z-oriented Pt(II) interacting orbitals in assembled complexes. In red the different HOMO-LUMO gap for single Pt(II) complexes and for interacting Pt(II) centres.

It has been shown that monometallic platinum complexes have lower quantum yields of emission, longer radiative decay times and blue-shifted emission wavelengths than related bimetallic Pt(II) complexes with bridging amidinate ligands.[31]

According to the literature, the sum of two Van der Waals radii for Au is 1.66 Å and for Pt is 1.72 Å.[41] Platinophilic interaction can be observed at a Pt···Pt distance between 2.9 and 3.5 Å.[36]

1.6 *N*-Oxy-heterocyclic carbenes (NOHCs)

Surprisingly, N-alkyloxy and N-aryloxy heterocyclic carbenes, namely NOHCs (Figure 11), have not been widely studied as NHC ligands in metal complexes.

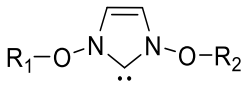

Figure 11. N-Oxy-imidazol-2-ylidene. R_1, R_2= alkyl-, aryl-.

The works of *Laus* and *Schottenberger* during the first decade of the 21st century marked the beginning in the study of these compounds and their Ni(II), Pd(II), Au(I), Ag(I) and Rh(I) complexes.[42–44] Not having any interesting application apart from being room temperature ionic liquids if asymmetrically substituted, the synthesis of these imidazolium salts was virtually neglected until 2021, when the research by *Schreiner, Lamaty* and *co-workers* put a new light on these compounds' synthesis and applications.[45–47]

The more interesting feature of N-aryloxy- and N-alkyloxyimidazol-based carbenes is the influence given by one or two oxygens to the overall aromatic system. Being the oxygen both a π-donor and a better σ-acceptor than nitrogen, the carbene carbon is more nucleophilic and generally an upfield shift of its ^{13}C NMR signal is observed (Figure 12). In a recent paper by *Schreiner et al.* two imidazole rings with adamantyl and adamantyloxy substituents were compared and both ^{13}C and ^{77}Se NMR confirmed a remarkable increase in the electron donor properties of the carbene when the adamantyloxy substituent was present.[46]

In the same work, they underlined how the presence of alkyl groups in the backbone of the imidazole must be carefully taken into consideration: the addition of electron density to C_4 and C_5 through inductive effect can decrease the electronic localization of the imidazole ring shifting the signals of the carbene centre down-field.[46]

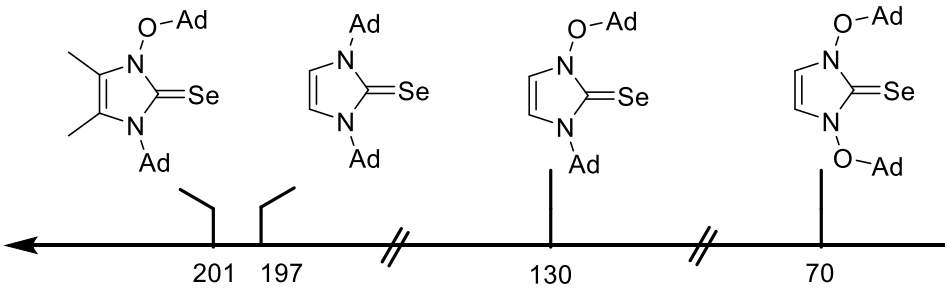

Figure 12. ^{77}Se NMR of the compounds synthetized by Schreiner and co-workers.

1.7 Synthesis and reactivity of *N*-oxy-imidazolium species

Single and double oxygenated N-oxy-imidazolium species have been studied so far, with short alkyl chains, benzyl and adamantyl moieties as oxygen-bound fragments.

1-hydroxyimidazole-3-oxide and its C_4 and C_5 substituted derivatives are the starting material for the two-oxygens NOHC proligands. Their syntheses are one-step condensations of monooximes of 1,2-diketones with either an aldehyde and ammonia or an adimine.[47,48] In particular, 1-hydroxyimidazole-3-oxide can be obtained in a one-step synthesis from glyoxal, formaldehyde, two equivalents of hydroxylamine and HCl in methanol basifying the mixture at 0°C afterwards.[48]

Further O-alkylation or O-arylation lead to the symmetrically or asymmetrically substituted species (Scheme 5). [42,45]

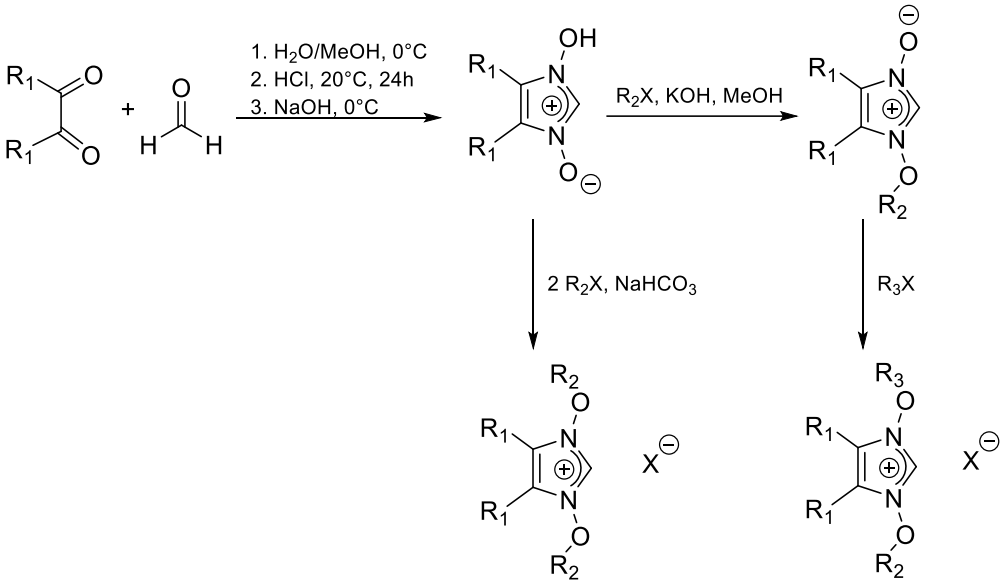

Scheme 5. Synthesis of N-oxyimidazolium ligand precursors (R_1=H, Me).

As alkylation and arylation require the oxygen atom to be deprotonated, a mild base is necessary. In presence of a strong base the formation of the carbene is possible. For the double benzylation of 1-hydroxyimidazole-3-oxide $NaHCO_3$ is used, whereas KOH in methanol is added for the two-step alkylation with different alkyl chains not longer than four carbon atoms.[43,44]

In a recent paper, vibratory ball milling (vbm) was used for a faster and solvent-free mechanosynthesis of 1-benzyloxyimidazole-3-oxide and their Ag(I), Au(I) and Cu(I) complexes with Cs_2CO_3 as the deprotonating agent (Scheme 6).[45]

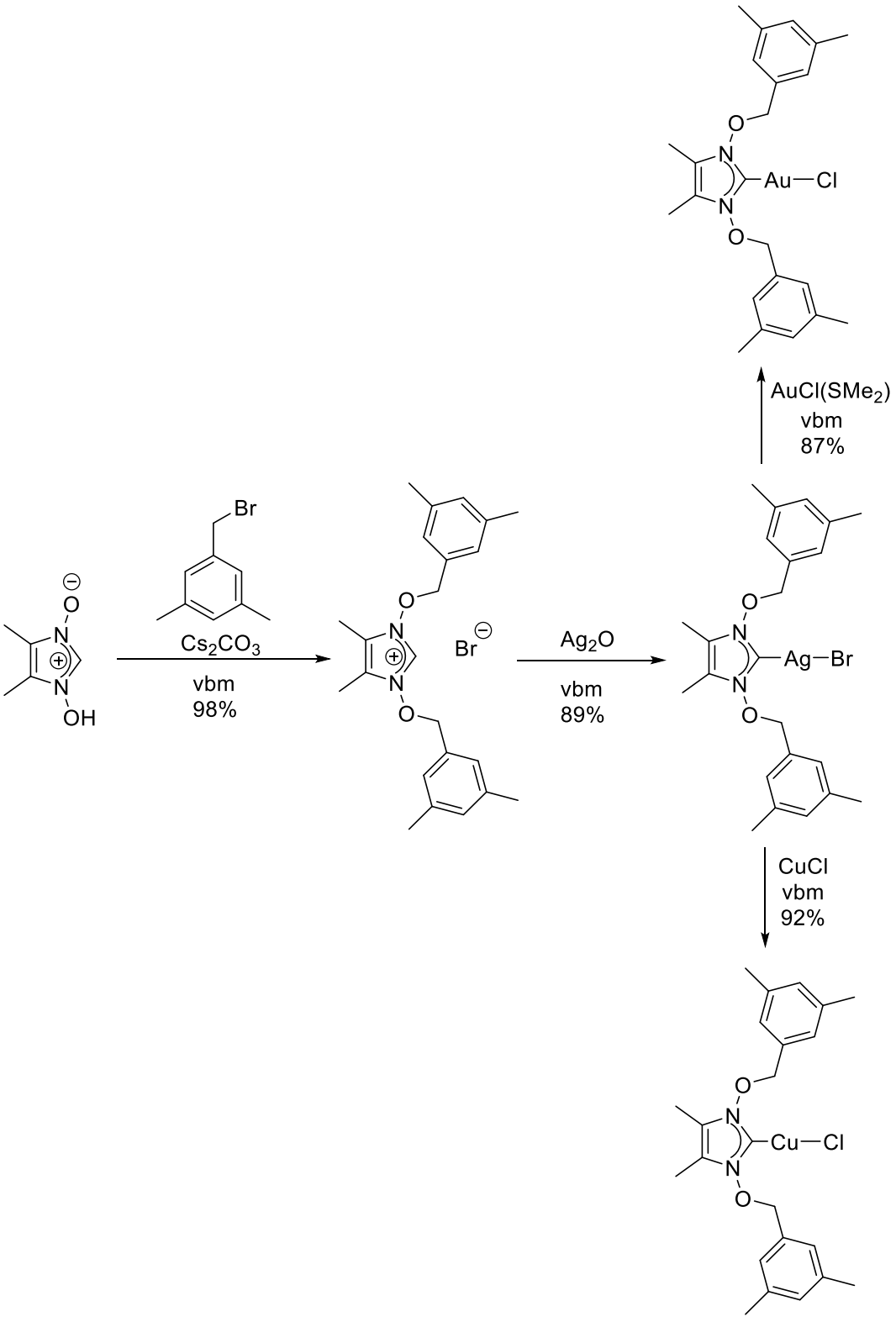

Scheme 6. Synthesis of symmetrically substituted proligand, Ag(I), Au(I) and Cu(I) complexes through mechanochemical vibratory ball milling.

As 1-hydroxyimidazole-3-oxide derivatives are easily accessible compared to mono-oxygenated analogues, they are the mostly used starting material for these compounds.

To study the behaviour of N-O bonds and to isolate single-oxygen NOHC species, the deoxygenation of a double-oxygenated NOHC has been explored by several research groups. PCl_3 and $TiCl_3$ in acid environment proved to be able to cleave the N-O bond of 1-hydroxy-3-benzyloxyimidazolium derivatives (Scheme 7, ***a***), whereas Pd/C can remove the benzyloxy moiety as well (Scheme 7, ***b***).[48]

The selective elimination of one of the two oxygen atoms in a double-oxygenated imidazolium salt has been obtained by *Heimgartner et al*. treating 1-adamantyloxyimidazolium-3-oxide with Raney-Nickel in methanol at room temperature or via sulfur-transfer mechanism with a dithione (Scheme 7, ***c***).[47]

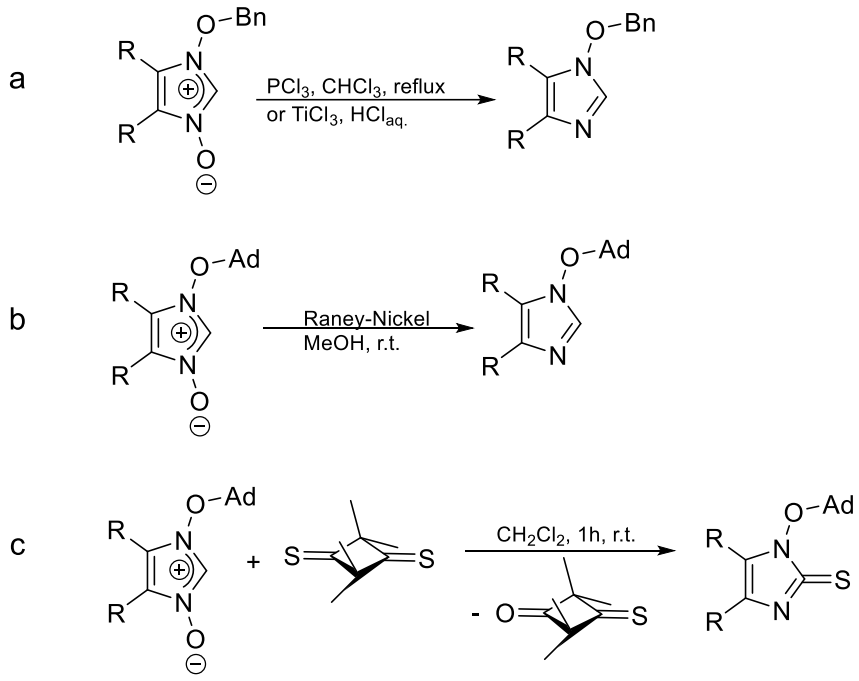

Scheme 7. Selective reduction of one N-O bond.

According to *Klötzer*, cleaving one of the two oxygen of 1-hydroxyimidazole-3-oxide is possible with Pd/C in a hydrogen atmosphere under mild heating (Scheme 8).[49]

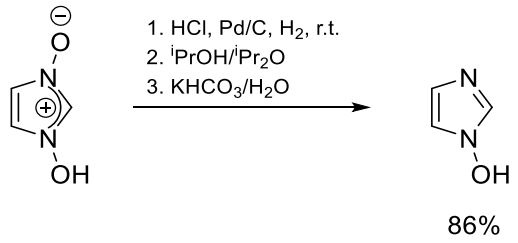

Scheme 8. Selective deoxygenation of 1-hydroxyimidazole-3-oxide with Pd/C.

1.8 Applications of *N*-oxy-imidazolium species

Silver(I), gold(I), copper(I), palladium(II) and rhodium(I) are the only metal centres with NOHC ligands reported in the literature so far. They are synthetized by deprotonation of the azolium salt or via transmetalation as shown previously.[43–45,50]

Not many applications which strongly diverge from the ones typical for NHC analogues have been investigated for this type of metal complexes. The catalytical activity of the palladium(II) complex in the Suzuki coupling proved to be worse than that with the correspondent NHC ligands because of a minor steric bulk next to the carbenoid centre which slows down the reaction rate (Scheme 9).[51]

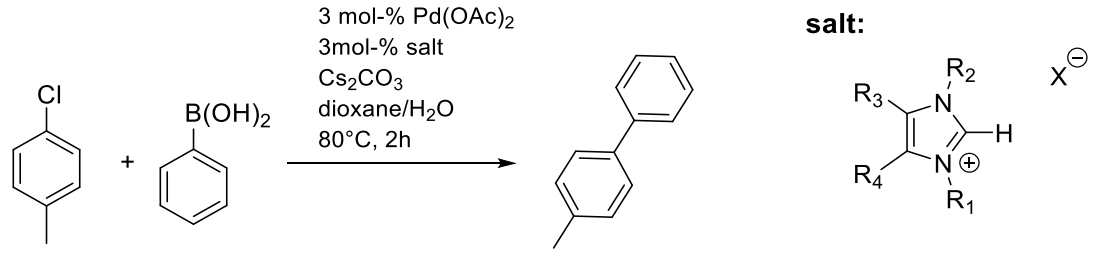

Scheme 9. Schematic representation of Suzuki coupling reaction of 4-chloro-toluene with benzene boronic acid catalysed by an in situ catalytic system reported by Wagner et al.[51] R_1, R_2 = OH,O^- (no X^-)/OMe (X^- = PF_6^-)/OEt(X^- = PF_6^-). R_3, R_4 = H/ Me/ Et/ Pr/ Ph.

Ruthenium(II) Grubbs catalysts in presence of NOH ligands lead to higher yields in ring closing metathesis than those observed in the same conditions without any additives, but the reason and the mechanism have not been studied yet.[52]

Cytotoxicity against colorectal cancer, promyelocytic leukemia and breast cancer cell lines have been tested using Au(I) and Ag(I) benzylated NOHC: the structural similarity leads to a release of the metal centre in the biological tissue analogous to what it is registered with NHC metal complexes.[45,53]

Furthermore, as already written previously, the imidazolium oxide species themselves are room temperature ionic liquids.[43,44]

1.9 Aim of the project

The research conducted in the framework of this master thesis is focused on the synthesis and characterization of N-oxyimidazolium proligands and their correspondent Ag(I), Au(I) mono-

and bis-carbene complexes as well as Pt(II) cyclometalated complexes. The synthetical interest is directed toward extended aromatic systems which have not been reported in the literature so far.

The type of proligands we plan to isolate are those reported in the following chart (Figure 13):

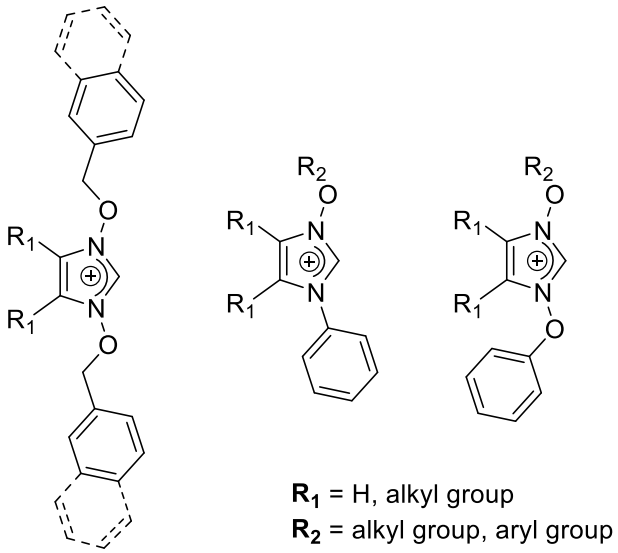

Figure 13. General representation of the synthetized proligands.

Concerning the Pt(II) complexes, the photophysical properties will be analysed in order to compare the results with those of similar NHC complexes already published. Absorption in a dichloromethane solution, emission from a PMMA doped matrix and decay time measurements will give an evaluation of which features are acquired by the molecules in the presence of an oxygen-bearing moiety. The optimization of the structural properties of these C^C* compounds look at the production of highly efficient deep-blue triplet emitters for OLED applications.

Quantum chemical optimization of the structure and calculation of both the excited triplet state electron density and HOMO and LUMO electron distribution can give further evidence on the emission and absorption results, respectively. The HOMO-LUMO gap will be analysed beyond with cyclic voltametric measurements.

Platinum species and their characterization will be realized in the Neubau Chemische Institute of the Technische Universität Dresden in the frame of a collaboration with the group of *Prof. Dr. Thomas Strassner*.

Chapter 2: RESULTS AND DISCUSSION

This Chapter is divided in three main sections. The first one (Section 2.1) regards the synthesis and the characterisation of silver(I) and gold(I) complexes with symmetrically substituted NOHC ligands, having benzyloxy or 2-methylnaphtalenyloxy substituents at the nitrogen atoms of the heterocyclic ring. The second part (Section 2.2) deals with the synthesis and characterisation of metal complexes (specifically platinum(II), silver(I) and gold(I)) with NOHC ligands bearing an oxy-moiety at one nitrogen atom and a phenyl ring as substituent at the second nitrogen atom. The last section (Section 2.3) summarizes all the attempts performed with the aim of isolating symmetrically and unsymmetrically substituted imidazolium salts different from those reported in the previous two sections. It can be anticipated that these attempts were mostly unsuccessful, but they are reported in order to underline the difficulties encountered in the broadening of this class of compounds.

2.1 Silver(I) and gold(I) complexes with symmetrically substituted NOHC ligands

2.1.1 Introduction

As reported in Chapter 1, the synthesis of both symmetrically and asymmetrically substituted NOHC proligands is already known in the literature, but the actual structures' library is far from being considered exhaustive.

The works of *Schottenberger et al.* focused on nucleophilic attack of deprotonated oxy-imidazolium rings to benzyl groups or short alkyl chains, such as methyl, butyl, allyl and propyl. Furthermore the only application reported to date for these compounds is their use as ionic liquids.[43,44,54]

In this Section the focus is on the synthesis of 1,3-disubstituted oxyimidazolium salts and their correspondent silver(I) and gold(I) complexes. The general structure of these species is described in Figure 14. The bis-benzyloxy-substituted NOHC is already known in the literature, however the bis-2-methylnaphtalenyloxy **3** is not.[43,44,54]

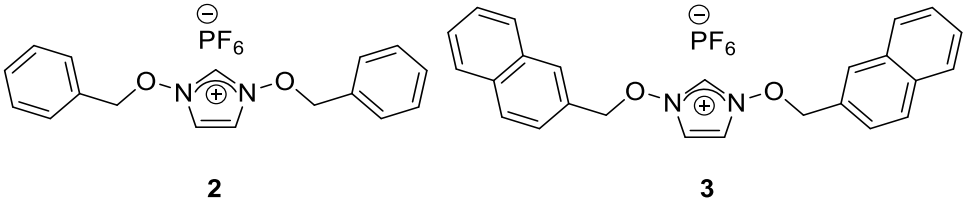

2 **3**

Figure 14. NOH proligands synthesized for Au(I) and Ag(I) complexation.

2.1.2 Synthesis and characterization of proligands

With a procedure already reported by *Eriksen et al.* 1-hydroxyimidazolium-3-oxide (**1**) was synthesized in large scale via condensation of glyoxal, formaldehyde and two equivalents of hydroxylammonium chloride in hydrochloric acid (Scheme 10). The pH was adjusted to 4.5 upon addition of NaOH, avoiding exceeding 20 °C because of the violent decomposition of the product at high temperature.[48] Even though part of the compound was lost due to the imprecise pH determination in water/methanol solution, the low cost of starting material, the scalability, the high yield and the absence of side products render this protocol efficient.

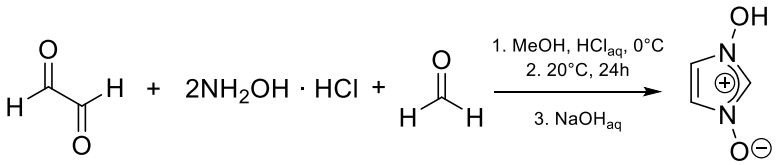

1

77-88%

*Scheme 10. Preparation of 1-hydroxyimidazole-3-oxide **1**.*

Following the procedures of *Schottenberger*, the nucleophilic attack of 1-hydroxyimidazolium-3-oxide (**1**) on two different bromide species was performed (Scheme 11).[54]

The last step of the synthesis involves the exchange between halide counterions and hexafluorophosphates, to obtain a solid soluble in most of the organic solvents in order to facilitate the subsequent metalation.

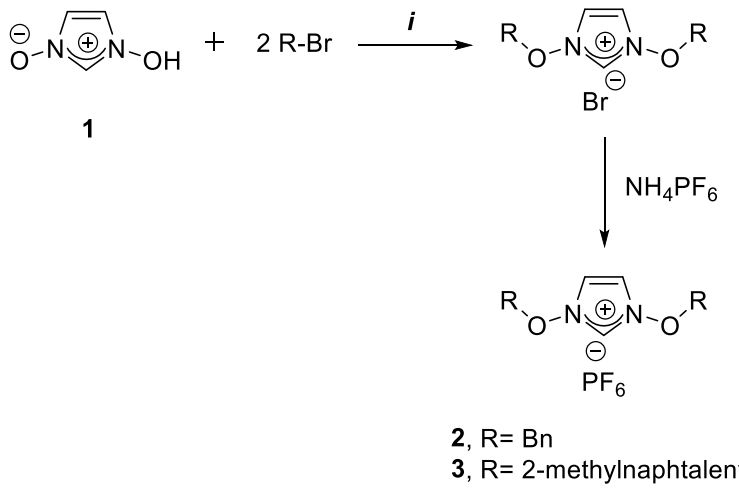

*Scheme 11. Synthesis of compound **2** (R=Bn, **i**= 1. neat, 2h 60°C; 3h r.t.; 2. $NaHCO_3$, H_2O, 17h, r.t., yield 48%) and **3** (R=2-methylnaphtyl, **i**= 1. neat, 2h 60°C; 3h r.t.; 2. $NaHCO_3$, H_2O, 3d, r.t.; **i'**= 1. CH_2Cl_2, 2h 60°C; 3h r.t.; 2. $NaHCO_3$, H_2O, 3d, r.t.).*

Compound **2** was isolated and characterised without problems. Benzylbromide was used as the solvent for the dissolution of the zwitterionic starting material **1**.

2-(Bromomethyl)naphtalene, however, has a higher melting point (52 °C). Therefore, two procedures were tried: i) neat conditions (60 °C) or ii) dissolution of the solids in dichloromethane and reflux.

NMR spectra of the solids obtained with both these procedures for the synthesis of **3** suggest some impurities were present. Two peaks, associable to the CH_2 benzylic protons, are observed at 5.59 and 4.88 ppm in the ^1H NMR spectrum registered in DMSO-d_6 after the nucleophilic substitution reaction with bromomethylnaphtalene; these two signals could be ascribed to the di- and mono-substituted compounds. Considering the relative intensities and the integrals, we can conclude that the peak at 5.59 ppm corresponds to the disubstituted compound **3** (with bromide as anion), whereas the one at 4.88 ppm to the monosubstituted one (Figure 15). A separation of these two compounds might be possible exploiting their different polarity, hence the solubility in different deuterated solvents (acetonitrile, DMSO, water, chloroform) was tested. Unfortunately, differential solubility was not satisfactory to separate the compounds; the NMR-experiments lead to the conclusion, that the mono- and the disubstituted products of compound **3** could not be separated by using different solubility.

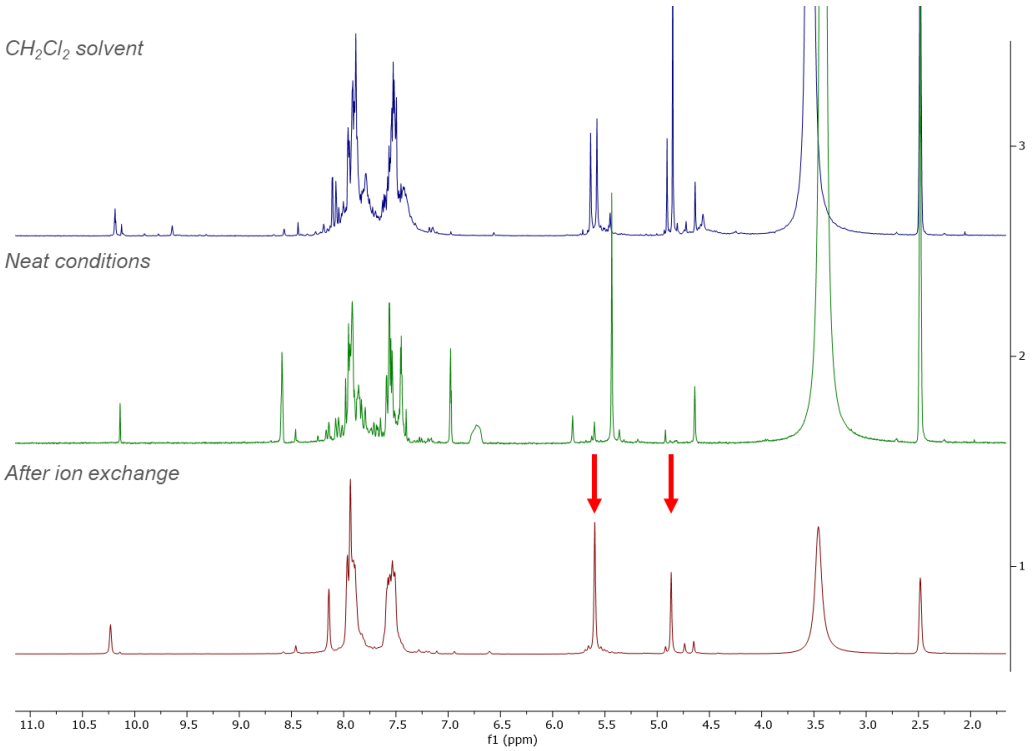

Figure 15. Comparison between the ^{1}H NMR spectra of 1,3-di(2-methylnaphtalenyloxy)imidazolium ions (25 °C, DMSO-d_6) obtained in neat conditions, in CH_2Cl_2 and after ion exchange with hexafluorophosphate. The red arrows mark the mono- and di-substituted CH_2 groups at 4.48 and 5.59 ppm, respectively.

ESI-MS analysis supports the formation of the disubstituted compound, as the most abundant signal is at *m/z* 381.16, which correspond to the singly charged positive ion (Figure 16).

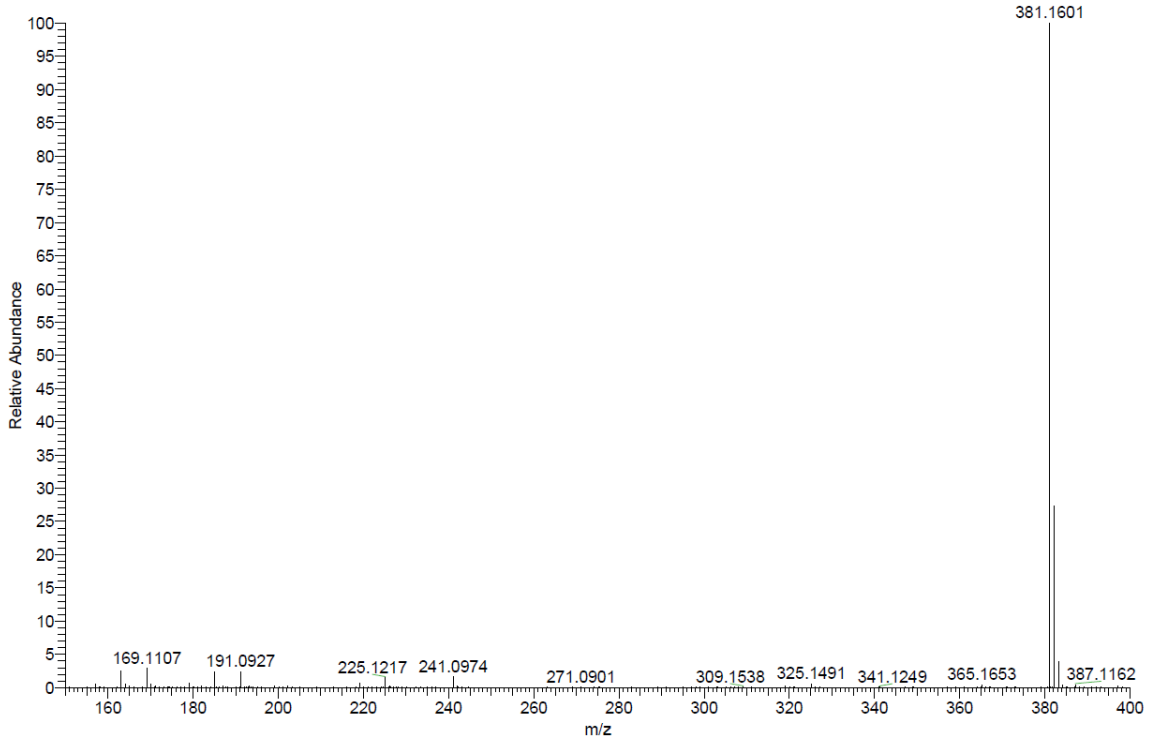

Figure 16. ESI-MS spectrum of 1,3-di(2-methylnaphtalenyloxy)imidazolium hexafluorophosphate.

The peak at 10.19 ppm in the ^{1}H NMR spectra of compound **3** can be assigned to the carbenic proton of the disubstituted compound because, as observed by comparing the ^{1}H NMR spectra of 1,3-di(benzyloxy)imidazolium hexafluorophosphate (**2**) and 1-benzyloxyimidazolium-3-oxide (compound **17**, see further in the text), the proton in C2 position is shifted down-field for the disubstituted compound (10.12 ppm compared to 8.53 ppm, Figure 17). This could be explained by the decrease in resonance stabilization given by the presence of two substituents bound to the O atoms.[46] The increase of the acidity of the disubstituted *N*-oxy imidazolium proligands can be observed in all disubstituted compounds compared to the single-substituted ones synthesised by *Schottenberger* and *co-workers*, as well.[42]

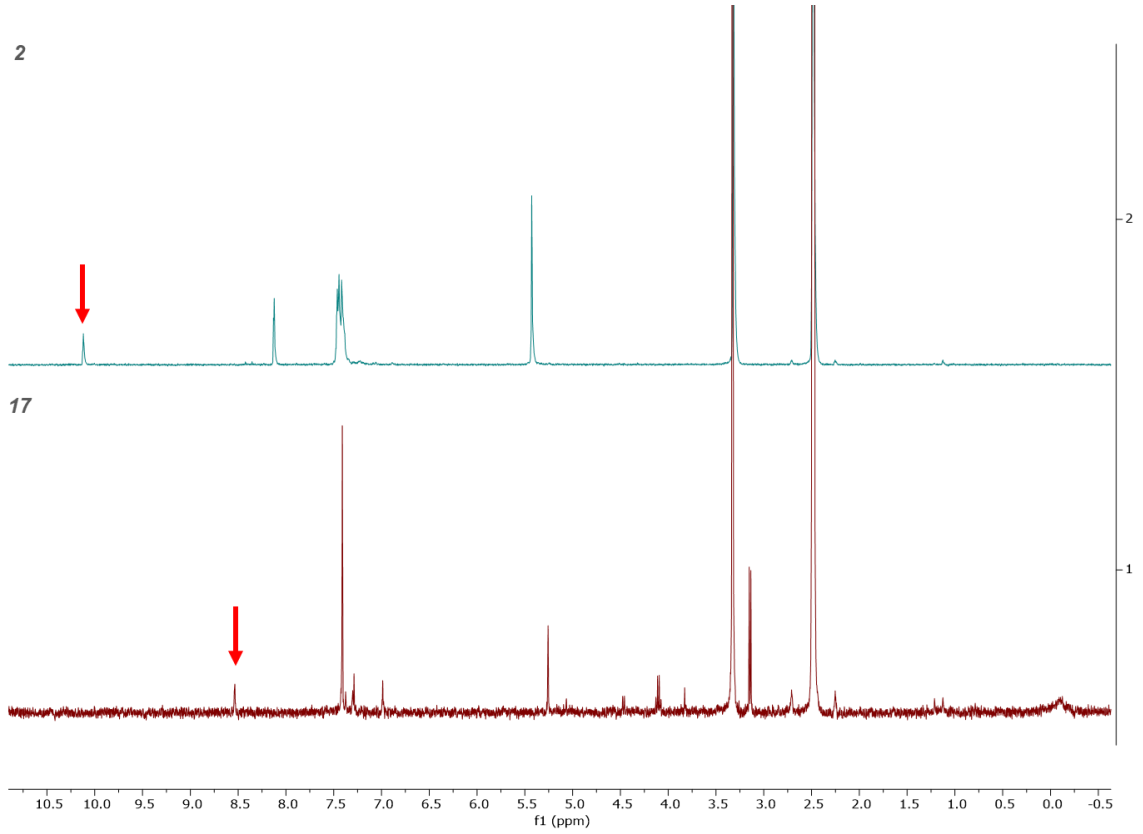

*Figure 17. Comparison between ^{1}H NMR spectra of 1,3-di(benzyloxy)imidazolium hexafluorophosphate **2** and 1-benzyloxyimidazole-3-oxide **17** (25°C, DMSO-d_6). The red arrows underline the C2 proton signals which correspond to 8.53 ppm for the monosubstituded **17** and to 10.12 ppm for the disubstituted **2**.*

1,3-Di(benzyloxy)imidazolium is a viscous liquid with bromide as a counterion, whereas its hexafluorophosphate salt is a solid. The difference in the ^{1}H NMR spectrum changing the Br^{-}

with the PF_6^- anion leads to a difference of almost 0.1 ppm in the C2-H proton resonance as described in the literature.[51]

The 1,3-di(2-methylnaphtalenyloxy)imidazolium salts, both bromide and hexafluorophosphate, are solids probably due to the larger aromatic system which allows for a better stacking of different units.

2.1.3 Silver(I) and gold(I) complexes

The obtained hexafluorophosphate NOHC precursors were employed for the synthesis of silver(I) complexes, even if compound **3** is not completely pure. In order to circumvent the photosensitive behaviour of silver(I) complexes, Au(I) complexes were obtained by transmetalation reactions. The procedure was derived from *Schottenberger et al.* using methanol as a solvent at room temperature under an inert atmosphere (Ar). The molar ratio between silver and ligand precursor was 1.2, hence some silver salt residues were expected to be present in the precipitate. Chloro(dimethylsulfide)gold(I) was used for the transmetalation reaction in dichloromethane (Scheme 12).

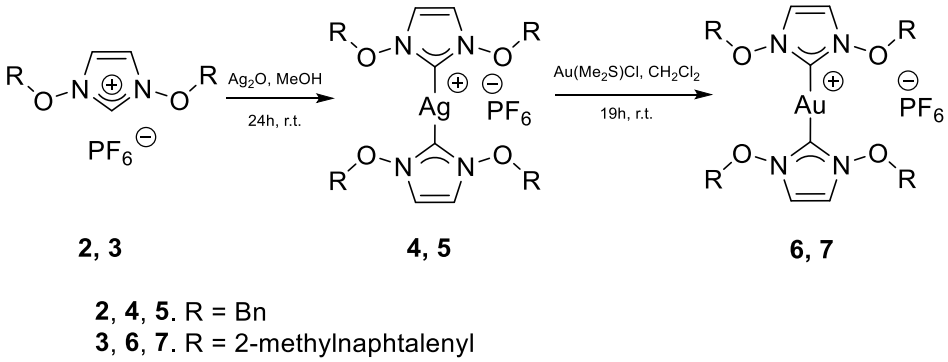

*Scheme 12. Synthesis of Ag and Au complexes **4-7**.*

The reaction for the synthesis of gold(I) complexes was continued for a longer time than what suggested by the literature (19h compared to 2.5h). The mixture should be filtered, and the product precipitated adding diethyl ether. However, gold complexes easily decompose at low pressure even at room temperature, hence we tried to promote crystallization storing the samples at 4°C. Since no solid precipitated, dichloromethane was removed under vacuum and a sample of each compound was dissolved in the minimum amount of dichloromethane with hexane added on top to promote crystallization.

Bis[1,3-di(benzyloxy)imidazolin-2-ylidene]gold(I) hexafluorophosphate is already literature known[54], so the colourless crystals obtained from its sample were not analysed through X-ray, but the ^{1}H and $^{13}C\{^{1}H\}$ NMR spectra were simply compared with the literature.

The absence of the carbene proton signal in the ^{1}H NMR indicates the formation of the metal-carbene complexes, as shown in Figure 18. Both ^{1}H and $^{13}C\{^{1}H\}$-NMR spectra confirm the complexation and the frequencies of the signals are corroborated by the literature.[54]

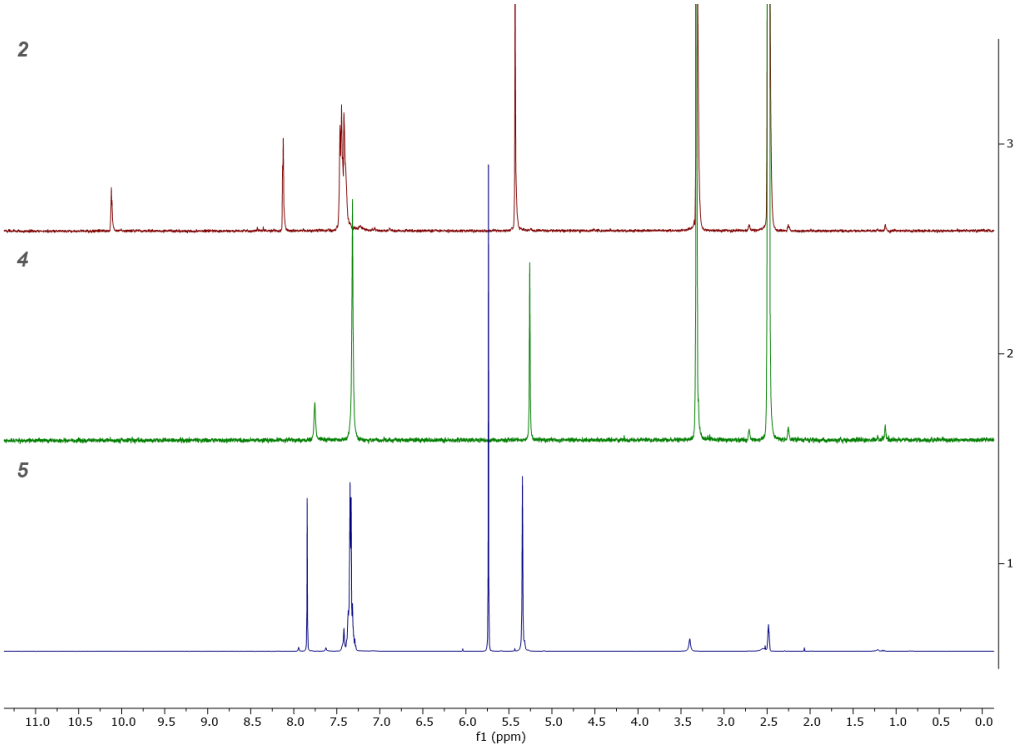

*Figure 18. Comparison between ^{1}H NMR spectra (25°C, DMSO-d_6) of compounds **2**, **4** and **5**.*

Concerning the 2-methylnaphtalenyloxy complex **6**,$^{13}C\{^{1}H\}$-NMR spectrum reports the expected signals, but ca.7-9% of the proligand was not converted in the silver complex (and thus in the gold complex as well) as it can be observed in the ^{1}H NMR spectrum in Figure 19. Moreover, for complex **7** the integrals of the signals in the ^{1}H NMR aromatic region, the presence of multiple peaks between 5.3 and 5.6 ppm and the high number of signals in the $^{13}C\{^{1}H\}$-NMR spectrum support the hypothesis of the presence of the free proligand and/or complexes without one or 2-methylnaphthalene moieties. These observations lead to the conclusion that the attempted experimental protocol does not provide access to the desired gold(I) complex in sufficient purity.

The binding of one or two benzyl fragments in NOHC structure was confirmed by these experiments but should be optimized for 2-methylnaphtalenoxy nucleophilic attack. A synthetic route which produces a purer methylnaphthalene-bearing precursor could lead to less impurities in the reaction mixture.

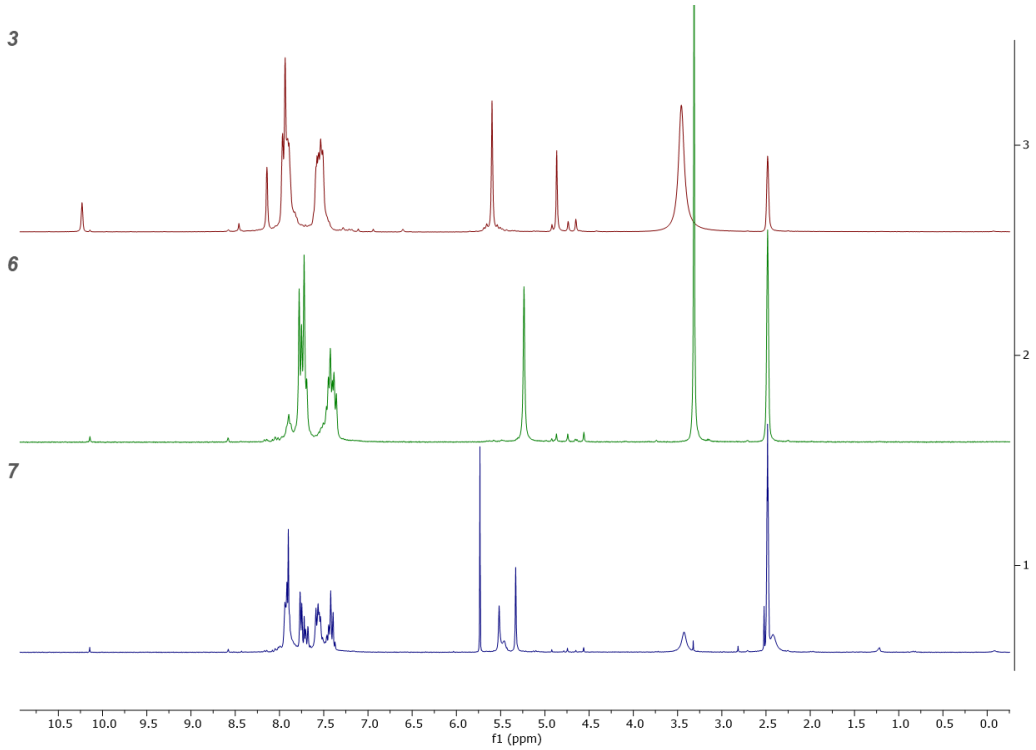

*Figure 19. Comparison between ^{1}H NMR spectra (25°C, DMSO-d_6) of **3**, **6** and **7**.*

2.2 Metal complexes with phenyl-substituted NOHC ligands

2.2.1 Introduction

Bidentate C^C* cyclometalated NHC Pt(II) complexes have been studied by *Strassner* and *co-workers* in the last decades. For OLED applications the thermal stability and charge neutrality of the compounds is fundamental as vapour deposition is the most used technique for the formation of layers.[23,30,34]

Therefore, Pt(II) compounds presented in this section are neutral to match industrial needs for applicability and more easily study the photophysical properties.

The melting point is also analysed in order to better understand and define the stability of the compounds.

Four Pt(II) complexes were synthesized combining two methoxy- and benzyloxy-substituted proligands with two different auxiliary ligands (acetylacetonate (acac) and mesityl-substituted acetylacetonate (1,3-bis(2,4,6-trimethylphenyl)propane-1,3-dione = mesacac)).
Additionally, proligand **10** (Scheme 14) was also complexated with silver (I) and gold (I) metal salts.

2.2.2 Synthesis and characterization of the proligands

The starting material for the generation of the C^C* proligands is 3-phenyl-4,5-dimethylimidazolium-1-oxide (**8**), chosen because the phenyl ring could be orthometalated by the platinum centre.

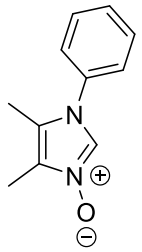

8

Figure 20. 3-phenyl-4,5-dimethylimidazolium-1-oxide.

Compound **8** was obtained according to a modified procedure reported by *Mlòston* for similar compounds with methyl and phenyl groups on the backbone and isopropyl, isobutyl and adamantyl groups bound to the nitrogen.[53]
Diacetyl monoxime and hexahydro-1,3,5-triazine were synthesized and used as starting materials in a 3:1 molar ratio in glacial acetic acid at room temperature for 40 h (Scheme 13).[55,56]

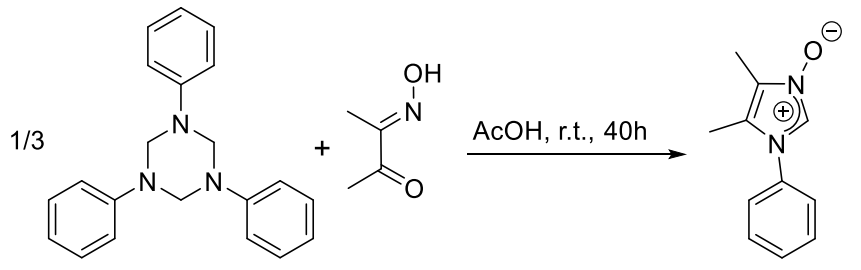

8

Yield: 9.9-51.2%

*Scheme 13. Synthesis of compound **8**.*

Concentrated sulphuric acid was added dropwise through a funnel into a flask charged with sodium chloride. Hydrogen chloride was generated and transferred via inlet into the reaction flask for 2 h. Excess of $HCl_{(g)}$ was directed into a 30% aqueous solution of sodium hydroxide. The system was not cooled down to 0°C as reported in the paper because that causes freezing of glacial acetic acid, hence the impossibility of stirring the solution. The formed hydrochloride salt of **8** was then precipitated with diethyl ether and cooled down to 4°C. After filtration, washing and dissolution in $CHCl_3$/MeOH 5:1 mixture, the product was basified with sodium carbonate which was filtered before purification by column chromatography. Four batches of compound **8** were synthetized on different scales: the yields varied between 9.9 and 51.2%. The poor scalability of this reaction should be mentioned at this point but considering the low cost of the production of the reagents and reactants it was considered worth the effort.

The hydrochloride salt of **8** showed a significant down-field shift for the carbene H-atom in the ^1H NMR. This could be explained with the higher polarity in relation to the zwitterionic species (Figure A 1).

Elemental analysis did not verify the calculated percentage, but this could be due to the hygroscopic nature of the species. High resolution mass spectrometry (HRMS) confirms the formation of this zwitterionic compound with a $[M+H]^+$ and a $[2M+H]^+$ signals at m/z 189.10 and 377.20, respectively.

The proligands **9** and **10** were obtained by mixing **8** with methyl iodide or benzyl bromide respectively, in anhydrous tetrahydrofurane in a pressure tube at room temperature (Scheme 14). Nucleophilic attack onto isobutyl bromide and several attempts of phenylation with a diphenyliodonium salt were not successful (see chapter 4.5.6). Methylation of oxyimidazolium rings using the Meerwein salt or dimethylsulphate was already reported.[43] Methyl iodide proved to give good results as no side products were present and the yield was in the range 81-94%.

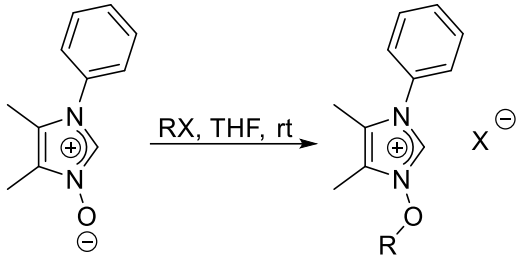

8

9. R = Me, X = I
10. R = Bn, X= Br

*Scheme 14. Methyl and benzyl substituted proligands. Yields: **9**, 93.5%; **10**, 61.8%.*

The obtained proligands **9** and **10** were successfully analysed and confirmed by NMR, EA and ESI-HRMS. The melting points of **9** and **10** are within the same range as for the adamantly analogues, reported in literature.[53,57]

2.2.3 Platinum(II) complexes based on *O*-methyl- and *O*-benzyl-substituted NOHCs

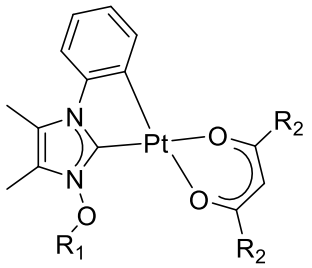

	R_1	R_2
11	Me	Me
12	Bn	Me
14	Bn	Mesityl

Figure 21. C^C cyclometalated Pt(II) complexes synthesized in this project.*

The methodology for the synthesis of complexes **11**-**14** was adapted from the one developed by the group of *Strassner* for the synthesis of C^C* cyclometalated NHC Pt(II) complexes (Scheme 14). Under inert conditions, 1-R-oxy-3-phenylimidazolium bromide (R=Me or Bn) was mixed with 0.5 eq. of silver(I) oxide in degassed and anhydrous dimethylformamide at room temperature to generate *in situ* the silver-NOHC complex. Then, transmetalation was achieved adding dichloro(1,5-cyclooctadiene)platinum(II) in equimolar amount with respect to the carbene precursor. According to the literature, cyclometalation of the proligand into the metal centre occurs when the Pt-NOHC complex is heated after the transmetalation.[58] Indeed, the mixture was heated overnight at 120 °C after the addition of $Pt(COD)Cl_2$. Acetylacetonate, which was provided as a sodium salt, was added without the presence of a

strong base, whereas for the isolation of the complexes with mesacac ligand, two equivalents of potassium tert-butoxide are required for *in situ* deprotonation of the diketone. After heating to 110°C and evaporating the solvent under mild heating, the products were extracted with dichloromethane and the silver by-products filtered through a Celite pad. After removal of the solvent and purification by column chromatography, the desired novel Pt(II) complexes were obtained in low yields (**11**: 23.9%, **12**: 6.4%, **13**: 5.0%, **14**: 9.0%).

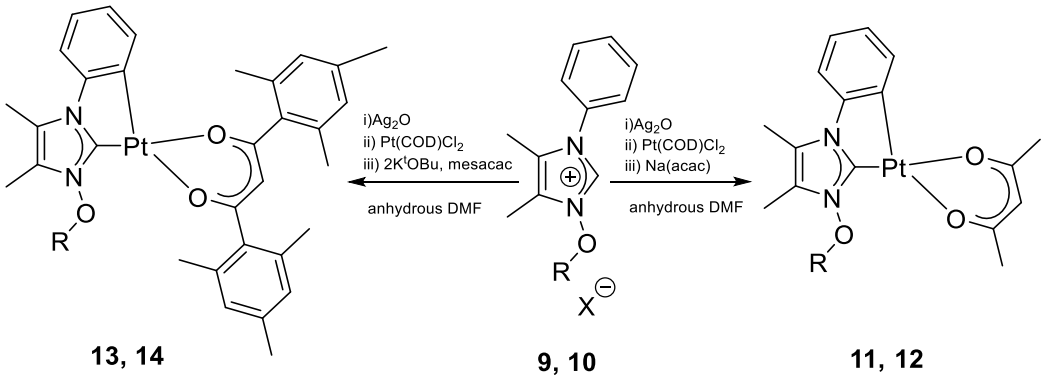

Scheme 15. Synthesis of Pt(II) C^C complexes. R= Me (**11**); R=Bn (**12**, **14**). The characterisation of complex **13** suggests the presence of R=H group or the replacement of the OMe group with a hydrogen (see further in the text).*

The obtained Pt(II) complexes were fully characterized, including ^{1}H, ^{13}C and ^{195}Pt NMR spectra as well as 2D-NMR experiments. For complexes **11** and **14**, solid state structures were obtained by X-ray diffractometry.

Successful cyclometalation was confirmed by the appearance of satellite peaks in the ^{1}H NMR of all Pt(II) complexes in the aromatic region (7.40 ppm-7.85 ppm). These smaller neighbouring signals typically indicate a ^{1}H-^{195}Pt-coupling (Figure 22).

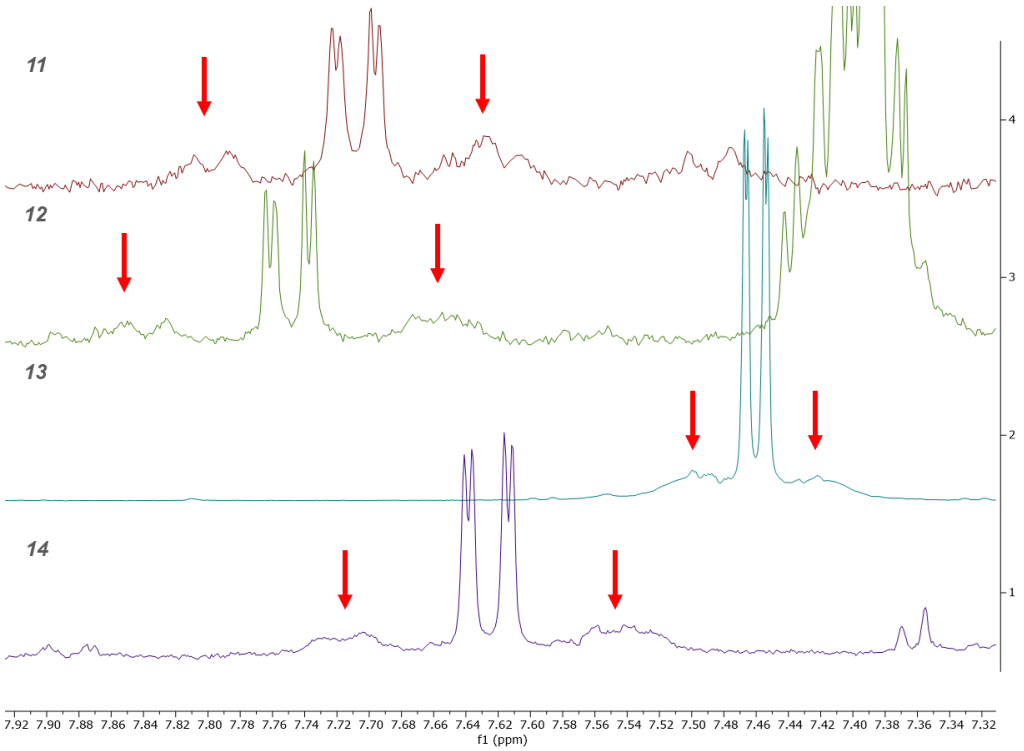

*Figure 22. Magnified ^{1}H NMR spectra of complexes **11**-**14** showing the characteristic ^{1}H-^{195}Pt coupling in the phenyl moiety.*

COSY, HSQC, HMBC and NOESY 2D NMR also give important information on the structure of the synthesized compounds. As an example, the correlations found in the 2D NMR spectra of compound **11** are reported (Figure 23).

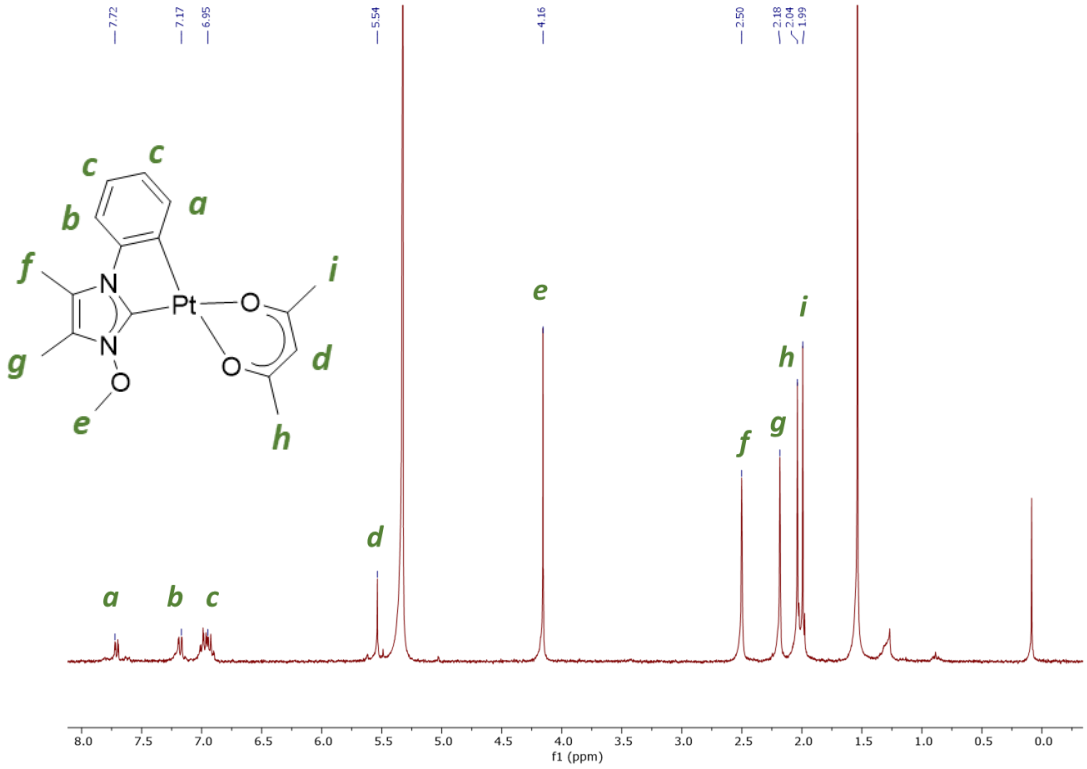

*Figure 23. ^{1}H NMR spectrum of compound **11** and its assignations.*

The COSY experiment proves the relationship between ^{1}H signals at 5.54 ppm and 2.04 ppm, that were assigned to the CH proton and a methyl group of the acetylacetonate ligand respectively. Moreover, the multiplet between 6.89 and 7.03 ppm integrating for 2 protons, should be designated to proton number 2 and 3 of the aromatic ring (numbering counterclockwise from the one next to the Pt centre), because they are coupled with the other two aromatic signals that, according to their coupling constants, are not correlated among themselves. The latter consideration is sustained by the evident ^{1}H-^{195}Pt coupling of the peak at 7.72 ppm, which is the one next to the platinum centre in the cyclometalated structure and by the NOESY ^{1}H-^{1}H correlation between the methyl group in the imidazole backbone and the aromatic signal at 7.17 ppm which can be assigned to proton 4 of the phenyl ring. Signal at 2.50 ppm can be attributed to the CH_3 group bound to carbon 5 of the imidazolylidene ring, whereas the OCH_3 group gives a signal at 4.16 ppm, which correlates with the methyl signals at 2.04 and 2.18 ppm, which should correspond to acetylacetonate and the C_4 imidazole methyl groups respectively. With HSQC and HMBC, carbons were associated with the respective groups in the molecules for the all four Pt(II) complexes.

^{195}Pt NMR signals are between -3454 ppm of **12** and -3397 ppm of **13**, in accordance with what has already been reported in the literature for C^C* Pt(II) complexes (Figure 24).

It is apparent that mesacac compounds **13** and **14** have an electron poorer Pt centre as their signals are up-field shifted in comparison to acac analogues. A further support of this conclusion comes from the photophysical analyses (*vide infra*).

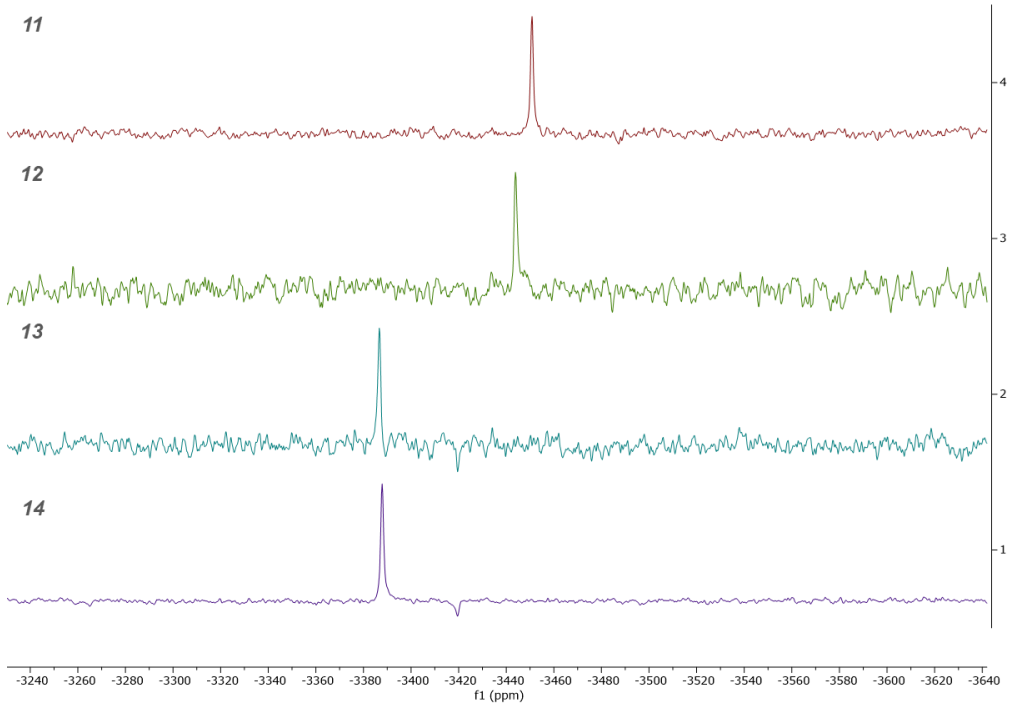

*Figure 24. ^{195}Pt NMR spectra (129 MHz, CD_2Cl_2, 25°C) of complexes **11**-**14**.*

Although elemental analyses of **11** and **12** do not perfectly fit the calculated percentages, the exact mass of **11**, **12** and **14** were detected in HRMS.

A surprising result is the absence of the methoxy group in the compound isolated in the attempt of synthesising complex **13**. In the ^{1}H and ^{13}C NMR spectra, no signal attributed to the methoxy group is present, as it is clearly evident by the comparison with the spectra of **9** and **11** (Figure 25).

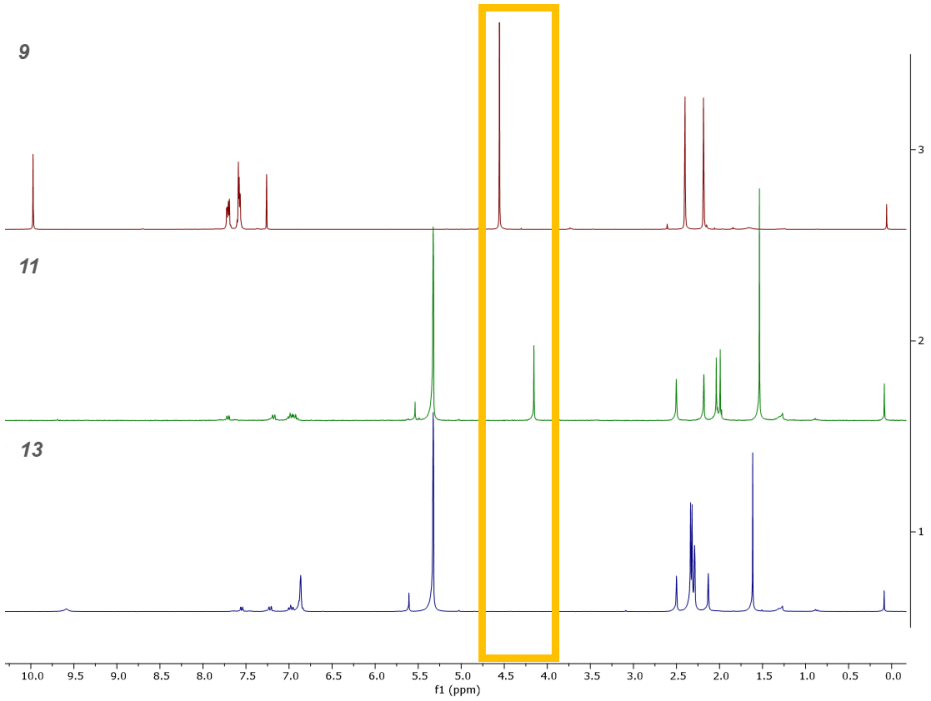

*Figure 25. ^{1}H NMR (600MHz, CD_2Cl_2, 25°C) spectra of the reported proligand and acetylacetonate complexes. In the yellow rectangle it is evidenced the signal attributed to the methoxy group bound to the N. In compound **13** this signal is not present.*

The so far only possibility to justify this result could be the presence of a strong base in the synthesis of **13**.

One equivalent of *tert*-butoxide might act as a nucleophile attacking either the imidazole nitrogen or the methoxy carbon of the positively charged cyclometalated Pt(II) complex generated before the addition of the diketonate ligand (Figure 26).

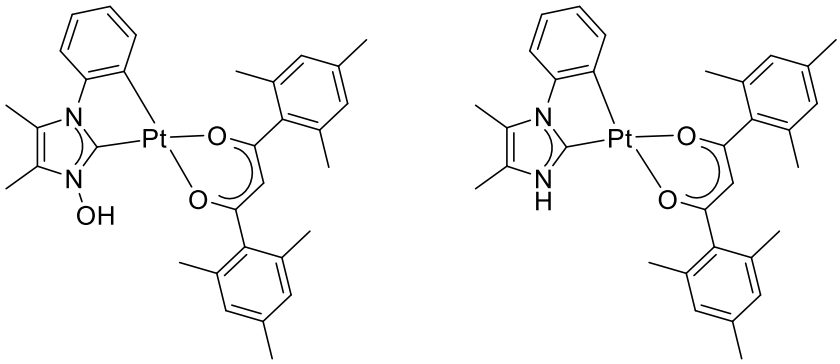

*Figure 26. Possible structure of compound **13** according to the analysis.*

Since no suitable single crystal of this compound could be grown, no proof of the assumed structure for complex **13** could be obtained. In the HRMS spectrum, the most intense m/z

peak correspond to a compound without a methoxy group, but we cannot consider this a sufficient proof for the absence of the oxygen as electron spray ionization can be particularly destructive for the N-O bond. A more reliable result could be obtained with a milder ionization method.

^{13}C NMR and 2D NMR experiments allow to assign the carbene carbon signal at the peaks between 148 and 151 ppm for all four Pt(II) complexes. The signal is down-field shifted if compared with the carbene carbon signal registered for the Pt(II) complex Pt(MPIM)(acac) (see Figure 36) reported by *Unger*[59], similar to complex **11** without the methyl groups in the backbone and with a methyl group instead of a methoxy at the imidazole nitrogen (between 125 and 147ppm): the minor resonance stabilization due to the methyl groups and the σ-withdrawing effect of the methoxy group could render electron donation towards the Pt centre less efficient.

The melting points are considerably low, between 150 and 170 °C, apart from **11** which melts at 216 °C without decomposition.[58]

Single crystals of **11** and **14** were grown by slow diffusion of isohexane in concentrated and filtered dichloromethane solution of the complexes.

X-ray diffractometry of compound **11** confirms the square planar geometry of the NOHC Pt(II) complex (Figure 27). The check-CIF generates one B-alert but the obtained data give a clear indication of the connectivity.

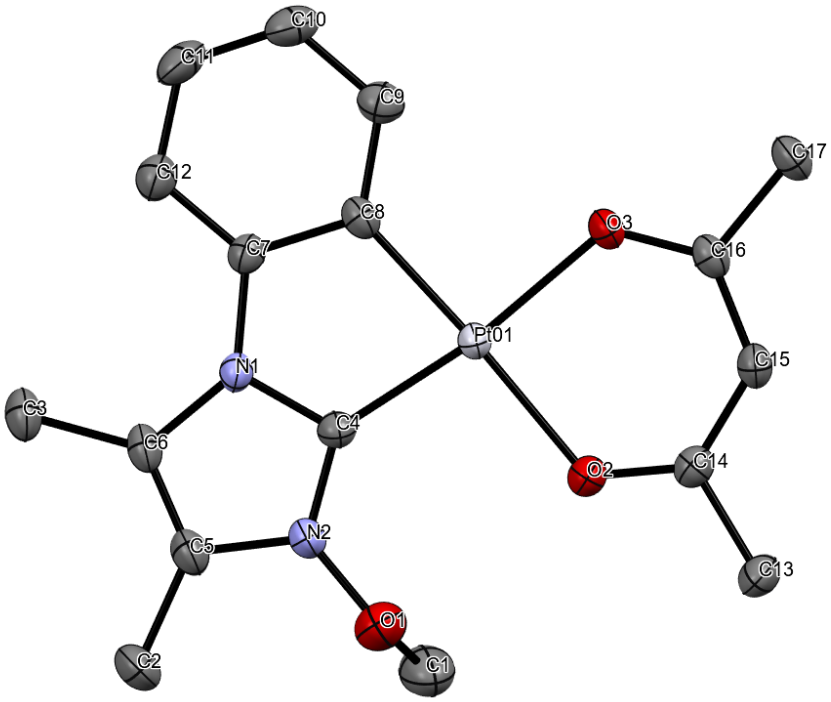

*Figure 27. ORTEP view of complex **11** (hydrogens have been omitted). Ellipsoids are drawn at their 50 % probability. Selected bond distances (Å) and angles (deg): N2-C4 1.334(5), C4-N1 1.369(6), N2-O1 1.382(6), C4-Pt01 1.941(4), C8-Pt01 1.985(5), O2-Pt01 2.081(3), O3-Pt01 2.051(3); C4-Pt01-C8 80.1(2), C4-Pt01-O2 97.0(2), C8-Pt01-O3 92.3(2), O2-Pt01-O3 90.6(1), O2-Pt01-C8 176.9(2).*

The five-membered ring is planar as confirmed by the small dihedral angle of the atoms C4-N1-C7-C8 (1.7(6)°). The C8-Pt01-C4 angle (80.1(2)°) differs from the ideal value of 90° for a square planar geometry, whereas the O2-Pt01-O3 angle (90.56(1)°) is in accordance with the anticipated angle value. Pt-$C_{carbene}$ bond length is in accordance with similar NHC Pt complexes reported in the literature, about 1.9 Å.[34,36,60,61] N2-O1 bond length of 1.38 Å is in accordance with N-O distances measured in similar NOH compounds, usually between 1.36 and 1.38 Å.[43] In general, the observed bond and angles compare well with the bond and angles of the NHC analogues without methyl groups in the backbone.[59]

The species crystallized in the $P\bar{1}$ space group with two molecules in the unit cell (Figure 28). Having the two solid state structures in the unit cell rotated by 180°, it becomes clear that the methoxy groups point away from each other and occupy the free space above and below the unit cell pair. The Pt-Pt distance is 6.988Å, hence a platinophilic interaction can be excluded.

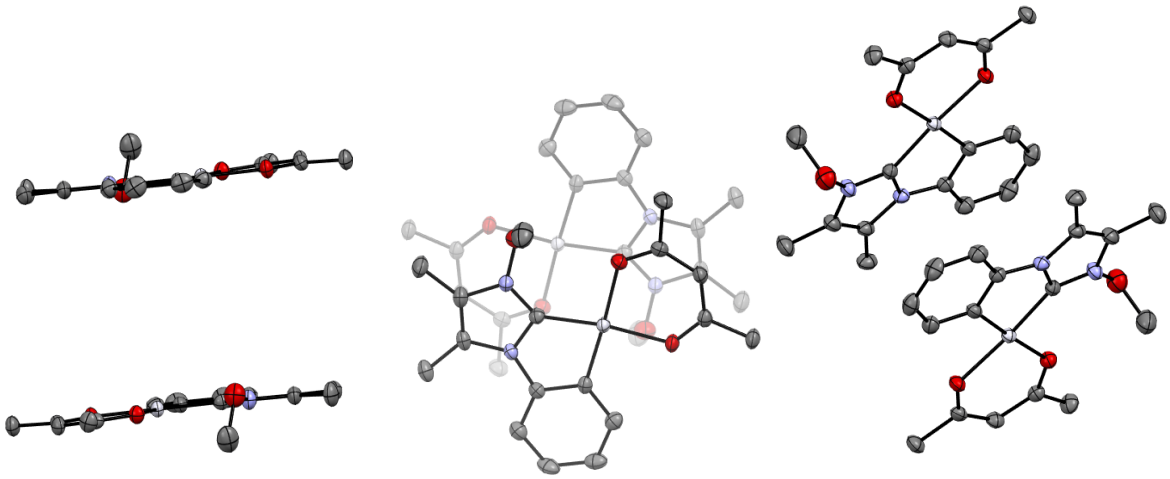

*Figure 28. ORTEP views of complex **11** crystallization cell structure (hydrogens have been omitted). Ellipsoids are drawn at their 50 % probability.*

A solid state structure of compound **14** was also obtained through X-ray diffractometry as shown in Figure 29 and Figure 30. Mesityl moieties are orthogonal to the plane defined by the β-diketonate auxiliary ligand, as the C20-C21-C22-C23 dihedral angle is 86.6(2)° and the C20-C19-C31-C38 dihedral is 57.0(3)°. The square-planar geometry is maintained, but it is more distorted as the four angles around the Pt centre diverge from 90° more than the corresponding angle in complex **11** (Figure 29).

The planarity of the central five-membered ring is confirmed by a 3.1(2)° angle between C5-N1-C6-C7.

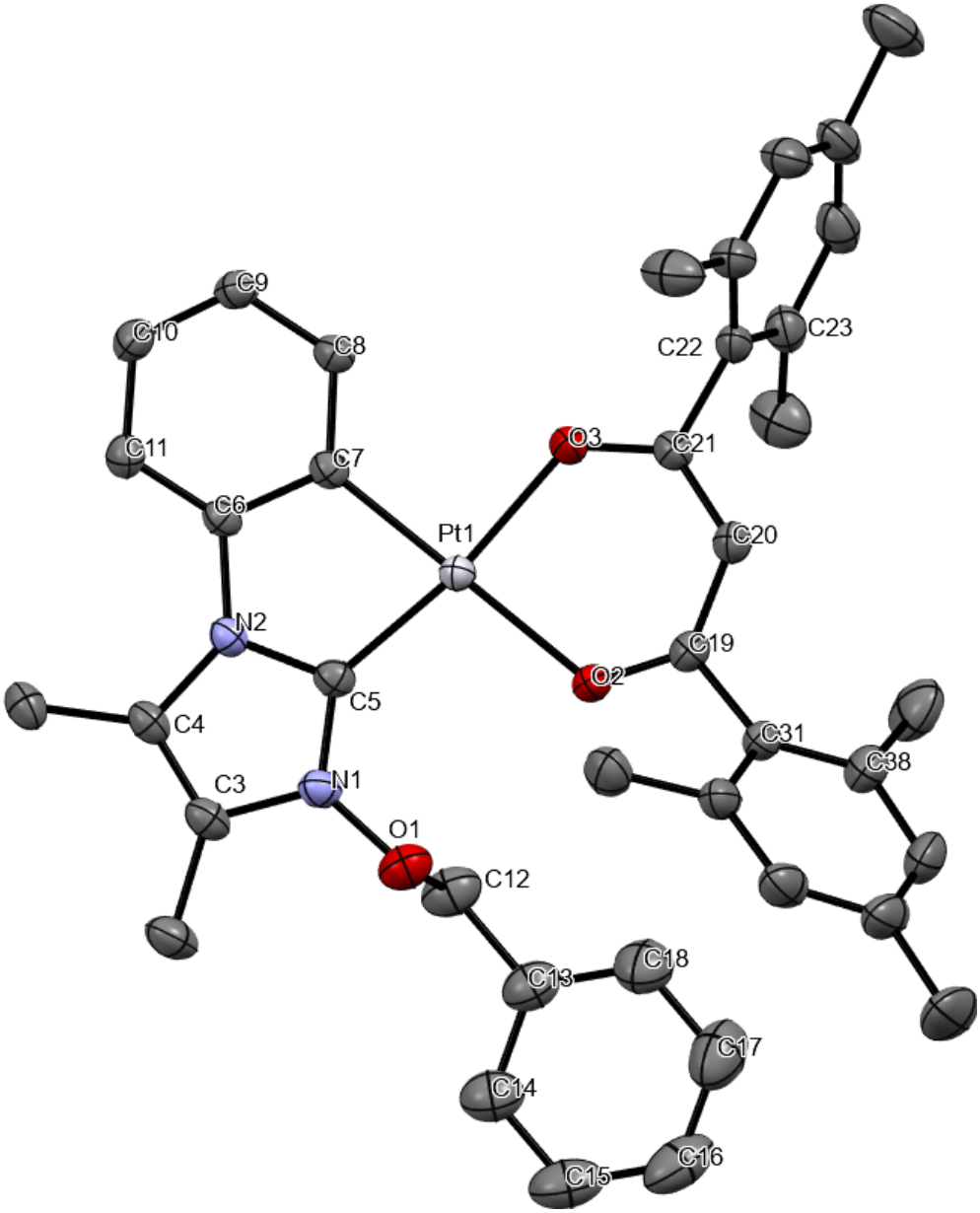

*Figure 29. ORTEP view of complex **14** (hydrogens have been omitted). Ellipsoids are drawn at their 50 % probability. Selected bond distances (Å) and angles (deg): N2-C4 1.400(3), C3-N1 1.395(2), N2-C5 1.365(2), C5-Pt1 1.942(2), C7-Pt1 1.977(2), O2-Pt1 2.102(1), O3-Pt1 2.046(2); C5-Pt1-C7 174.70(6), C5-Pt1-O2 99.57(6), C7-Pt1-O3 91.69(6), O2-Pt1-O3 89.31(6), O2-Pt1-C7 79.66(7).*

No Pt-Pt interaction is verified as the metal centres are not superimposed, hence their distance in larger than the sum of their Van der Waals radii. The crystallization is defined by a $P\bar{1}$ space group with the aromatic cyclometalated ring and the imidazolium ring stacked by a 180° on-plane rotation (Figure 30). As in the previous sample, the moiety bound to the oxygen, in this case the benzyl fragment, lays over the volume in between the two units cell molecules.

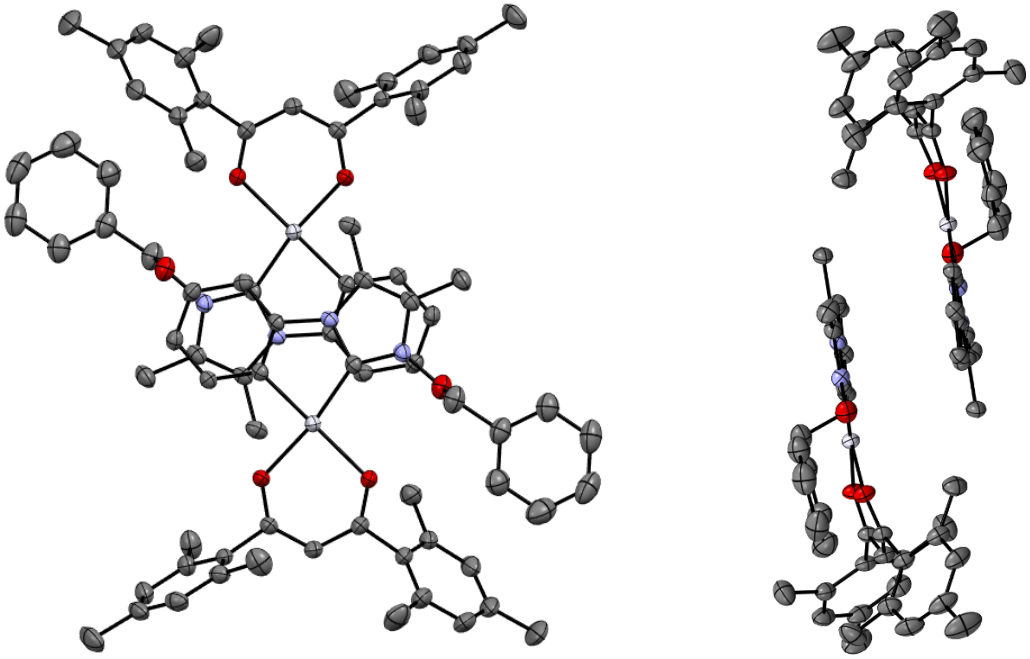

*Figure 30. ORTEP views of complex **14** crystallization cell structure (hydrogens have been omitted). Ellipsoids are drawn at their 50 % probability.*

2.2.4 Silver(I) and gold(I) complexes based on *O*-benzyl-substituted phenyl NOHCs

Monocarbene gold(I) complexes of proligand **10** was synthetized according to two different procedures already reported by *Tubaro* [18,24–26], namely the transmetalation of Ag(I) complexes and the weak base direct metalation (Scheme 16).

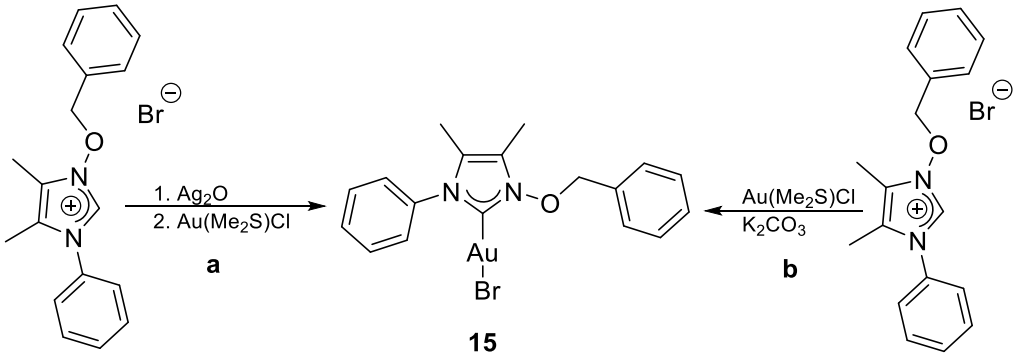

*Scheme 16. Au (I) complex obtained through transmetalation (route a) (**15a**) and via direct synthesis (route b) (**15b**).*

The two protocols used acetonitrile as a solvent and were performed under inert atmosphere (Ar). Bases were not necessary in the transmetalation protocol as Ag_2O itself acts as a base.

No ligand residues were detected in the ^{1}H NMR spectrum of both the Ag(I) and the Au(I) complexes from the transmetalation reaction. However, no crystal was obtained from this procedure.

The direct synthesis involves the use of a base to deprotonate the carbene C-atom, in this case potassium carbonate. After 48h some residual ligand was detected on the ^{1}H NMR spectrum due to the carbene proton still present. Moreover, some gold complex decomposed to a black powder during the concentration of acetonitrile in the rotary evaporator. Hence the mixture was filtrated again and stored at 4°C to promote the formation of crystals which were then analysed at the X-ray diffraction (Figure 31).

The ^{1}H and $^{13}C\{^{1}H\}$ NMR of the crystals in CD_3CN and the HRMS confirm the composition of the complex and the absence of free proligand.

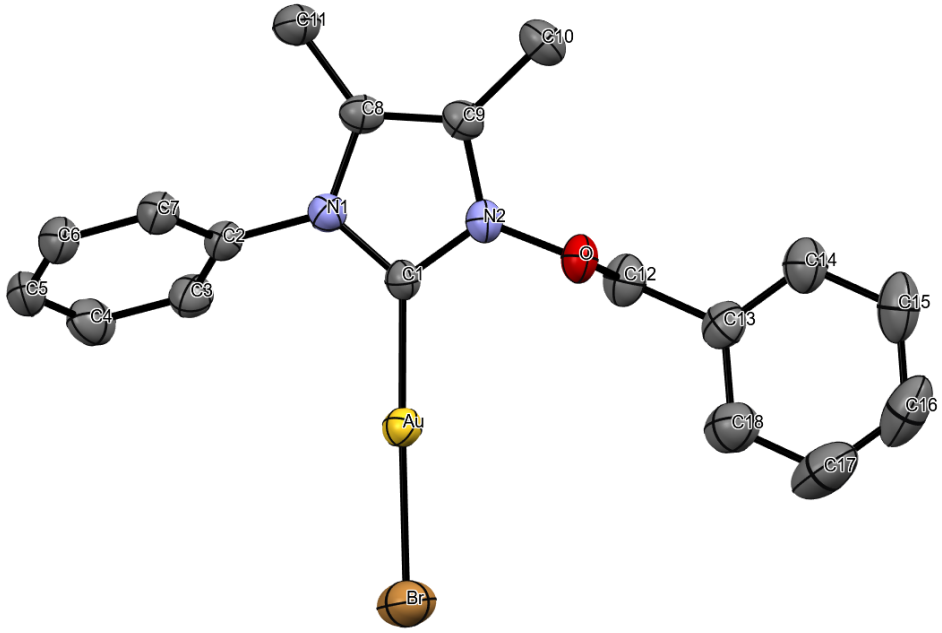

*Figure 31. ORTEP view of complex **15** (hydrogens have been omitted). Ellipsoids are drawn at their 50 % probability. Selected bond distances (Å) and angles (deg): Br-Au 2365(1), Au-C1 1.975(5), C1-N2 1.353(6), C1-N1 1.353(6), N2-O 1.382(6), N1-C2 1.345(8); Br-Au-C1 178.4(2), N2-C1-N1 102.7(4), C12-O-N2 110.9(4).*

The ligands are oriented in a linear geometry along the Au(I) centre ($C_{carbene}$-Au-Br 178.36°) and there is accordance between the Au-$C_{carbene}$ distance (1.975Å) and the values reported in the literature for this bond.

The cell has a $P2_1/n$ space group containing four molecules. Complexes are not superimposed, therefore Au(I) centres are not next to the others (Figure 32). Imidazolium rings are overlapped, but 180° rotated.

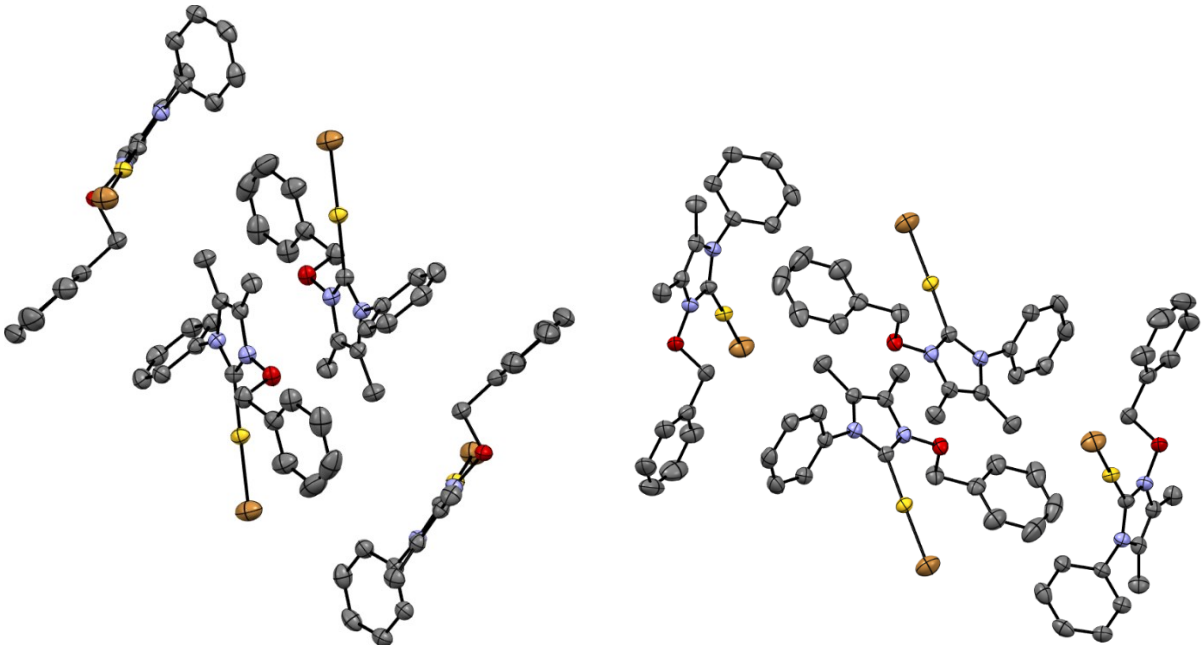

*Figure 32. ORTEP views of complex **15** crystallization cell structure (hydrogens have been omitted). Ellipsoids are drawn at their 50 % probability.*

2.2.5 Photophysical properties of the Pt(II) complexes

Photoluminescence is one of the main industrially known and applied feature of (heavy-) metals organometallic complexes and gold(I) and platinum(II) species have interesting features.[18,28]

Three spectroscopic terms give rise from the d^8 configuration of Pt(II) complexes, that when excited, can undergo three d→d transitions, namely to the A_{2g}, B_{1g} and E_g states, the order is highly dependent on the extent of the spin-orbit coupling.[62]

Hence, three absorption bands should be visible in the UV-Vis spectra of these compounds.

Cyclometalation is important in defining the properties of these compounds as structure rigidity makes it possible to better maintain the pseudo-square planar geometry in the excited state, therefore enhancing the radiative decay rate towards the ground state.

Absorption data were collected at room temperature with a $5 \cdot 10^{-5}$M dichloromethane solution (Figure 33). As expected, three bands are observable in each of the four spectra, because the metal centre is in a d^8 configuration and the spectral range is in the UV-Vis.

Referring the wavelength maxima, no significant difference in the absorption is observed when changing the hydrocarbon moiety bound to the oxygen atom at the NOHC or the diketonate auxiliary ligand (

Table *1*).

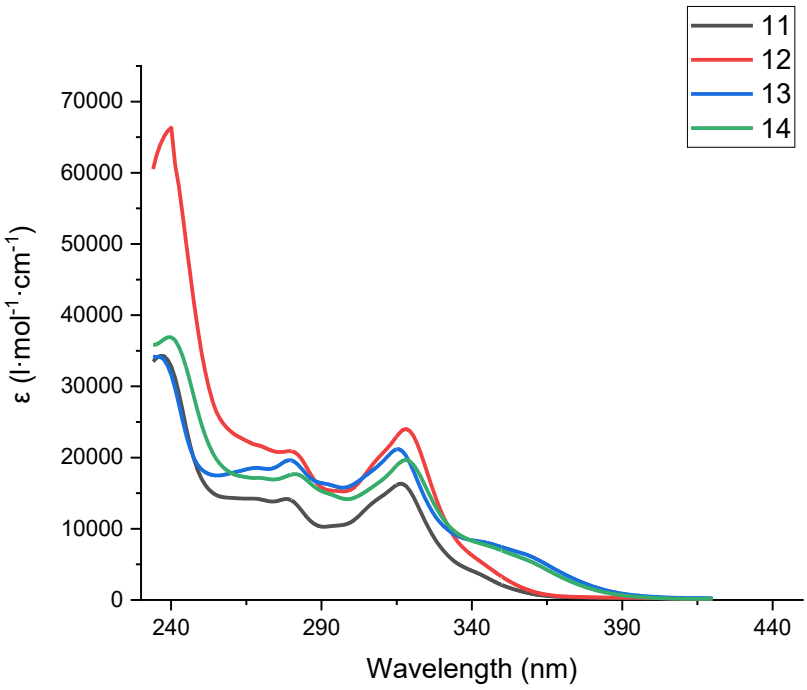

*Figure 33. Absorption spectra of compounds **11**-**14** recorded in CH_2Cl_2 solutions ($5 \cdot 10^{-5}$M) at room temperature. Cuvette length d=1 cm.*

*Table 1. The maxima wavelengths detected in the absorption spectra of compounds **11**-**14** in CH_2Cl_2 solution $5 \cdot 10^{-5}$M at room temperature.*

	Absorption wavelength (nm)		
Compound	band n.1	band n.2	band n.3
11	317	279	237
12	318	281	240
13	315	280	237
14	319	282	240

The emission spectra were recorded in a 2 wt % matrices of PMMA (0.6 µm) on a quartz glass substrate under N_2 atmosphere at room temperature (Figure 34). Compounds **13** and **14** show a significant bathochromic shift of 33-35 nm with the respect to the main emission band of the corresponding acac complexes **11** and **12**. This effect is accompanied by a massive increase in the quantum yield and a decrease of the decay time (Table 2). These latter properties make the mesacac complexes more suitable for OLED applications. Previous reports observed for

other acac and mesacac Pt(II) complexes and duryl diketonates suggest similar conclusions (*vide infra*).[36,57]

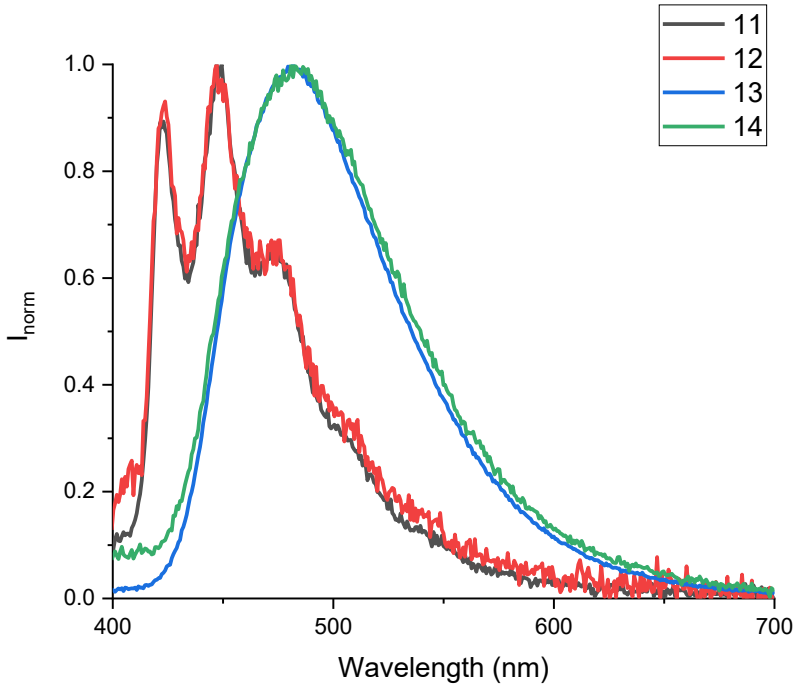

*Figure 34. Normalized emission spectra of compounds **11**-**14** in a 2 wt % emitter load in a PMMA matrix on a quartz glass substrate at room temperature (λ_{exc}= 320 nm, N_2 atmosphere).*

The profiles of the emission spectra are virtually unchanged by the alkyloxy moiety bound to the C^C* ligands, confirming that the presence of Me or Bn substituent moieties do not alter the photophysical properties of the Pt(II) complexes.

*Table 2. Photoluminescence data from emission spectra of compounds **11**-**14** in a 2 wt % emitter load in a PMMA matrix on a quartz glass substrate at room temperature (λ_{exc}= 320 nm, N_2 atmosphere).*

Compound	ϕ	λ_{em} (nm)	CIE coordinates (x,y)	τ_{exp} (μs)	τ_0 (μs)	k_r (x10^3 s^{-1})	k_{nr} (x10^3 s^{-1})
11	0.07	423; 449; 472	0.162; 0.128	2.0	28.1	35.6	473.1
12	0.04	424; 447; 475	0.169; 0.142	2.4	61.2	16.3	392.2
13	0.70	482	0.192; 0.319	1.1	1.5	659.9	282.8
14	0.17	482	0.198; 0.318	1.1	6.3	157.9	770.9

Experimental emission lifetimes τ_{exp} were determined from the decay time biexponential fit, measured in the 2 wt% doped PMMA films. The emission lifetimes τ_0 were then calculated according to Equation 2.

$$\tau_0 = \frac{\tau_{exp}}{\phi} \quad \text{[Eq. 2]}$$

τ_{exp} was calculated by a biexponential fit at the emission maximum wavelength of the decay kinetics values τ_1 and τ_2, which were chosen by the software after having obtained the a suitable fit quality, given by the χ^2 parameter (Table A 1).

k_r and k_{nr} were obtained as reported in Equation 3 and Equation 4.

$$k_r = \frac{\phi}{\tau_{exp}} \quad \text{[Eq. 3]}$$

$$k_{nr} = \frac{1-\phi}{\tau_{exp}} \quad \text{[Eq. 4]}$$

The low photoluminescence quantum yield of emission (PLQY) of acac compounds is connected to the long decay times. As previously mentioned, this should be between 1 and 2 µs to have a stable phosphorescent emitter. These lead to the conclusion that compound **13** only is suitable for this application as both τ_0 and the PLQY are not outstanding for the others. Considering that the triplet spin density of complexes **11**, **12** and **14** is mainly distributed on the auxiliary ligand and on different extent on the metal, and that in the HOMO is more localized in the C^C* ligand (Figure A 37), suggests a metal-perturbed ligand-to-ligand charge transfer (LLCT) from the acac to the C^C*.[34] The short decay time, the loss of vibronic fine structure and the higher PLQY in **13** point toward MLCT. Undesirable radiationless d-d transitions could be the cause for the lower PLQY and the larger k_{nr} of complex **14**.

CIE (*Commission internationale de l'éclairage*) colour coordinates were investigated. The compounds can be classified in the blue and green-blue region of the spectrum (Figure 35). In order to be designated as a deep blue emitter, the CIE coordinates of a compound should be below (0.150; 0.150).[34]

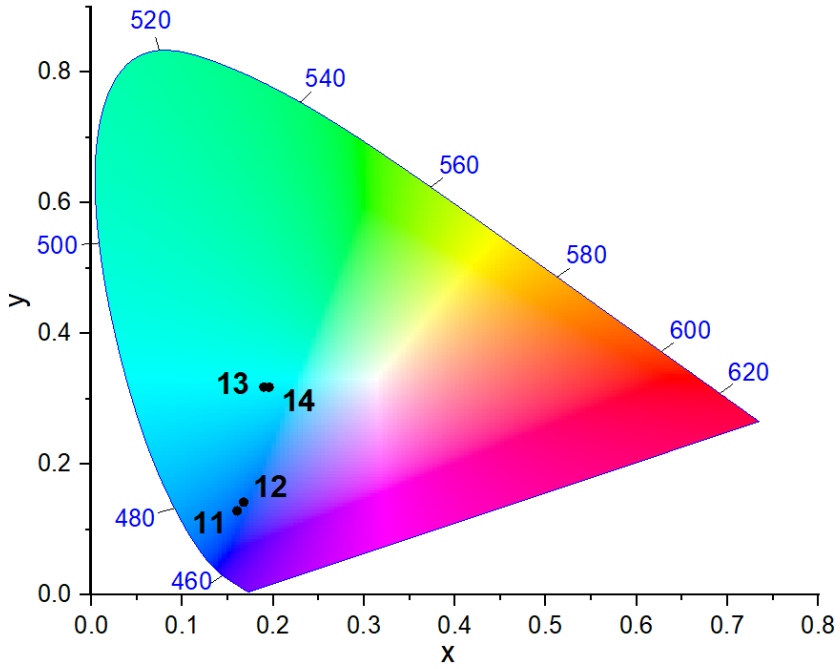

*Figure 35. CIE color coordinates of compounds **11**-**14** in a 2 wt % emitter load in a PMMA matrix at room temperature (λ_{exc}=320 nm, N_2 atmosphere).*

The rigidity of the compound is responsible for both the high PLQY and the low k_{nr}, as vibrational and rotational transitions should be disadvantaged with the respect to radiative decay to the ground state.[23] Out of plane bending is more favoured in case of a less sterically hindered β-diketonate ligand such as acetylacetonate, hence rearranging to a pseudo-square planar geometry of the ground state is more challenging.[31]

11 and the related compound synthesized by *Strassner* and *co-workers* Pt(MPIM)(acac) exhibit the same PLQY and very similar emission wavelength, highlighting that both the oxygen and the methyl groups in the backbone have a negligible effect on the emission parameters (Figure 36, Table 3).[36,60,63]

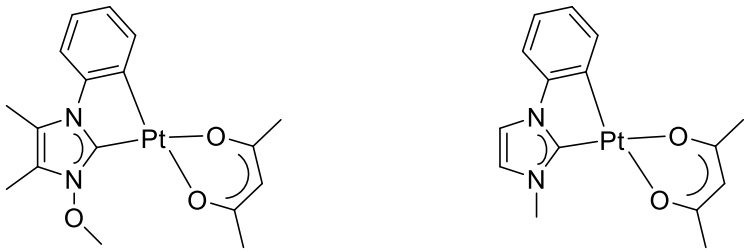

Figure 36. Structures of the compounds under comparison. Pt(MPIM)(acac) was reported by Strassner.[63]

*Table 3. Photoluminescence data of complexes **13** and Pt(MPIM)(mes) in a 2 wt % emitter load in a PMMA matrix at room temperature (λ_{exc}= 320 nm, N_2 atmosphere).*

Compound	ϕ	λ_{em} (nm)	CIE coordinates (x,y)	τ_0 (μs)
11	0.07	423; 449; 472	0.162; 0.128	28.1
Pt(MIPM)(acac)	0.07	416; 441; 464	0.190; 0.190	-

Electron donating groups in the backbone can reduce the electronic delocalization on the imidazole ring decreasing the electron donation toward the Pt centre but being the oxygen π-electron-donating the former effect can be partly or totally balanced. Although the structures are not perfectly identical, we can conclude that the addition of the oxygen does not significantly modify the photophysical parameters.

A confirm of what already stated comes from the comparison between compound **13** the mesacac Pt(II) cyclometalated complex Pt(MPIM)(mesacac) reported by *Strassner* (Figure 37, Table 4).[36]

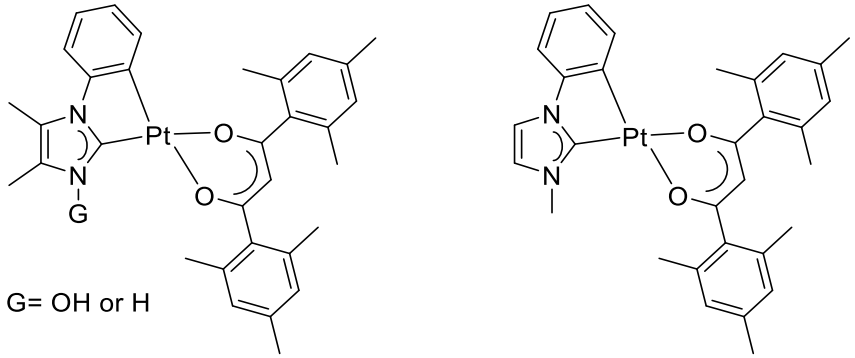

13 **Pt(MPIM)(mesacac)**

Figure 37. Structures of the compounds under comparison. Pt(MPIM)(mesacac) was reported by Strassner.[36]

*Table 4. Photoluminescence data of complexes **13** and Pt(MPIM)(mes) in a 2 wt % emitter load in a PMMA matrix at room temperature (λ_{exc}= 320 nm, N_2 atmosphere).[36]*

Compound	ϕ	λ_{em} (nm)	CIE coordinates (x;y)	τ_{exp} (μs)	τ_0 (μs)	k_r (x10^3 s^{-1})	k_{nr} (x10^3 s^{-1})
13	0.70	482	0.192; 0.319	1.1	1.5	659.9	282.8
Pt(MPIM)(mes)	0.82	482	0.196; 0.326	2.6	3.1	320.5	70.4

The fragment bound to the nitrogen and the methyl groups on C_4 and C_5 apparently do not generate any difference on the photophysical behaviour of the complexes, as the two PLQY are high, the emission wavelength is the same and the radiative decay time is considerably low for both the two compounds (Table 4). Unfortunately, the absence of a crystalline form

of compound **13** makes it impossible to judge whether the high PLQY is due to the absence of an hydrocarbon chain or due to the absence of the oxygen atom.

The red-shift of the mesacac compounds can be clearly observed in the PMMA films as the acac complexes **11** and **12** emit in a deeper blue region of the visible part of the spectra when irradiated with an ultraviolet light (365 nm, Figure 38).

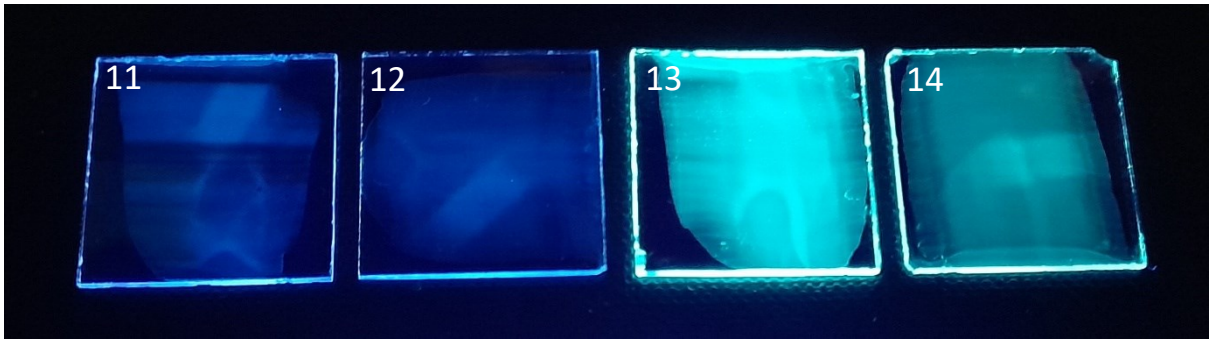

*Figure 38. 2 wt % emitters in PMMA 0.6 µm films on a quartz glass substrate irradiated with 365 nm light. Confirming the analytical results, samples of complexes **13** and **14** emitted light is red-shifted. The intensity of light emitted by **13** is noticeably higher as its PQY is 4-10 times the others.*

As a conclusion based on the observations of complexes **11**, **12** and **14**, the nature of the β-diketonate ligand is mainly responsible for the photophysical properties of the synthesized complexes. The localization of electron density in the auxiliary ligand of mesacac compounds in their triplet states results in a bathochromic shift of the emitted light. Evaluating the effects of the fragments bound to the oxygen atom of the C^C* ligand is only possible for the compounds **11**, **12** and **14** for the problems in the synthetic procedure of **13** already reported. However, even from the comparison of **13** and **14**, we can conclude that the benzyl- moiety has a negligible effect on the absorption and emission spectra profiles, but strongly influences the PLQY and the radiative decay time. These effects can be ascribed to the enhanced π-π stacking promoted by the benzyl ring, which is responsible for the shortening of the radiative lifetime, hence of a worse PLQY.[20] For cyclometalated 1-alkyl-3-phenylimidazolium diketonate Pt(II) complexes the major influence proved to be given by the substituents at the aromatic ring and the ancillary ligand rather than by the nitrogen N1 substituents.[63]

2.2.6 Electrochemistry

Cyclic voltammetry is an important analysis tool to calculate the energy of the HOMO-LUMO gap of cyclometalated Pt (II) complexes. The potentials here presented belong to the first oxidative and first reductive events derived from the DPV experiments and are referenced internally vs Fc/Fc^{+}. None of the event under consideration is reversible, and this is a typical feature of Pt(II) complexes as in their d^8 configuration a radical structural change is involved in every redox event, thus irreversibility is a usual property (Figure 39 and Figure 40).

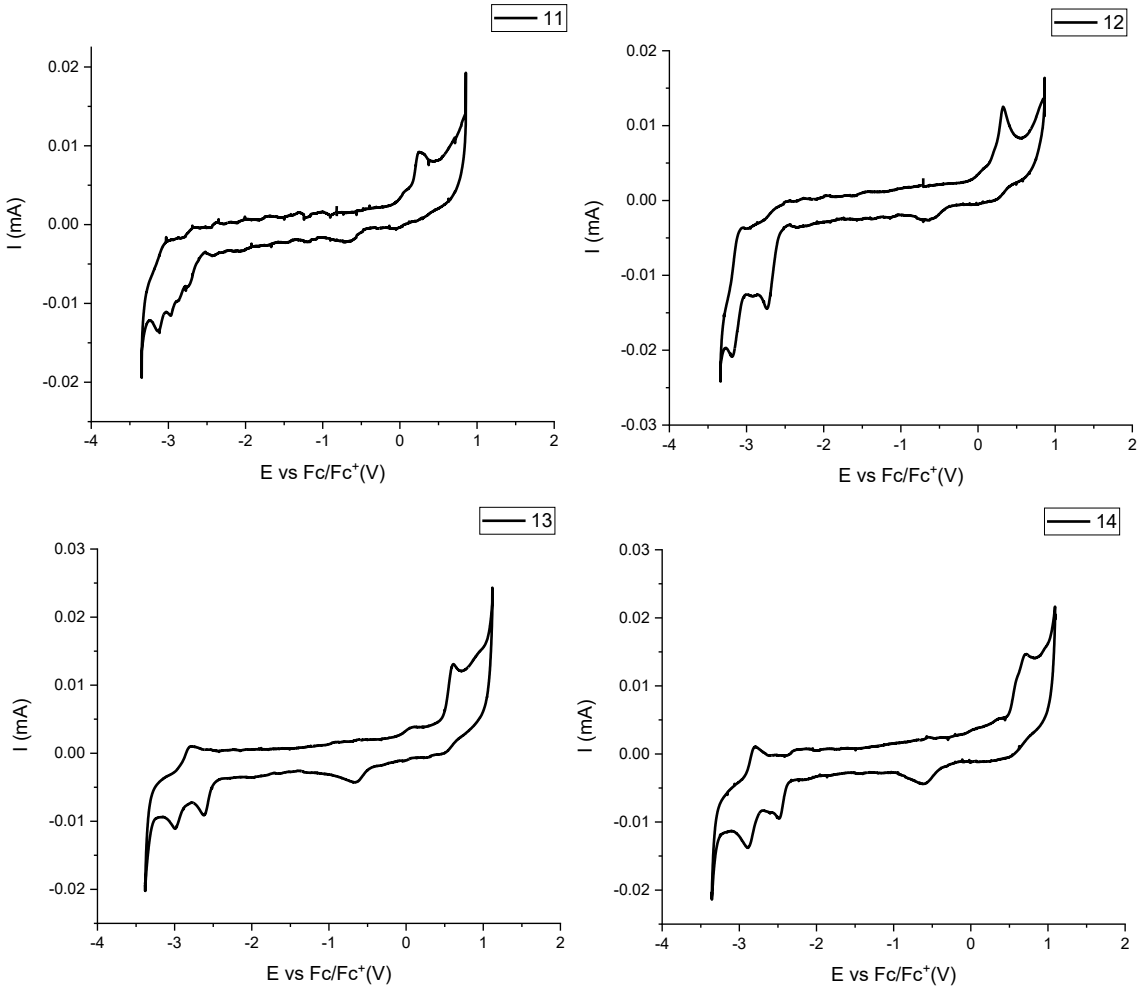

*Figure 39. Cyclic voltammograms of complexes **11-14** in dimethylformamide, referenced internally against Fc/Fc^{+}.*

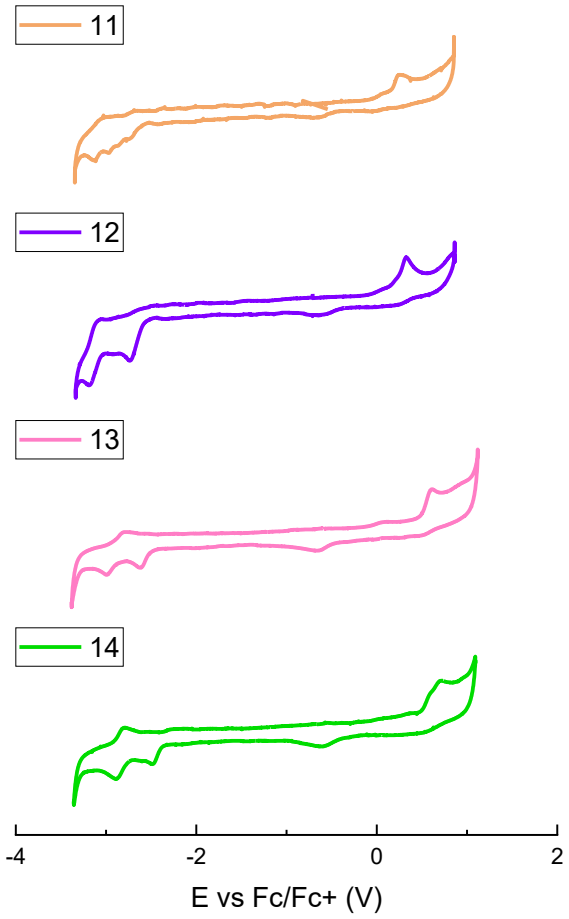

*Figure 40. Stacked cyclic voltammograms of complexes **11-14** in dimethylformamide, referenced internally against Fc/Fc^{+}.*

The potential of the LUMO levels of compounds **11** and **12** is close (ca. -1.51 V). The DFT calculations for these complexes support this result as the electron density in the LUMO level is mostly concentrated in the acac ligand, and it is almost identical for the two species (see Chapter 2.2.7). A minimal difference in the oxidation potential is highlighted between the two acac and the two mesacac complexes; which is consistent with a major concentration of electron density on the orthometalated phenyl ring evidenced by the DFT calculations.

Table 5. Redox potentials and calculated energies for HOMO, LUMO and band gap of compounds **11-14**. E_{ox} *and* E_{red} result from DPV data, referenced internally vs. Fc/Fc^{+}. E_{HOMO} [eV]= - 1.4*E_{ox} - 4.6.[64] E_{LUMO} [eV]= - 1.19*E_{red} - 4.78.[65] Eg= E_{HOMO} - E_{LUMO}.

Compound	E_{ox} (V)	E_{HOMO} (eV)	E_{red} (V)	E_{LUMO} (eV)	E_g (eV)
11	0.25	-4.95	-2.73	-1.53	3.43
12	0.32	-5.05	-2.75	-1.51	3.54
13	0.63	-5.48	-2.60	-1.69	3.80
14	0.61	-5.59	-1.86	-2.51	3.08

As displayed for similar compounds, the substitution of the acac with the mesacac ligand leads to a positive shift of both HOMO potentials.[57]

2.2.7 Quantum chemistry

As confirmation of the photophysical properties, density functional theory (DFT) calculations with PBE0 functional and 6-311G* basis set was employed to optimize the geometries of the complexes and define the energies of both ground singlet and excited triplet states, confirming true minima by the absence of negative eigenvalues in the vibrational frequencies. LANL2TZ ECP was combined with the aforementioned method in order to consider only the valence electron behaviour of the metal, reducing the calculation time and cost.[57,66]

Geometries of both ground singlet and excited triplet states have been calculated, together with the HOMO and LUMO plots of the ground state and spin density plots of the emissive triplet state.

Considering that the structure of compound **13** could not be confirmed so far, only complexes **11**, **12** and **14** have been investigated (Figure 41).

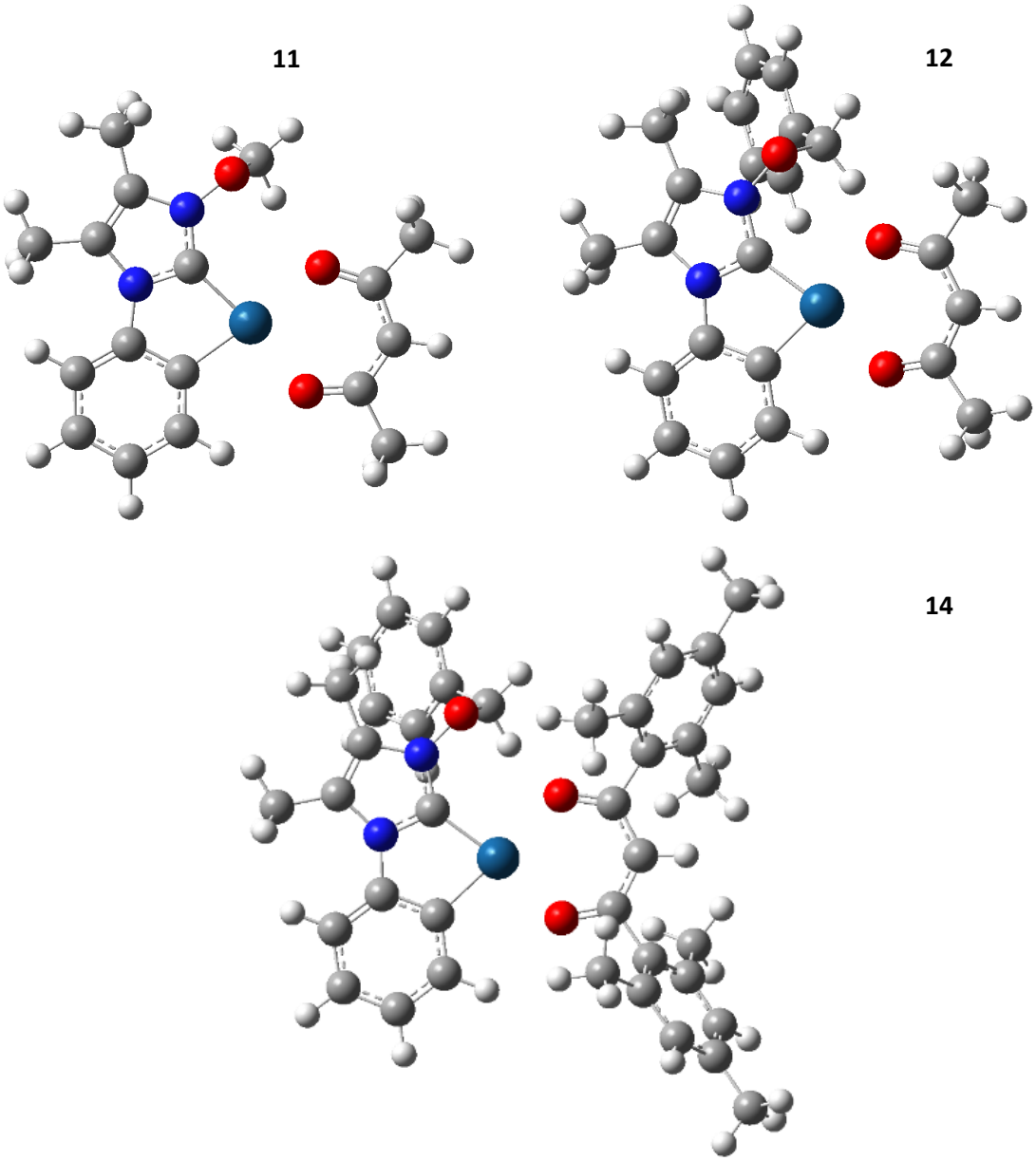

*Figure 41. Optimized geometries of complex **11**, **12** and **14** in the ground state.*

The more bent the geometry in the excited triplet state, the less efficient is the emission from the triplet state because the superimposition of the wavefunction of the triplet state with the wavefunction of the ground state becomes smaller. Therefore, the lower is the Franck-Condon integral the lower the PLQY of the compound. Acetylacetonate complexes triplet state geometries are distorted, and this factor can strongly reduce the emission.[21]

The β-diketonate ligand of compound **11** in the triplet state is bent respect to the plane defined by the platinum centre, the orthometalated ring and the oxygen atoms of the diketonate ligand. In **12**, instead, the diketonate ligand is perpendicular to the planar

geometry defined in the singlet state (Figure 42). The steric hindrance of the mesityl fragments in complex **14** allows for a reduced bending of the aromatic rings in the triplet state. All these observations can be related to the measured higher PLQY of **14** related to **11** and **12**.

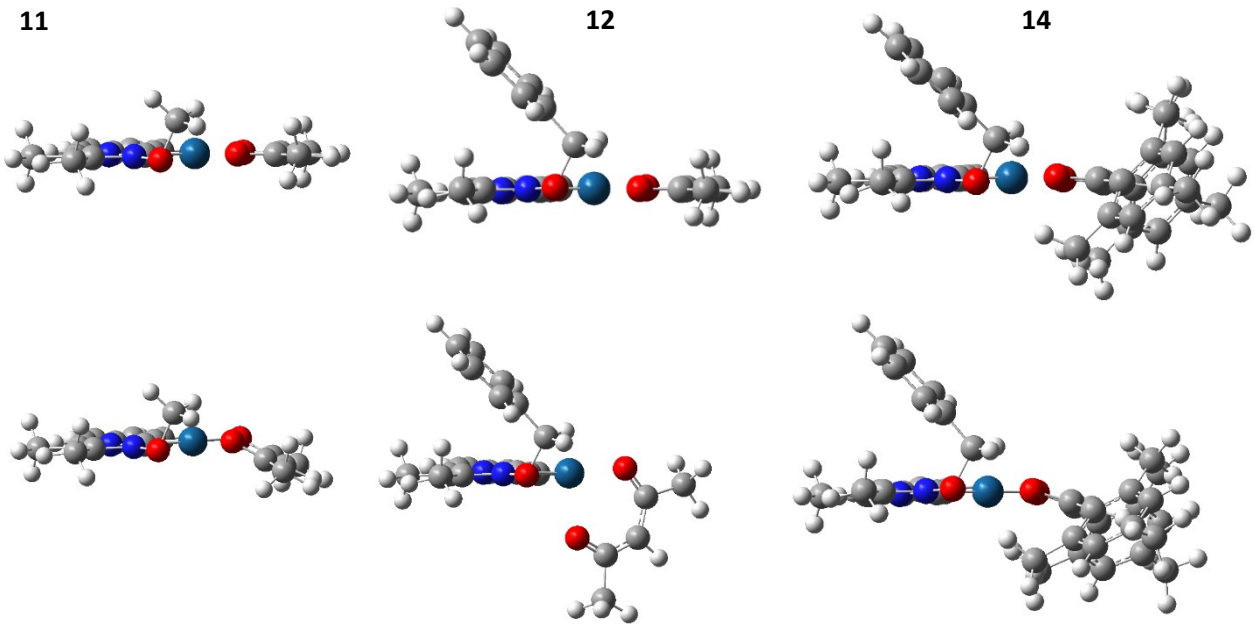

*Figure 42. Side views of the square-planar coordination of the Pt(II) centre in the ground singlet state (top) and excited triplet state (bottom) of complexes **11**, **12**, **14**.*

The localization of electron density in the triplet state (Figure 43) is prevalently centred in the β-diketonate ligand in **11**, whereas in **12** a significant contribution on the metal centre is present, thus they exhibit a LLCT emitting state, with an higher metal contribution in **12**. These observations explain the very low PLQY of complex **11** and **12** (7 and 4% respectively).

The rigidity of **14** can be responsible for its higher PLQY, as observed the triplet and singlet states geometries in Figure 42.

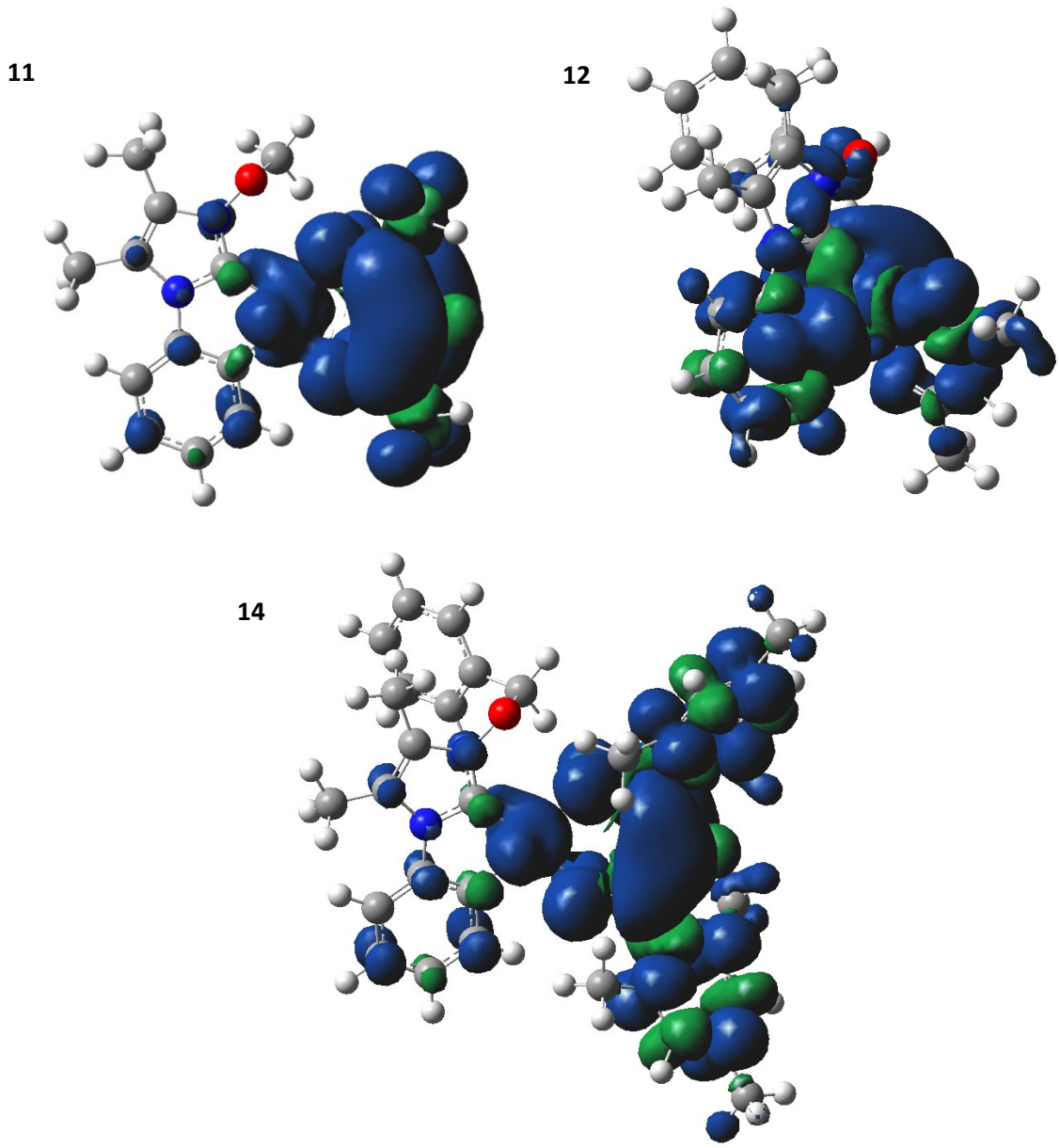

*Figure 43. Localization of the spin density in the triplet state for compounds **11**, **12** and **14** (B3LYP/6-311G*, ECP LANL2DZ, isovalue 0.04).*

A rotation of the aromatic rings of the mesacac ligand in the triplet state favours a larger π-system, hence a stronger participation of the ancillary ligand in this state. Therefore, the dihedral angle between O-C-C_{arom}-C_{arom} of the mesityl aromatic ring of **14** closer to the benzyl ring changes from 56.43° of the singlet ground state to 51.11° of the triplet. For this reason the LUMO of **14** is more strongly influenced by the β-diketonate ligand than the LUMOs of compounds with acac ligand.

Using the sum of electronic and thermal free energies at 298.15 K (25.0°C) provided by the calculation results, we estimate the energy difference between the excited triplet state and the singlet ground state, thus obtaining the approximated energy of the emission process and the wavelength of the emitted light (*Table 6*).[32]

As reported by Pinter, in case of vibronically resolved spectra such as the ones of **11** and **12**, we compared the more intense band's wavelengths.[32]

Table 6. Sum of electronic and thermal free energies (ΔG°), sum of electronic and thermal enthalpies (ΔH°), difference between triplet and singlet states free energies ($\Delta\Delta G°_{T-S}$), predicted emission wavelength ($\lambda_{em\ calc}$) and more intense experimental emission wavelength ($\lambda_{em\ exp}$) at 298.15 K. ***12_7MR*** *= compound* ***12*** *in a seven-member-ring geometry (see Figure 44).*

	Singlet		*Triplet*					
	ΔG° (kcal/mol)	ΔH° (kcal/mol)	ΔG° (kcal/mol)	ΔH° (kcal/mol)	$\Delta\Delta G°_{T-S}$ (kcal/mol)	$\Delta\Delta G°_{T-S}$ (eV)	$\lambda_{em\ calc}$ (nm)	$\lambda_{em\ exp}$ (nm)
11	-698412	-698363	-698346	-698296	66	2.85	435	449
12	-843219	-843163	-843154	-843095	65	2.81	442	447
12_7MR	-843211	-843154						
14	-1231354	-1231272	-1231294	-1231211	60	2.60	477	482

The comparison between experimental and calculated emission wavelengths confirms the validity of this method, as a difference between 5 and 14 nm is detected for the three compounds.

Compound **12** structure was analysed particularly in detail as it contains two aromatic rings, namely the phenyl and benzyloxy moieties bound to each of the nitrogen atoms, therefore during the synthesis of the complex the formation of either a five-member-ring (by metalation of the phenyl nitrogen substituent, as evidenced by experimental results) or a seven-member-ring (by metalation of the benzyloxy nitrogen substituent) is possible. Being the energy of the seven-member-ring complex **12_7MR** almost 0.4 eV higher than the 5-membered ring of **12**, the latter can be considered thermodynamically more stable (Figure 44).

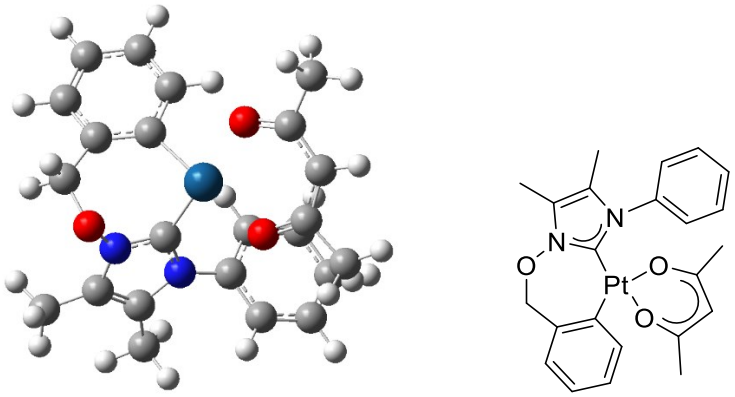

*Figure 44. Optimized geometries of complex **12_MR** in a seven-member-ring geometry in the ground state, not detected in the experimental results.*

2.3 Attempted synthesis of unsymmetrically functionalised NOHC proligands

One of the aims of the thesis is to expand the class of NOHC ligand, deriving from imidazolium rings with one or both nitrogen atoms having an oxygen atom in the sidearm, like those depicted in the following figure:

The strategies followed during this thesis to reach this goal were (Scheme 17):

i) deoxygenation of one of the two nitrogen atoms, followed by arylation of the oxygen and finally quaternization of the second nitrogen atom;

ii) stepwise functionalization of the oxygen atoms.

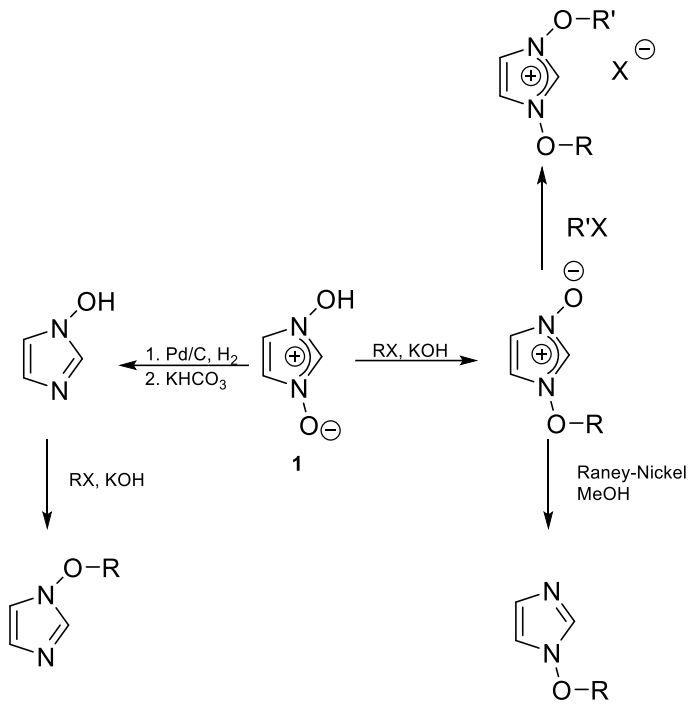

*Scheme 17. Synthetic pathways for the synthesis of unsymmetrically functionalised NOHC proligands followed in this project starting from 1-hydroxyimidazolium-3-oxide (**1**).*

2.3.1 Deoxygenation attempts

Being aware of the simple accessibility of 1-hydroxyimidazole-3-oxide (**1**), a possible approach to isolate the imidazolium with only one oxygen function is to cleave one N-O moiety afterwards. Previous literature reports involve the use of Pd/C and H_2 or Raney Nickel.[47,49] We tried both these approaches with different substrates, but none of these worked as reported in the following sections.

Pd/C and H_2

The selective deoxygenation of 1-hydroxyimidazolium-3-oxide (**1**) to 1-hydroxyimidazole (**16**) was reported in a paper of *Laus* of 1989, isolating compound **16** in 86% yield (Scheme 18).[49]

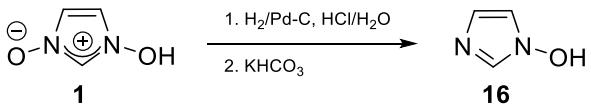

Scheme 18. Selective deoxigenation of 1-hydroxyimidazolium-3-oxide into 1-hydroxyimidazole.

They used Pd/C as a catalyst in an H_2 atmosphere and noticed a more rapid hydrogen uptake when hydrochloric acid is dissolved in the solution, with the formation of the hydrochlorides of **1**, **16** and imidazole. In our case, the reaction was followed analysing the integrals of the C_2 proton of the three compounds with time (Figure 45).

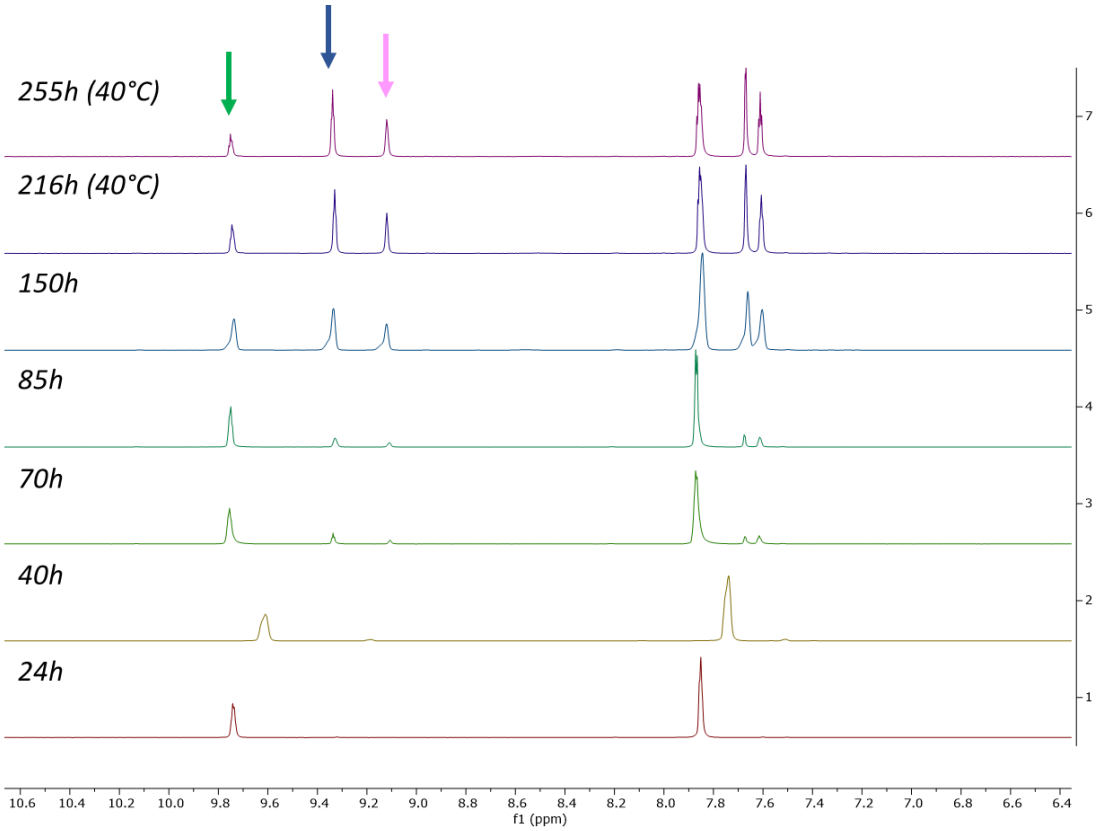

Figure 45. ^{1}H NMR (25°C, DMSO-d_6) spectra of the hydrogenation reaction under atmospheric pressure of H_2 at different times. A rough estimation of the concentration of the compounds was obtained from the C2-H peak integrals as reported by Laus et al.[49] *(vide infra Chapter 4.4.1). Assignments: 1-hydroxy-1H-imidazole-3-oxide hydrochloride (**1***HCl, green arrow) 9.67ppm; 1-hydroxy-1H-imidazole hydrochloride (**16***HCl, blue arrow) 9.29 ppm; imidazole hydrochloride (pink arrow) 9.09 ppm.*

As evident from Figure 45, we were not able to fully convert compound **1** to compound **16**, even at very long reaction times: formation of the completely deoxygenated product, namely simple imidazole, was observed. Moreover, when we tried to isolate compound **16**, following a multi-step purification procedure (crystallization in ^{i}PrOH/^{i}Pr$_2$O, basification with $KHCO_3$ and the dissolution in acetone) the desired singly-deoxygenated compound could not be obtained. To optimize the reaction process and the product yield and to minimize the quantity of imidazole, some parameters have been modified: H_2 pressure, temperature, the quantity and

the type of catalyst as well as the reaction time. Three trials were performed in an autoclave at almost 1.5 bar H_2 pressure, at 40°C (Table 7) but without a significant improvement.

Table 7. Reaction parameters of autoclave deoxygenations. The relative percentages of the compounds in hydrochloride solvent were evaluated comparing the H2 peaks integrals of ^{1}H NMR spectra using the data provided by Laus et al.[49].

Trial	T (°C)	P_0 (bar)	Time (h)	Pd/C	H_2 uptake (mmol)	**1** (%)	**16** (%)	Imidazole (%)
1	40	1.51	24	10% wt	1.2	36	42	22
2	40	1.58	24	1% wt	1.2	50	50	0
3	40	1.62	48	1% wt	2.2	20	64	15

Considering the difficulties in both the reaction parameters' control and the purification, no further trials on this synthesis were carried out.

Raney-Nickel

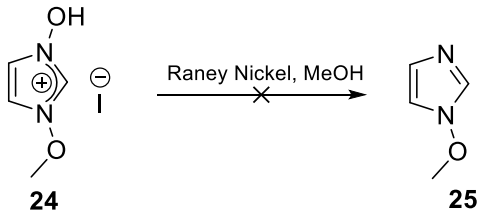

Scheme 19. Selective deoxygenation with Raney-Nickel.

The selective N-O cleavage of 1-(adamantyloxy)imidazole-3-oxides was reported by *Heimgartner* in 2019.[47] They isolated 1-(adamantyloxy)imidazole in 39% yield and similar results were obtained with C4 and C5 substituted imidazolium rings. Raney-Nickel is a stronger reducing agent than Pd/C, hence protecting one of the N-O moieties with an organic fragment proved to be sufficient.

Following the same procedure reported by the literature, we tried the selective deoxygenation of 1-methyloxy-3-hydroxy-imidazolium hexafluorophosphate in methanol with this reducing agent, but no analytically pure products were detected. ^{1}H NMR and TLC proved the final mixture had no soluble organic species nor photoactive species, respectively.

In HRMS polymerization patterns were detected which could not be attributed to a chemical structure (Figure A 29).

Begrup et al. successfully performed the N-O cleavage of 1-benzyloxy-imidazole-3-oxide into 1-benzyloxy-imidazole, using excess of phosphorous trichloride. It will be interesting to investigate this strategy in future research.

2.3.2 Additional synthesis attempts

2.3.2.1 Asymmetrically substituted 1-hydroxyimidazolium-3-oxide

The synthesis of an asymmetric imidazolium oxide species was attempted starting from the literature known 1-benzyloxyimidazolium-3-oxide (**17**, Scheme 20).[42]

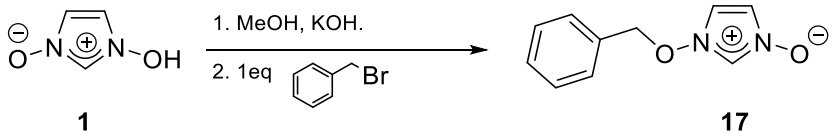

Scheme 20. Synthesis of 1-benzyloxyimidazolium-3-oxide. Yields: literature 83%, this work 81%.

Employing commercially available 2-(bromomethyl)naphthalene, the reaction was performed in dichloromethane under reflux (Scheme 21).

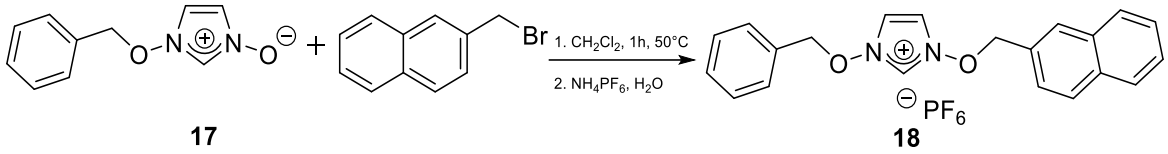

Scheme 21. Synthesis attempt of 1-Benzyloxy-3-methylnaftalenoxyimidazolim hexafluorophosphate.

Several products were detected in the ^{1}H NMR spectrum, including the disubstituted compounds **2** and **3**, the starting material **17** and probably the methylnaphtalenyloxy-monosubstituted product, identified by comparison with literature data. Hence product **18** was not isolate in a pure form.

2.3.2.2 Attempted syntheses of 1-phenyloxy-4,5-dimethylimidazole-3-oxides

The synthesis of 1-adamantyloxy-4,5-dimethylimidazole-3-oxides was reported by *Heimgartner et al.* reacting *N*-adamantyloxy imine and α-hydroxyiminoketones.[47] A similar procedure was used in order to obtain the analogous 1-phenyloxy-4,5-dimethylimidazole-3-oxide (**22**, Scheme 22).

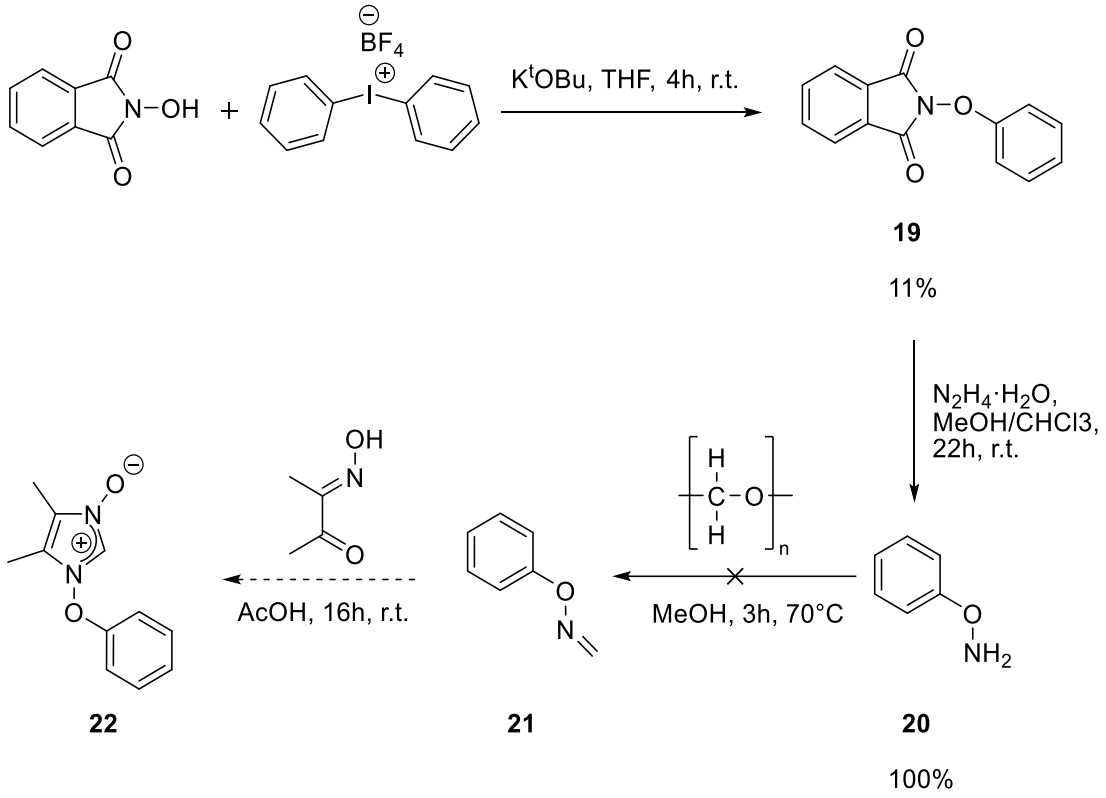

*Scheme 22. Synthetic route developed and experimentally exerted to obtain compound **22**.*

The *N*-phenoxy substituted intermediate **19** was synthesized via nucleophilic attack of deprotonated *N*-hydroxyphtalimide and diphenyliodonium tetrafluoroborate in anhydrous tetrahydrofurane.[67] Purification by column chromatography and crystallization lead to **19** with 11% yield. Treating **19** with hydrazine in a methanol/chloroform mixture produced the amine **20** without further purification in contrast to what suggested in the literature.[67] The material was dissolved in methanol and reacted with paraformaldehyde under reflux, but after the work up the product decomposed quickly (Figure A 30).[67,68]

Since *N*-phenoxy imine (**21**) is unstable, considerations lead to attempts for *in situ* formation of **21** and to add 3-(hydroxyimino)butan-2-one subsequently to in the reaction mixture, but

this pathway was abandoned in favour of nucleophilic attack on the double oxygenated NOH proligand (see Chapter 2.1.2).

2.3.2.3 Attempted syntheses of macrocyclic NOHC precursors

The nucleophilic attack toward a benzylbromide species was also exploited for two attempts in synthetizing a NOHC-bearing macrocyclic ligand. 1-hydroxyimidazole-3-oxide and α,α'-dibromometaxylene were chosen as the starting materials.

Two approaches were tested using different solvents in high dilution:

- Deprotonation of two equivalent of 1-hydroxyimidazole-3-oxide in methanol (85mM) with potassium hydroxide, as reported for a single nucleophilic attack carried out by N-O imidazolic species. Slow addition of one equivalent of α,α'-dibromometaxylene to the mixture and heating under reflux for 2h. Cooling down to room temperature and addition of the second equivalent of α,α'-dibromometaxylene (Scheme 23).

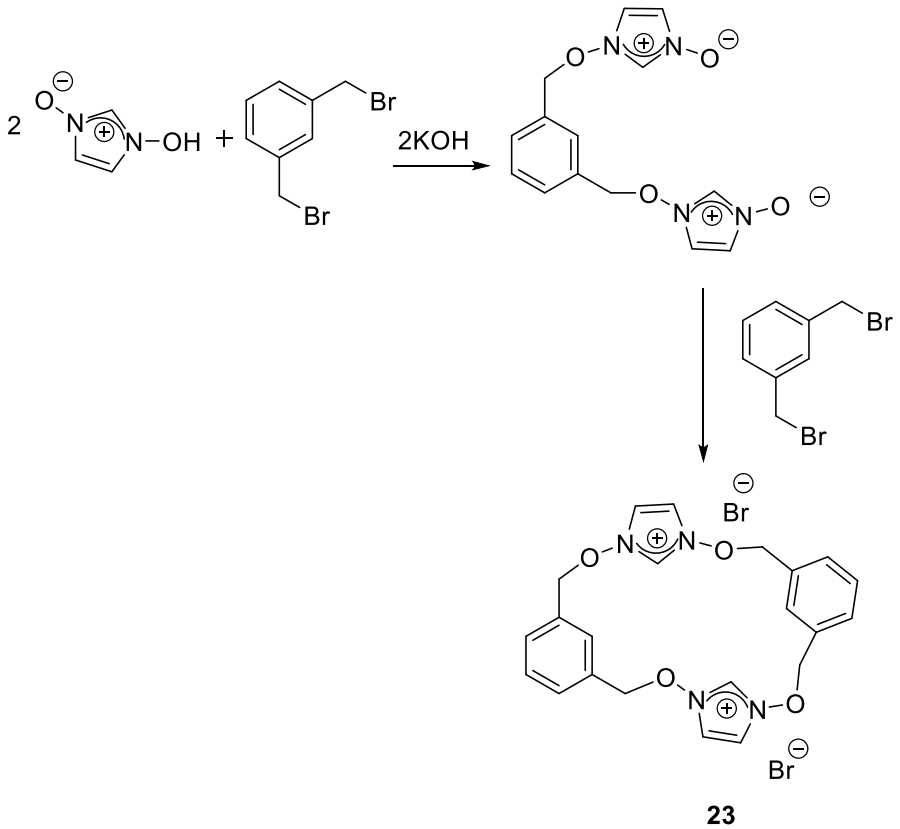

23

Scheme 23. First synthesis attempt of a macrocyclic NOH-bearing species: deprotonation with a base of the nucleophilic centre.

- Slow addition of one equivalent of α,α'-dibromometaxylene to an acetone solution (40 mM) of 1-hydroxyimidazole-3-oxide without previous deprotonation to separate the tridentate ligand (Scheme 24).

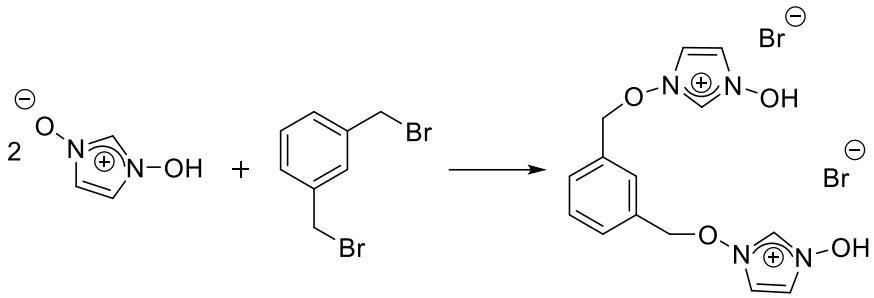

Scheme 24. Second synthesis attempt of a macrocyclic NOHC-bearing species.

None of these attempts worked, as evidenced by ^{1}H NMR spectrum and HRMS spectra where a polymerization pattern (Figure A 31) is observed.

Using a syringe pump to have an even slower addition of α,α'-dibromometaxylene or a templating agent to move the charged extremities closer or a singly-oxygenated NOH precursor can been evaluated for further trials.

Chapter 3: CONCLUSIONS

In this thesis project we focused on the synthesis of mono- and di-oxygenated imidazolium precursors starting from 1-hydroxyimidazole-3-oxide (Scheme 25) and from 1-phenylimidazole-4,5-dimethyl-3-oxide (Scheme 26). The synthesis of the proligands is not simple and it must be underlined that the substituents on the scaffold cannot be easily changed, going for example from aryl to alkyl groups. The proligands that have been successfully isolated and characterised are highlighted in Scheme 25 and Scheme 26, which summarise also all the attempted synthesis to broaden the scope of the reactions.

Starting from proligands **9** and **10**, and following synthetic procedures already reported by *Strassner et al*., the platinum(II) complexes **11**-**14** were isolated. To the best of our knowledge, they are the first Pt(II)-NOHC compounds ever reported. The structures of **11** and **14** were also solved with X-ray diffraction analysis. The structure of complex **13** was not unambiguously defined as no signals ascribable to the methyl group bound to the oxygen are present and the single crystal was not obtained; the presence of the oxygen bound to the imidazolium nitrogen is still unclear. The yields of the complexes are quite low (5 -24%) if compared with those of similar complexes with simple imidazole-based carbenes (5-44%). This further underlines the instability of this oxy-substituted compounds. It must be remarked, in fact, that they must be handled with care, since in the literature the decomposition of similar compounds when heated at 150 °C is reported.

Absorption and emission features of compound **11** compared to the analogous compound of *Strassner* without the oxygen bound to the imidazolic nitrogen, proved that this modification in the structure does not lead to a significative change in the photophysical properties. A more consistent difference is caused by exchanging the β-diketonate ligand from acetylacetonate to the mesityl derivative. As already reported, a red-shift of the emitted wavelength and a shortening of the decay time were verified in mesacac compounds **13** and **14**.

No reversible first oxidative and first reductive events were detected in the cyclic voltammograms of **11**-**14**, as expected from d^8 square-planar compounds. The HOMO-LUMO gap was calculated from these results after referencing internally against Fc/Fc^+.

Quantum chemistry calculation showed how the electronic density is spread over the frontier orbitals and in the triplet excited state, leading to considerations on which type of emission and PLQY is expected in comparison with similar compounds. Finally, the emission wavelength

is calculated through the difference in the free energy between the ground singlet and the excited triplet. The theoretical values fit well with the experimental ones.

The Au(I) complex **15** was isolated from the proligand **10** both through Ag(I) transmetalation and via direct synthesis, with good and moderate yield respectively. The yields are higher with this metal centre compared to the platinum ones, probably because of milder reaction conditions. The structure of complex **15** has been solved with XRD as well and shows the typical linear coordination of gold(I) centres.

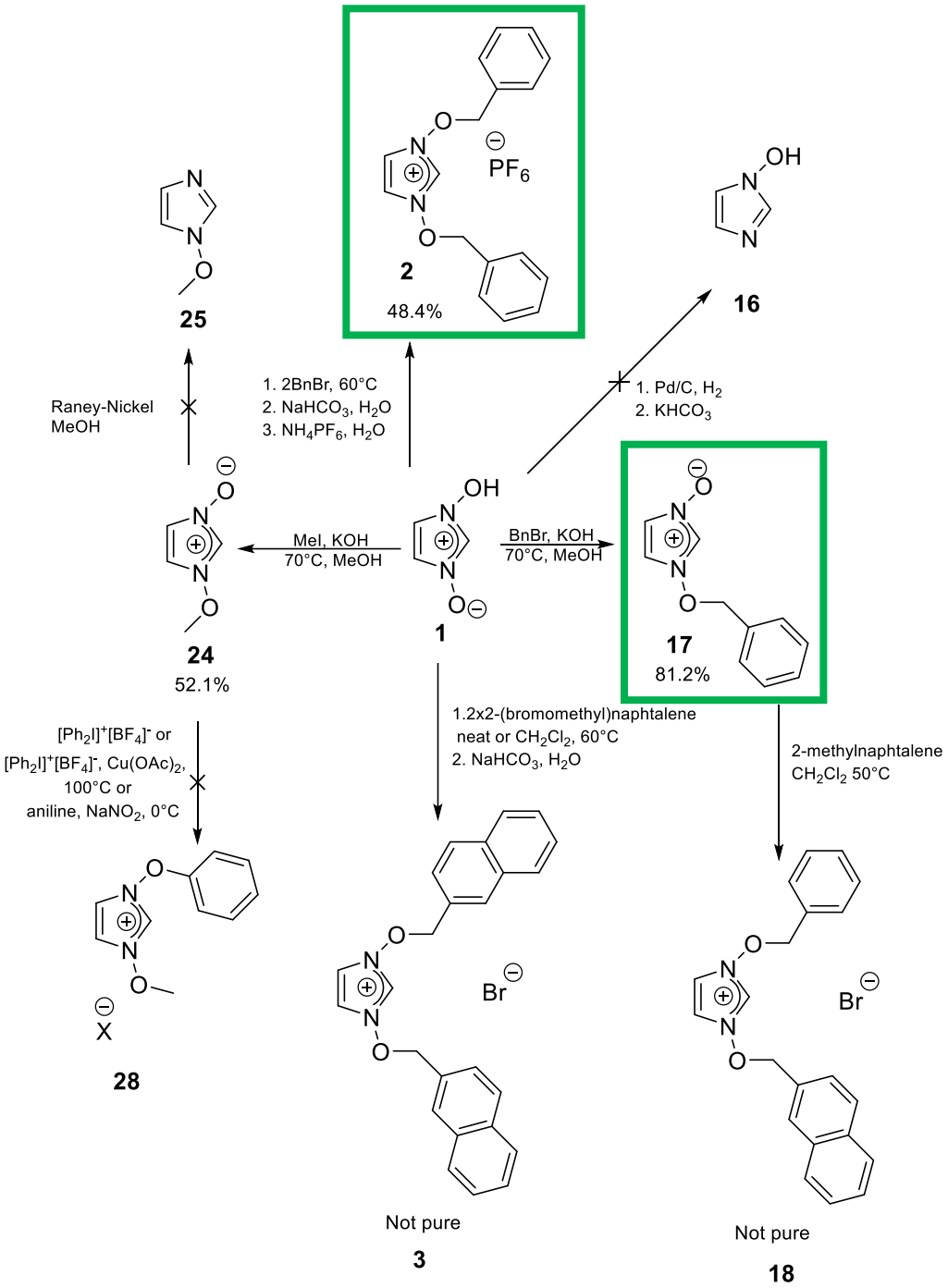

Scheme 25. Summary of synthesized species starting from 1-hydroxyimidazole-3-oxide. In a green rectangle the species obtained in a pure form.

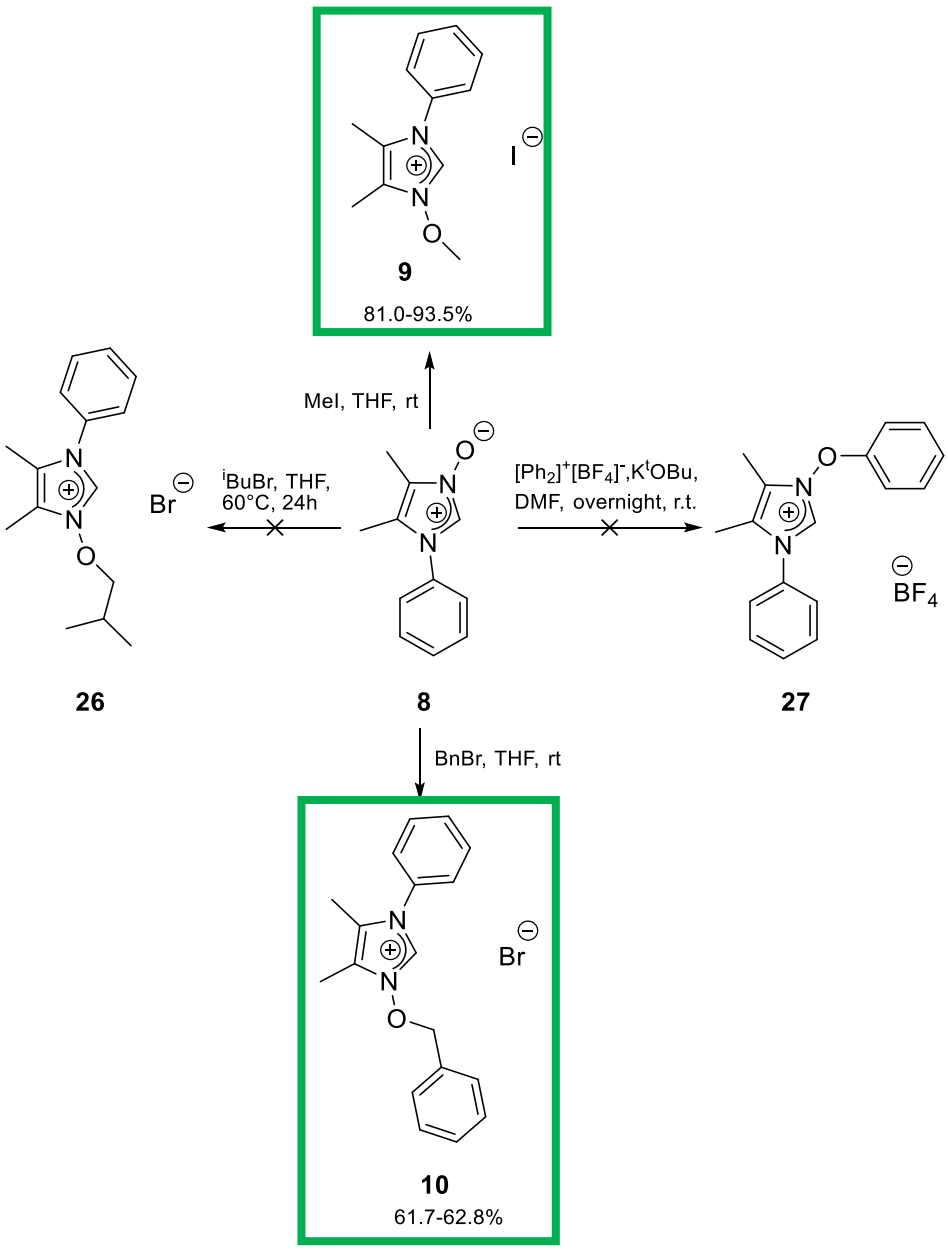

Scheme 26. Summary of synthesized species starting from 1-phenylimidazole-4,5-dimethyl-3-oxide. In a green rectangle the species obtained in a pure form.

Chapter 4: EXPERIMENTAL SECTION

4.1 Materials and methods

The reactions in this work were performed with Schlenk techniques under Ar inert atmosphere (99.999%). Dimethylformamide (DMF) was dried over activated molecular sieves (3 Å) and degassed by freeze-pump-thaw cycles. Dichloromethane, isohexane, ethyl acetate and tetrahydrofuran were distilled before use; other solvents were used without further purifications. Column chromatography was carried out using silica gel 60 (230–400 mesh). Chemicals were obtained from suppliers and were used without further purification.

NMR spectra were recorded on a Bruker Avance 300 MHz (300.1 MHz for ^{1}H, 75.5 MHz for ^{13}C, 282.2 MHz for ^{19}F, 121.5 MHz for ^{31}P and) spectrometer or on Avance 300P and Avance III 600 Bruker (600 MHz for ^{1}H, 150 MHz for ^{13}C and 129 MHz for ^{195}Pt) spectrometers. All the spectra have been recorded at 298 K. The chemical shift values (δ) are reported in units of ppm relative to the residual of the deuterated solvent; the ^{195}Pt NMR spectra were referenced externally by using K_2PtCl_4 in D_2O (δ =−1617.2 ppm in D_2O for $PtCl_4^{2-}$) and the ^{31}P spectra were referenced externally against triphenyl phosphate in acetone-d_6 (−17.9 ppm vs. H_3PO_4). All the coupling constants (*J)* are reported in Hertz. The multiplicities of the signals are reported using these abbreviations: singlet (s), doublet (d), triplet (t), multiplet (m) and broad (br).

The following experiments have been carried out: ^{1}H-NMR, $^{13}C\{^{1}H\}$-NMR, $^{31}P\{^{1}H\}$-NMR, $^{19}F\{^{1}H\}$-NMR, $^{195}Pt\{^{1}H\}$-NMR, HMQC (*H*eteonuclear *M*ultiple *Q*uantum *C*oherence), HMBC (*H*eteronuclear *M*ultiple *B*ond *C*oherence) and NOESY (*N*uclear *O*verhauser *E*nhancement *S*pectroscopY).

Elemental analyses were performed with a FlashSmart Elemental Anlyzer EA IsoLink or with a Thermo Scientific FLASH 2000 apparatus.

HRMS measurements were carried out with a Q-Exactive hybrid quadrupole-Orbitrapt mass spectrometer (Thermo Fisher Scientific, Waltham, Massachusetts, USA). MS conditions were as followed: electrospray ionization in positive mode, resolution 70 000, AGC target 1 x 10^6, max injection time of 50 ms, scan range 150–2000 amu, capillary voltage 3.5 kV and RF voltage at 50 V, capillary temperature 320°C and probe temperature 350°C; nitrogen was used as shealth gas at 11 psi. Calibration was performed with a standard solution purchased by Thermo Fisher Scientific (Pierces ESI positive Ion Calibration Solution). The software for

analysis of MS data was Xcalibur 3.1 (Thermo Fisher Scientific). Otherwise, HR-ESI mass spectra were recorded on a Waters Xevo G2-XS QTOF mass spectrometer.

EI mass spectra were recorded by GC-MS coupling on an Agilent Technologies 6890N GC system equipped with a 5973 N mass-selective detector (70 eV) detecting positive and negative ions.

Hydrogenation trials with Pd/C and H_2 were performed in a Büchi miniclave steel (up to 10 bar, 300 ml) in borosilicate glass 3.3, stainless steel, Hastelloy®, PTFE.

Absorption spectra were measured on a Perkin Elmer Lambda 365 UV-vis spectrometer in dichloromethane $5x10^{-5}$ M solutions, with a quartz cuvette (cell length of 1 cm). The spectra were recorded with a scan speed of 600 nm/min.

The emission spectra were measured with a Hamamatsu Quantaurus Quantum Yield Spectrometer C11347-01. The samples were prepared by doctor blading a solution with the respective concentration of emitter in a 10 wt% PMMA solution in dichloromethane on a quartz substrate with a 60 µm doctor blade. The film was dried under nitrogen flow, and the emission was measured under nitrogen at room temperature.

The phosphorescence decay was measured with an Edinburgh Instruments mini-τ by excitation with pulses of an EPLED (360 nm, 20 kHz) and time-resolved photon counting (TCSPC).

Melting points were measured by a Wagner and Munz PolyTherm A system and were not corrected.

Cyclic voltammetry and differential scanning voltammetry experiments were carried out using a Biologic SP-150 potentiostat in degassed, anhydrous DMF 0.5 mM solutions with 0.1M supporting electrolyte ($N(^nBu)_4ClO_4$), employing a platinum wire counter electrode, a glassy carbon working electrode and a Ag/Ag^+ pseudo reference electrode. The measurements were conducted with a sweep rate of 100 mV/s and internally referenced against Fc/Fc^+, whereas the DPV measurements were carried out with a sweep rate of 50 mV/s.

The Gaussian16[69] package was used for all quantum chemical calculations employing the hybrid functional PBE0[70,71] and the 6-311G*[72–74] basis set. Platinum was described through the LANL2TZ ECP and basis set[75–78]. Dispersion forces were employed by using the D3 dispersion correction with Becke-Johnson damping (D3BJ).[79,80] All given structures were verified as true minima by vibrational frequency analysis and the absence of negative eigenvalues. Calculated geometries were visualized with GaussView.[81]

4.2 Silver(I) and gold(I) complexes with symmetrically substituted *N*-Oxy heterocyclic carbene ligands

Dichloro(1,5-cyclooctadiene)platinum(II) [Pt(COD)Cl_2]

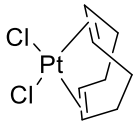

In a 500 mL single-necked round bottom flask open to air, potassium tetrachloroplatinate(II) (4.98 g, 12 mmol) was stirred in a mixture of water/glacial acetic acid (4:5, 180 ml) at 50°C. 1,5-cyclooctadiene (3.96 g, 36.6 mmol) was added dropwise with a syringe and the mixture was heated at 110°C under reflux conditions. After having cooled down to room temperature, the mixture was concentrated at the rotary evaporator to about 1/3 of its volume and kept overnight in the fridge. The precipitated was filtered and washed twice with distilled water (3x5 ml), ethanol (3x5 ml) and diethyl ether (20 ml). The solid was further crystallized, dissolving the sample in CH_2Cl_2 and adding isohexane as precipitation solvent. The beige solid was filtrated and washed with diethyl ether. Yield: 2.81 g, 7.5mmol, 62.1%.

EA: Calcd for $C_{11}H_{12}N_2O$ (188.09 g mol^{-1}): C, 25.68; H, 3.23%. Found: C, 26.17; H, 3.25.%

4.2.1 Preparation of 1-hydroxyimidazolium-3-oxide[48]

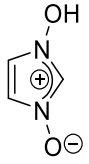

1

Glyoxal (7.6 ml, 66.5 mmol 40% aqueous solution), formaldehyde (6.0 ml, 80.6 mmol, 37% in water and methanol solution) and methanol (15 ml) were stirred in a 200 ml three-necked round bottom flask at 0°C. A saturated aqueous solution of hydroxylammonium chloride (9.28 g, 133.5 mmol in 12.2 ml) and hydrochloric acid (37% w/w, 1.33 ml, 44 mmol) were added to the solution while stirring. Stirring was continued for 2h at 0°C and for 22h at 20°C. The pH was adjusted to 4.5 (pH meter) adding slowly sodium hydroxide (about 20 ml, 33%

aqueous solution) avoiding exceeding 15°C. The white powdery solid was washed with cold water (20 ml, 0°C), methanol (10 ml, 0°C) and diethyl ether (20 ml) and dried under vacuum. Yield: 5.10 g, 50.9 mmol, 77.0%.

^{1}H NMR (300 MHz, D_2O): δ (ppm) = 7.02 (d, J=2Hz, 2H), 8.23 (t, J=2Hz, 1H).
^{1}H NMR (300 MHz, DMSO-d_6): δ (ppm) = 7.20 (d, J=2Hz, 2H), 8.50 (t, J=2Hz, 1H).

The NMR characterisation of the product coincides with that reported in the literature.[48]

4.2.2 Preparation of 1,3-disubstitutedoxyimidazolium hexafluorophosphate

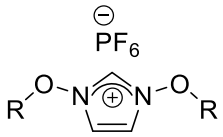

2 R=benzyl
3 R=methylnaphtalenyl

2.

1-hydroxylimidazole-3-oxide (0.50 g, 5.1 mmol) was stirred in a 100 ml two-necked round bottom flask for 2h at 60°C (oil bath) with benzyl bromide (0.12 ml, 9.9 mmol). 1-hydroxylimidazole-3-oxide dissolved in a few minutes after the beginning of the heating.
The mixture was initially white, later yellowish and at the end brown. It was then stirred for 3h at room temperature. Sodium hydrogencarbonate (0.43 g, 5.1 mmol) and water (2 ml) were added and the mixture was stirred for 17 h at room temperature. The yellow-brown oil was separated from the aqueous layer with a separating funnel. The product was washed with H_2O (5ml) and Et_2O (5ml) and dissolved in CH_2Cl_2 (10 ml). The organic phase was dried over magnesium sulphate it was dried under vacuum. A yellow-brown wax was obtained.
1,3-di(benzyloxyl)-imidazolium bromide (1.84 g, 5.1 mmol) was stirred with water (10 ml) in a 100 ml two-necked round bottom flask for 3h. The dense oil was not miscible in water and drops were dispersed in the solvent. A solution of NH_4PF_6 (0.85 g, 5.2 mmol) in water (3.5 ml) was added slowly to the mixture and a white precipitate formed as soon as the solution of

NH_4PF_6 was added. The solution was stirred for three days. The white powdery solid was filtered under vacuum and washed with water (25 ml). Yield: 1.03 g, 2.42 mmol, 48.4%.

^{1}H NMR (300 MHz, DMSO-d_6): δ (ppm) = 5.42 (s, CH2, 4H), 7.43 (m, H_{arom}, 10H), 8.13 (d, J=2 Hz, H4 and H5 imidazole, 2H), 10.12 (t, J=2 Hz, H2 imidazole, 1H). The NMR characterisation of the product coincides with that reported in the literature.
EA: Calcd for $C_{17}H_{17}N_2O_2\,PF_6$ (426.29 g mol^{-1}): C, 47.00; H, 4.02; N, 6.57%. Found: C, 44.85; H, 4.07; N, 6.03%.

3.

Neat conditions. 1-hydroxyimidazole-3-oxide (0.50 g, 5.1 mmol) was mixed with 2-bromo(methyl)naphthalene (2.2 g, 10 mmol) in a glove box because of the toxicity of the latter compound. The two solids were stirred in a 100 ml two-necked round bottom flask for 2h at 60°C to melt the 2-bromo(methyl)naphthalene. The white mixture was then stirred for 3h at room temperature.
Sodium hydrogencarbonate (0.42 g, 5.0 mmol) and water (8 ml) were added, and the mixture was stirred for 3 days at room temperature. The water-immiscible wax was filtered, washed with water (10 ml), Et_2O (10 ml) and dissolved in CH_2Cl_2 (10 ml). The solvent was evaporated in vacuo and a greyish solid was obtained. The solid was stirred in water and a solution of NH_4PF_6 (0.82g, 5mmol) in water (3.5ml) was slowly added. The stirring was continued for 30 minutes and the formed pale pink solid was filtered in a sintered glass filter and washed with water (2x10 ml). The ^{1}H NMR of the product present two set of signals (this is particularly evident in the CH_2 benzylic region) attributed to the monosubstituted OR and the bis-functionalized compounds in 3:5 ratio. Some solubilities trials in deuterated solvents were performed:

- D_2O: no dissolved species.
- CD_3CN: no precipitate is present, everything is dissolved.
- $CDCl_3$: a white precipitate is visible.

The solid and liquid phases of the $CHCl_3$ mixture were separated and dissolved in DMSO-d_6. In the solid phase a lower amount of monosubstituted product was present as it can be seen by the relative intensities of the CH_2 benzyl peaks of the di- and monosubstituted at 5.59 and

4.86 ppm in the DMSO spectra, respectively. Differential solubility was not satisfactory to separate the compounds.

^{1}H NMR (300 MHz, DMSO-d6): δ (ppm) = 5.59 (s, benzylic CH_2, 4H), 7.42-7.63 (m, 13H), 7.76-8.04 (m, 16H), 8.13 (s, 2H), 10.22 (t, H2, 1H).
EA: Calcd for $C_{25}H_{21}N_2O_2PF_6$ (526.41 g mol^{-1}): C, 57.04; H, 4.02; N, 5.32%. Found: C, 51.43; H, 3.80; N, 3.23%.
HRMS (ESI): (m/z) 382.1632 ([M+H]$^+$), 381.1601 (M$^+$).

In CH_2Cl_2. 1-hydroxylimidazole-3-oxide (0.26 g, 2.6 mmol) was mixed with 2-bromo(methyl)naphthalene (1.1 g, 5.0 mmol) in CH_2Cl_2 (4 ml) in the glove box. The mixture was stirred in a 100 ml two-necked round bottom flask for 2h at 30°C and then for 3h at room temperature. The mixture was pale yellow and after the solvent was evaporated under vacuum a brown wax was obtained. Sodium hydrogencarbonate (0.22 g, 2.6 mmol) and water (10 ml) were added and the mixture was stirred for 3 days at room temperature.
The product was washed with water, ethanol, diethyl ether and dried in the Schlenk line.
No significative difference between this batch and the former was detected at the ^{1}H NMR spectra: both the mono- and the disubstituted species were present.

4.2.3 General procedure for the synthesis of metal complexes 4-7

Silver (I) complexes 4 and 6

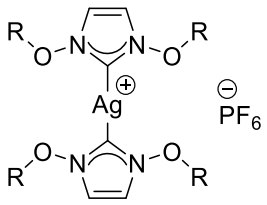

4 R=benzyl
6 R=2-methylnaphtalenyl

1,3-disubstituted-oxyimidazolium hexafluorophosphate (1 mmol) was stirred with Ag_2O (0.1336 g, 0.58 mmol) in methanol (10 ml) in a 100 ml three-necked round bottom flask for 24 h. The glass flask was covered with aluminium foil to prevent the photodecomposition of

the Ag complex. A beige solid was filtrated and washed with methanol. It was stored under inert atmosphere (Ar) overnight before the transmetalation toward the more stable Au complex.

4.

Yield: 285.4 mg (0.32 mmol, 68.1%)

^{1}H NMR (300 MHz, DMSO-d6): δ (ppm) = 5.26 (s, CH_2, 4H), 7.32 (s, H_{arom}, 10H), 7.75 (s, H4 and H5, 2H).
$^{13}C\{^{1}H\}$-NMR (75 MHz, $CDCl_3$): δ (ppm) = 81.6 (CH_2); 117.1, 128.5, 129.4, 129.8, 132.8 (C_{arom}, CH_{arom}, C_i) The carbene signal was not detected.

6.

Yield first batch: 228 mg, 225 mmol, 45%. Yield second batch: 562 mg, 0.55 mmol, 37%.

^{1}H NMR (300 MHz, DMSO-d6): δ (ppm) = 5.26 (s, CH_2, 4H), 7.31-7.56 (m, H_{arom}, 7H), 7.60-7.94 (m, H_{arom} and H4 and H5, 11H).
$^{13}C\{^{1}H\}$-NMR (75.475 MHz, $CDCl_3$): δ (ppm) = 81.8 (CH_2); 117.1, 126.3, 126.7, 127.4, 127.8, 128.3, 129.2, 130.4, 132.3, 132.9 (C_{arom}, CH_{arom}, C_i). The carbene signal was not detected.

Gold (I) complexes 5 and 7

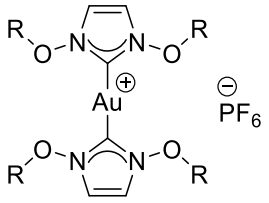

5 R=benzyl
7 R=methylnaphtalenyl

5.

Compounds **4** (0.13 mmol) was mixed with $Au(Me_2S)Cl$ (0.15 mmol) in CH_2Cl_2 (3 ml) for 19 h at room temperature in a 100 ml three-necked round bottom flask covered with aluminium foil under inert atmosphere (Ar). The mixture was filtered with filter syringes (25 mm, PTFE,

0.45 µm) to remove the silver salt. The solvent was removed under vacuum (Schlenk line). The powder was solubilized in the minimum quantity of CH_2Cl_2 (10 ml) and was stored at 4°C for 18 days covered with aluminium foil. A crystalline solid was obtained. Yield: 77.8 mg, 0.09 mmol, 66.3%.

The stabilities of both the Ag and Au complexes with silica were validated by TLC plates (hexane and EtOAc/hexane). The spots were fully retained by the silica and that can be explained considering they are salts.

^{1}H NMR (300 MHz, DMSO-d6): δ (ppm) = 5.34 (s, CH_2, 4H), 7.34 (m, H_{arom}, 10H), 7.85 (s, H4 and H5, 2H)

7.

Same procedure reported for complex **5**, although using complex **6** (0.23 mmol) as starting material and Au(Me_2S)Cl (0.23 mmol).

^{1}H NMR (300 MHz, DMSO-d6): δ (ppm) = 5.33 (s, CH_2, 4H), 5.41-5.55 (4.5 H), 7.34-7.49 (m, 8H), 7.50-7.63 (m, 7H), 7.65-7.81 (m, 7H), 7.84-7.97 (13H), 10.15 (0.1H).

^{13}C{^{1}H}-NMR was not defined due to the presence of many peaks.

4.3 Metal complexes with phenyl-substituted NOHC ligands

4.3.1 Preparation of hexahydro-1,3,5-triphenyl-1,3,5-triazine[56]

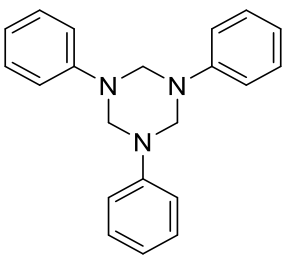

Aniline (5.5 ml, 60 mmol) and paraformaldehyde (2.0 g, 66 mmol) were mixed with n-hexane (10 ml) under reflux for 30 minutes in a one-necked round bottom flask. A viscous liquid was separated after the removal of the solvent (rotary evaporator, 100 mbar), but a solid was expected (literature melting point: 144°C). After 17 h a solid was present at the bottom of the flask, so 10 ml of n-hexane were added and the stirring was continued for other 3h until a beige solid precipitated.

The solvent was removed (rotary evaporator, 500 mbar), and the remaining white solid was dried with the Schlenk line (10^{-2} mbar). Yield: 3.09 g, 9.8 mmol, 49.0%.

A second and a third batch with twice the amount of the starting material were performed and the reaction mixture were kept stirring overnight.

Yield second batch: 10.58 g, 33.5 mmol, 83.8%. Yield third batch: 10.44 g, 33.1 mmol, 82.8%.

^{1}H NMR (300 MHz, $CDCl_3$): δ (ppm) = 4.90 (s, CH_2, 2H), 6.88 (t, J=7.6 Hz, 1H), 6.99-7.06 (m, H_{arom}, 2H) 7.18-7.27 (m, CH_{arom}, 2H).

4.3.2 Preparation of 3-(hydroxyimino)butan-2-one[55]

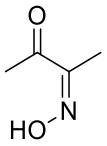

Pyridine (9 ml, 111 mmol) was added dropwise with a syringe during 15 minutes to a solution of diacetyl (9 ml, 103 mmol) and hydroxylamine hydrochloride (7.35 g, 105 mmol) in methanol (190 mL) in a one-necked round bottom flask at room temperature. The solution was initially pale yellow, but during pyridine addition it became colourless and produced white vapours because of the acid-base reaction between pyridine and HCl. The mixture was stirred for 2 h and then the solvent was removed under vacuum. The residue was extracted with ethyl acetate (50 mL) and then washed with distilled water (50 ml) and a saturated aqueous solution of NH_4Cl (19 g/50 ml). The organic layer was separated with a separating funnel and dried over Na_2SO_4 for 15 minutes. After filtration of the salt, the solvent was removed under vacuum. As confirmed by the ^{1}H NMR spectrum, organic side-products were not present,

hence no column chromatography was performed as otherwise stated in the literature.[55] The compound was vacuum dried at the Schlenk line to evaporate the residual pyridine. Yield: 5.57 g, 55.1 mmol, 53.5%.

A new batch with twice the amount of the first was synthetized. Yield: 15.9 g, 77.2 mmol, 76.3%.

^{1}H NMR (300 MHz, $CDCl_3$): δ (ppm) = 1.97 (s, CH_3, 3H), 2.37 (s, CH_3, 3H), 8.70 (s br, NOH, 1H).

4.3.3 Preparation of 1-phenylimidazolium-3-oxide

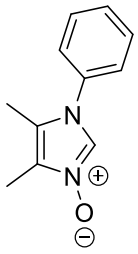

8

3-(hydroxyimino)butan-2-one was stirred with hexahydro-1,3,5-triazine in glacial acetic acid for 40 h at room temperature in a two-necked round bottom flask. The yellow solution changed its colour to orange after 40 h. Then, HCl (g) was bubbled into the solution for 2h at room temperature. Diethyl ether (almost 200 ml) was added until the solution became turbid, and a white precipitate appeared. The mixture was kept at 4°C overnight. The hydrochloride was filtrated with a sintered glass filter, washed with diethyl ether (4x50 ml) and dissolved in the mixture $CHCl_3$/MeOH (5:1, 30 ml). Na_2CO_3 was added in excess to the solution, which was stirred for 30 minutes. The solid was filtrated with a paper filter and the solvent was evaporated to dryness under vacuum at the rotary evaporator. The product was isolated by column chromatography (EtOAc/MeOH 1:1 or 1:2) and the solvent was evaporated. The reaction was repeated in batches of different size. The results of each reaction are presented below (cf. Table 8).

*Table 8. Quantities of starting materials and reagents for compound **8** synthesis.*

Trial	Diacetyl monoxime	Hexahydro-1,3,5-triazine	Solvent	Na_2CO_3	N-phenylimidazole-3-oxide	Yield
1	21 mmol, 2.13 g	7 mmol, 2.19 g	60 ml	26 mmol, 2.8 g	10.3 mmol, 1.45 g	36.7%
2	60 mmol, 6.07 g	20 mmol, 6.31 g	40 ml	78 mmol, 8.4 g	6.0 mmol, 1.12 g	9.9 %
3	39 mmol, 3.95 g	13 mmol, 4.10 g	20 ml	52 mmol, 1.9 g	6.5 mmol, 1.22 g	16.7 %
4	39 mmol, 3.95 g	13 mmol, 4.10 g	20 ml	52 mmol, 1.9 g	20 mmol, 3.76 g	51.2%

^{1}H NMR (300 MHz, $CDCl_3$): δ (ppm) = 2.11 (s, CH_3, 3H), 2.30 (s, CH_3, 3H), 7.28-7.33 (m, CH_{arom}, 2H), 7.47-7.58 (m, CH_{arom}, 3H), 8.23 (s, H2, 1H).

$^{13}C\{^1H\}$-NMR (75.475 MHz, $CDCl_3$): δ (ppm) = 7.6 (1C, CH_3), 9.6 (1C, CH_3), 77.2 (t, $CDCl_3$), 122.2 (1C, C_i), 125.7 (1C, C_{arom}), 126.1 (2C, C_{arom}), 127.4 (1C, C_i), 129.7 (1C, NC(H)N), 130.1 (2C, CH_{arom}), 134.9 (1C, CH_{arom}).

$^{13}C\{^1H\}$-NMR (75.475 MHz dept., $CDCl_3$): δ (ppm) = 7.6 (1C, CH_3), 9.6 (1C, CH_3), 125.7 (1C, C_{arom}), 126.1 (2C, C_{arom}), 129.7 (1C, NC(H)N), 130.1 (2C, CH_{arom}).

HRMS (TOF, 0.5 mM NH_4OAc): (m/z) 189.1032 $[M+H]^+$; 377.1983 $[2M+H]^+$.

EA: Calcd for $C_{11}H_{12}N_2O$ (188.09 g mol^{-1}): C, 70.24; H, 6.43; N, 14.89%. Found: C, 66.90; H, 6.15; N, 14.06; S, 0.68%.

Melting point (°C): 170.6.

4.3.4 Preparation of 1-phenyl-3-alkyloxyimidazolium halide

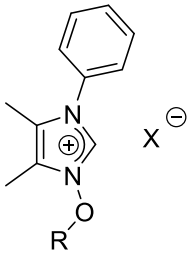

9 R=Me, X=I
10 R=Bn, X=Br

9.

1-phenylimidazole-3-oxide (**8**, 0.67 g, 3.56 mmol) and methyl iodide (0.22 ml, 3.56 mmol) were dissolved in anhydrous THF (10 ml) and stirred for 24h at room temperature in a pressure tube. The reaction was controlled with TLC in MeOH/EtOAc 1:1. The reaction was

stopped after 24 h when no significant amount of starting material was detected in the reaction mixture. The product was filtered, washed with diethyl ether and dried *in vacuo*. Yield: 0.952 g, 2.9 mmol, 81.0%.
This synthesis was performed again with half the amount of the starting materials. Yield: 0.338 g, 1.7 mmol, 93.5%.

^{1}H NMR (300 MHz, $CDCl_3$): δ (ppm) = 2.16 (s, 3H, CH_3), 2.38 (s, 3H, CH_3), 4.50 (s, 3H, OCH_3), 7.51-7.59 (m, 3H, CH_{arom}), 7.64-7.72 (m, 2H, CH_{arom}), 10.00 (s, 1H, H2).
$^{13}C\{^{1}H\}$-NMR (75.475 MHz, $CDCl_3$): δ (ppm) = 7.8 (1C, CH_3), 9.8 (1C, CH_3), 70.5 (1C, $NOCH_3$), 125.0 (1C, C_i), 127.0 (1C, C_i), 126.6 (2C, CH_{arom}), 130.4 (2C, CH_{arom}), 130.8 (1C, CH_{arom}), 131.2 (1C, $NC_{NOHC}N$), 132.9 (1C, CH_{arom}).
EA: Calcd for $C_{12}H_{15}N_2OI$ (330.17 g mol^{-1}): C, 43.65; H, 4.58; N, 8.48%. Found: C, 43.48; H, 4.29; N, 8.88%.
HRMS (TOF, 0.5 mM NH_4OAc): (m/z) 172.0999 $[M\text{-}OCH_3]^+$; 203.1189 $[M]^+$; 204.1221 $[M+H]^+$; 126.9039 $[I^-]$.
Melting point (°C): 123.7.

10.

1-phenylimidazole-3-oxide (0.50g, 2,66 mmol) and benzyl bromide (0.32 ml, 2.66 mmol) were dissolved in anhydrous THF (10 ml) and stirred for 6 days at room temperature in a pressure tube. The beige solid was filtrated and washed with diethyl ether. Yield: 0.59 g, 1.64 mmol, 61.7%.
A second batch with twice the amounts of starting materials was synthesized. Yield: 1.20 g, 3.3 mmol, 62.8%.

^{1}H NMR (300 MHz, $CDCl_3$): δ (ppm) = 2.11 (s, 3H, CH_3), 2.13 (s, 3H, CH_3), 5.89 (s, 2H, CH_2), 7.26 ($CHCl_3$), 7.35-7.44 (m, 3H, CH_{arom}), 7.52-7.59 (m, 3H, CH_{arom}), 7.60-7.69 (m, 4H, CH_{arom}), 10.65 (s, 1H, H2).
$^{13}C\{^{1}H\}$-NMR (300 MHz, $CDCl_3$): δ (ppm) = 7.6 (1C, CH_3), 9.6 (1C, CH_3), 84.5 (1C, $NOCH_2$), 124.7 (1C, C_i), 125.4 (1C, C_i), 126.3 (2C, CH_{arom}), 129.1 (2C, CH_{arom}), 130.3 (1C, CH_{arom}), 130.5 (2C,

CH_{arom}), 131.0 (2C, CH_{arom}), 131.1 (1C, $NC_{NOHC}N$), 132.4 (1C, CH_{arom}), 132.6 (1C, CH_{arom}), 133.0 (1C, CH_{arom}).

EA: Calcd for $C_{18}H_{19}N_2OBr$ (359.27 g mol^{-1}): C, 60.18; H, 5.33; N, 7.80%. Found: C, 56.81; H, 4.94; N, 6.87%.

HRMS (TOF, 0.5 mM NH_4OAc): (m/z) 280.1531 $[M+H]^+$; 279.1497 $[M]^+$; 78.9174 and 80.9159 $[Br]^-$.

Melting point (°C): 124.7.

4.3.5 General procedure for the synthesis of metal complexes 11 and 12

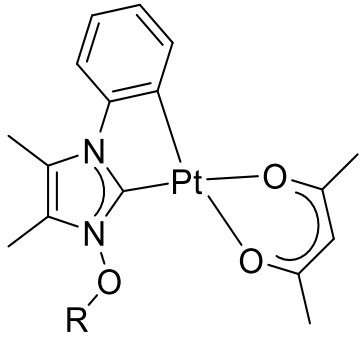

11 R=Me
12 R=Bn

Compounds **8** or **9** (0.80 mmol) and silver(I) oxide (0.40 mmol) were added in a dried Schlenk tube. Ar atmosphere was provided and anhydrous dimethylformamide was added in counterflow. The reaction was stirred overnight at room temperature. Dichloro(1,5-cyclooctadiene)platinum(II) (0.80 mmol) was then added in Ar counterflow. The mixture was stirred for 24h at room temperature and overnight at 120°C. Na(acac) (1.60 mmol) was added in Ar counterflow. The mixture was stirred 110°C for 5h and cooled down to room temperature. The solvent was evaporated in high vacuum (Schlenk line) under mild heating. The black crude solid was extracted with dichloromethane and the mixture filtered through a Celite pad. The red-purple liquid was evaporated under vacuum (rotary evaporator) to give a residue that was purified as specified below.

11.

The crude solid was purified through a chromatographic column with pure dichloromethane as an eluent (R_f=0.5). A yellow solid was obtained from fractions: 17-21. It was washed with diethyl ether and distilled pentane and ^{1}H NMR confirmed the removal of undesired compounds. Yield: 95.0 mg, 0.20 mmol, 23.9%.

^{1}H NMR (600 MHz, CD_2Cl_2): δ (ppm) = 1.99 (s, 3H, CH_3 acac), 2.04 (s, 3H, CH_3 acac), 2.18 (s, 3H, $CH_{3,i}$), 2.50 (s, 3H, $CH_{3,i}$), 4.16 (s, 3H, OCH_3), 5.54 (s, 1H, CH_{acac}) 6.89-7.03 (m, 2H, CH_{arom}), 7.17 (dd; J=1.5 Hz, 7.9 Hz; 1H, CH_{arom}), 7.72 (dd; J=1.7 Hz, 7.2 Hz; 1H, CH_{arom}).

^{13}C{^{1}H}-NMR (150.92 MHz, CD_2Cl_2): δ (ppm) = 7.1 ($CH_{3,i}$), 11.2 ($CH_{3,i}$), 27.9 ($CH_{3,acac}$), 28.1 ($CH_{3,acac}$), 67.4 (OCH_3), 102.1 (CH_{acac}), 112.5 (CH_{arom}), 120.8 (C_i), 121.5 (C_i), 123.7 (CH_{arom}), 126.0 (NC_{arom}), 131.9 (CH_{arom}), 144.4 (C_{arom}), 149.6 ($NC_{NOHC}N$), 184.8 (C_{acac}), 186.1 (C_{acac}).

^{195}Pt NMR (129 MHz, CD_2Cl_2): δ (ppm) = -3450.8.

HRMS (TOF, 0.5 mM NH_4OAc): (m/z) 496.1204 $[M+H]^+$; 496.1204 $[M+H]^+$; 465.1073 $[M-OMe+H]^+$; 831.1592 $[2M-2OMe-acac+H]^+$; 861.1699 $[2M-OMe-acac+H]^+$; 891.1812 $[2M-acac+H]^+$.

EA: Calcd for $C_{17}H_{20}N_2O_3Pt\cdot$ ½ CH_2Cl_2 (1075.74 g·mol^{-1}): C, 39.07; H, 3.93; N, 5.21%. Found: C, 39.24; H, 3.92; N, 5.27%.

Melting point (°C): 216.0.

In a precedent trial, milder reaction conditions were employed as the NOHC ligand is a temperature sensitive species. However, the very low yield suggests using the general protocol established by *Strassner* and *co-workers* is preferable.

First trial 11.

1-methyloxy-3-phenylimidazolim iodide (265 mg, 0.80 mmol) and silver(I) oxide (93 mg, 0.40 mmol) were added in a dried Schlenk tube. Ar atmosphere was provided and anhydrous dimethylformamide was added in counterflow. The reaction was stirred overnight at room temperature. Dichloro(1,5-cyclooctadiene)platinum(II) (0.30 mg, 0.80 mmol) was added in Ar counterflow. The mixture was stirred for 2h at rt, for 4h at 110°C and overnight at rt. Na(acac) was added in Ar counterflow. The mixture was stirred for 30 minutes at room temperature, for 1h at 110°C and cooled down to room temperature. The solvent was evaporated in high

vacuum (Schlenk line) under mild heating. The black crude was extracted with dichoromethane and filtered through a Celite pad. The red-purple coloured liquid was evaporated under vacuum (rotavapor). The crude was separated through a chromatographic column (2:1 CH_2Cl_2:isohexane). A pale yellow solid was obtained. The low quantity of isolated material enabled only to register the NMR spectra, which are in agreement with those reported above for complex **11**. Yield: 25.6 mg, 0.052 mmol, 6.4%.

The product was solubilized in dichloromethane and 2 ml of isohexane were added on top to promote crystallization. The tube was stored in the fridge for 5 days and the crystals emitted orange light when irradiated with the long wave UV light. A sample of the crystals was observed under the microscope and the structure was determined with XRD analysis.

12.

The crude was separated through two chromatographic columns (1:1 CH_2Cl_2/isohexane R_f=0,3 and then 3:2 CH_2Cl_2/isohexane R_f=0.4). A white solid was obtained after removal of the solvents. The solid was washed with isohexane and finally dried in the Schlenk line.

Yield: 38.3 mg, 0.07 mmol, 6.4%.

^{1}H NMR (600 MHz, CD_2Cl_2): δ (ppm) = ^{1}H NMR (300.13 MHz, CD_2Cl_2): δ (ppm) = 1.75 (s, 3H, CH_3), 1.86 (s, 3H, CH_3), 2.04 (s, 3H, CH_3), 2.44 (s, 3H, CH_3), 5.44 (s, 2H, $CH_{2,benzyl}$), 5.52 (s, 1H, CH_{acac}), 6.88-7.04 (m, 2H, CH_{arom}), 7.18 (dd; J=7.7 Hz, 1.4 Hz; 1H; CH_{arom}), 7.33-7.46 (m, 5H, CH_{arom}), 7.76 (dd; J=1.7 Hz, 7.2 Hz; 1H; CH_{arom}).

^{13}C{^{1}H}-NMR (150.92 MHz, CD_2Cl_2): δ (ppm) = 8.9 (CH_3), 12.8 (CH_3), 29.5 (CH_3), 29.7 (CH_3), 83.5 (CH_2), 103.8 (CH_{arom}), 114.1 (CH_{arom}), 122.0 (C_i), 124.1 (C_i), 125.3 (CH_{arom}), 125.4 (CH_{arom}), 127.5 (C_{arom}), 130.5 (CH_{arom}), 130.9 (CH_{arom}), 131.4 (CH_{arom}), 133.4 (CH_{arom}), 136.5 (C_{arom}), 146.0 (C_{arom}), 151.2 ($NC_{NOHC}N$), 186.4 (C_{acac}), 187.9 (C_{acac}).

^{195}Pt NMR (129 MHz, CD_2Cl_2): δ (ppm) = -3454.3.

HRMS (TOF, 0.5 mM NH_4OAc): (m/z) 594.1332 $[M+Na]^+$; 487.0865 $[M-OBn+Na]^+$; 1165.2794 $[2M+Na]^+$.

EA: Calcd for $C_{23}H_{24}N_2O_3Pt\cdot$ ½ $CH_2Cl_2\cdot$ ⅛ C_6H_{14} (2414.00 g·mol^{-1}): C, 47.76; H, 4.38; N, 4.64%. Found: C, 47.72; H, 4.09; N, 4.58%.

Melting point (°C): 154.7.

4.3.6 General procedure for the synthesis of metal complexes 13 and 14

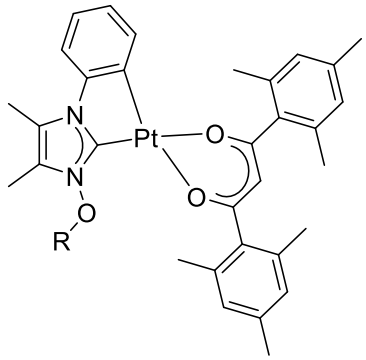

13 R=Me
14 R=Bn

Compounds **8** or **9** (1.0 mmol) and silver(I) oxide (0.60 mmol) were added in a dried Schlenk tube. Ar atmosphere was provided and anhydrous dimethylformamide was added in counterflow. The reaction was stirred overnight at room temperature. Dichloro(1,5-cyclooctadiene)platinum(II) (1.0 mmol) was added in Ar counterflow. The mixture was stirred for 24h at room temperature and overnight at 120°C. Dried potassium *tert*-butoxide (2.0 mmol) and 1,3-bis(2,4,6-trimethylphenyl)propane-1,3-dione (2.0 mmol) were added in Ar counterflow. The mixture was stirred 110°C for 5h and cooled down to room temperature. The solvent was evaporated in high vacuum (Schlenk line) under mild heating. The black crude was extracted with dichloromethane and filtered through a Celite pad. The dark red liquid was evaporated under vacuum (rotary evaporator) to give a residue that was purified as specified below.

13.

The crude was separated through a chromatographic column (1:9 EtOAc/isohexane, R_f=0,5 and then 1:5 EtOAc/isohexane, R_f=0,4). A yellow liquid was obtained. The solvent was dried in the Schlenk line. The crystallization from CH_2Cl_2/pentane was unsuccessful. The product was dissolved in 10 ml of distilled pentane and after sonication a solid precipitated.

A second column was performed to separate the side-products increasing the polarity of the eluent, from 2:1 CH_2Cl_2/isohexane to 4:1 CH_2Cl_2/isohexane (R_f=0.4, fractions: 35-52). The yellow powder was washed with isohexane and sonicated twice before drying in the Schlenk

line. The crossed spot with **11** showed that the new compound is less polar due to the presence of the mesytilene moiety. Yield: 33.9 mg, 0.05 mmol, 5.0%.

^{1}H NMR (600 MHz, CD_2Cl_2): δ (ppm) = 2.13 (s, 3H, CH_3), 2.28-2.36 (m, 18H, $CH_{3,mesacac}$), 2.50 (s, 3H, CH_3), 5.64 (s, 1H, $CH_{mesacac}$), 6.83-6.98 (m, 5H, CH_{arom}), 6.98 (td; J=1.5 Hz, 7.8Hz; 1H; CH_{arom}), 7.22 (dd; J=7.8 Hz, 1.1 Hz; 1H; CH_{arom}), 7.55 (dd; J=1.5 Hz, 7.5 Hz; 1H; CH_{arom}), 9.59 (s, 1H, OH or NH or CH_i).

^{13}C{^{1}H}-NMR (150.92 MHz, CD_2Cl_2): δ (ppm) = 8.4 (CH_3), 9.4 (CH_3), 18.5 ($CH_{3,mesacac}$), 18.8 ($CH_{3,mesacac}$), 20.0 (CH_3), 20.1 (CH_3), 106.3 (CH_{arom}), 111.0 (CH_{arom}), 120.8 (C_i), 121.3 (Ci), 122.6 (CH_{arom}), 122.7 (CH_{arom}), 125.5 (C_{arom}), 127.3 ($CH_{arom,mesacac}$), 127.4 ($CH_{arom,mesacac}$), 131.2 (CH_{arom}), 132.9 ($C_{arom,mesacac}$), 133.2 ($C_{arom,mesacac}$), 137.0 ($C_{arom,mesacac}$), 138.6 (C), 138.7 (C), 147.5 (C), 148.4 ($NC_{NOHC}N$), 184.2 ($C_{mesacac}$), 184.4 ($C_{mesacac}$).

^{195}Pt NMR (129 MHz, CD_2Cl_2): δ (ppm) = -3396.8.

HRMS (TOF, 0.5 mM NH_4OAc): (m/z) 674.2347 $[M\text{-}OMe+2H]^+$; 696.2167 $[M\text{-}OMe+H+Na]^+$.

14.

The crude was separated through a chromatographic column with 1:2 CH_2Cl_2/isohexane (Rf=0.2). A second column was performed to separate the free mesacac (from 1:3 CH_2Cl_2/isohexane to 1:2 CH_2Cl_2/isohexane, Rf=0.1). The solid was washed with distilled pentane and sonicated twice before drying in the Schlenk line. Yield: 80.4 mg, 0.10 mmol, 9.0%.

^{1}H NMR (600 MHz, CD_2Cl_2): δ (ppm) = 2.27-2.38 (m, 21H, $CH_{3,mesacac}$ + CH_3), 2.50 (s, 3H, CH_3), 5.24 (s, 2H, CH_2), 5.68 (s, 1H, $CH_{mesacac}$), 6.77-7.12 (m, 10H, CH_{arom}), 7.15-7.31 (m, 2H, CH_{arom}), 7.63 (dd; J=7.6 Hz, 1.5 Hz; 1H; CH_{arom}).

^{13}C{^{1}H}-NMR (150.92 MHz, CD_2Cl_2): δ (ppm) = 7.6 (CH_3), 11.4 (CH_3), 19.7 (CH_3), 20.0 (CH_3), 21.2 (CH_3), 21.3 (CH_3), 82.1 (CH_2), 107.6 (CH_{arom}), 112.6 (CH_{arom}), 120.7 (C_i), 122.2 (C_i), 123.8 (CH_{arom}), 123.9 (CH_{arom}), 125.8 (NC_{arom}), 128.4 (CH_{acac}), 128.5 (CH_{arom}), 128.6 (CH_{arom}), 128.7 (CH_{arom}), 129.1 (CH_{arom}), 132.0 (CH_{arom}), 134.0 (C_{arom}), 134.2 (C_{arom}), 134.4 (C_{arom}), 184.3 ($C_{mesacac}$), 186.6 ($C_{mesacac}$).

^{195}Pt NMR (129 MHz, CD_2Cl_2): δ (ppm) = -3398.1.

HRMS (TOF, 0.5 mM NH_4OAc): (m/z) 696.2163 $[M\text{-}OBn+H+Na]^+$; 780.2770 $[M+H]^+$; 802.2599 $[M+Na]^+$.

4.3.7 Synthesis of bromo(1-phenyl-3-benzyloxyimidazolydene) gold(I) complex

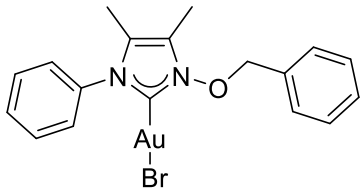

15

Transmetalation procedure.

1-phenyl-3-benzyloxyimidazolium bromide (72 mg, 0.2 mmol) was stirred with Ag_2O (28 mg, 0.12 mmol) in acetonitrile (40 ml) for 24h at room temperature under inert atmosphere in a 250 ml two-necked round bottom flask. ^1H NMR of a small amount of the reaction mixture proved the proligand was not present anymore. Chloro(dimethylsulfide)gold(I) (30 mg, 0.1mmol) was added in Ar counterflow to the mixture which was stirred for three more hours. The mixture was then filtrated in a syringe filter (25 mm, PTFE, 0.45 µm) and kept at 4°C but no solid precipitated. The solvent was removed under vacuum to give an off-white solid.

^1H NMR (300 MHz, CD_3CN): δ (ppm) = 1.96 (s, 6H, CH_3), 5.44 (s, 2H, CH_2), 6.40-7.53 (m, 5H, CH_{arom}), 7.54-7.64 (m, 5H, CH_{arom}).

Direct synthesis procedure.

1-phenyl-3-benzyloxyimidazolium bromide (72 mg, 0.2 mmol) was stirred with $Au(Me_2S)Cl$ (59 mg, 0.2 mmol) and K_2CO_3 (276 mg, 2 mmol) in acetonitrile (40 ml) overnight at room temperature under inert atmosphere in a 250 ml two-necked round bottom flask. ^1H NMR of reaction mixture withdrawals after 24 h and 48 h detected the presence of some residual ligand (5:2 complex:proligand). Hence, the mixture was concentrated (rotary evaporator) and almost 30 ml of diethyl ether were added. During the evaporation of acetonitrile some gold complex decomposed in a black powder, hence the mixture was filtrated and stored for three days at 4°C until some crystals formed. They were analysed with the X-Ray and used for NMR and HRMS experiments. Yield: 31.9 mg, 0.06 mmol, 30.3%.

^{1}H NMR (300 MHz, CD_3CN): δ (ppm) = 1.96 (s, 6H, CH_3), 5.44 (s, 2H, CH_2), 6.40-7.53 (m, 5H, CH_{arom}), 7.54-7.64 (m, 5H, CH_{arom}).

$^{13}C\{^{1}H\}$-NMR (75.475 MHz, CD_3CN): δ (ppm) = 6.9 (CH_3); 8.9 (CH_3); 82.3 (CH_2); 100.0, 127.4, 127.5, 128.9, 129.6, 129.7, 130.3, 130.4 (C, CH_{arom}, C_i). The carbene signal was not detected.

HRMS (TOF): (m/z) 753.2494 $[L_2Au]^+$.

4.4 Attempts to isolate compound 16

4.4.1 Pd/C and H_2

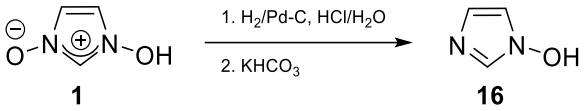

1 **16**

Balloon containing H_2.

1-hydroxyimidazolium-3-oxide (3.0095 g, 30 mmol) was stirred with HCl (3.5 ml, 10 M) and Pd/C 10% (0.1512g) in water (20 ml) in a 250 ml three-necked round bottom flask. H_2 atmosphere was provided using a balloon as a container (approximately 1.5 L). The reaction progression was followed with ^{1}H NMR spectra on mixture withdrawals (Table 9).

Table 9. ^{1}H-NMR data of hydrochloride mixtures: species percentages in aqueous mixture.

	1-Hydroxy-1H-imidazole-3-oxide Hydrochloride **1**·HCl		1-Hydroxy-1H-imidazole Hydrochloride **16**·HCl		Imidazole Hydrochloride	
	H2	H4, H5	H2	H4, H5	H2	H4, H5
δ (ppm)	9.67 (t, J=2)	7.80 (d, J=2, 2H)	9.29 (t, J=1.5)	7.57 (t, J=1.5)	9.09 (t, J=1.1)	7.63 (d, J=1.1, 2H)
24h	100		-		-	
40h	97		3		-	
70h	73		19		8	
85h	73		19		8	
150h	33		41		26	
216h (Heating)	25		47		28	
255h (Heating)	20		49		31	

Comparing the results of ^{1}H NMR spectra and the data provided by Laus *et al.*[49] for the species in hydrochloride solvent, a rough estimation of the concentration of the compounds was obtained from the H2 peaks integrals. After nine days H_2 was recharged, and the mixture was gently heated (40°C) for 3 days as suggested by literature. We stopped the reaction after 255 h, when no significative increase of **16** hydrochloride from the previous sample collection was detected.

Despite the numerous attempts, following the procedure reported in the literature it was not possible to separate compound **16** from **1** and the imidazole.

Autoclave trials.

Three attempts were performed using autoclave to ensure a controlled H_2 uptake.

- 1-hydroxy-1H-imidazole-3-oxide (0.525 g, 6.2 mmol) was stirred with Pd/C catalyst (10% wt, 0.025 g) and HCl (10 M, 0.6 ml) in water (5 ml) for 24 h. The pressure drop was 0.13 bar (1.2 mmol).
- 1-hydroxy-1H-imidazole-3-oxide (0.500 g, 5.9 mmol) was stirred with Pd/C catalyst (1% wt, 0.030 g) and HCl (10 M, 0.6 ml) in water (5 ml) for 24 h. The pressure drop was 0.13 bar (1.2 mmol).
- 1-hydroxy-1H-imidazole-3-oxide (0.516 g, 6.1 mmol) was stirred with Pd/C catalyst (1% wt, 0.026 g) and HCl (10 M, 0.6 ml) in water (5 ml) for 48 h. The pressure drop was 0.23 bar (2.2 mmol).

The second batch was purify as reported in the literature (centrifugation to separate Pd/C, precipitation from i-Pr_2O, washing with i-Pr_2O/i-PrOH, treatment with H_2O and $KHCO_3$, solubilization in acetone and vacuum drying of the mixture), but a very low amount of product was obtained.

^{1}H NMR (300 MHz, DMSO-d_6): δ (ppm) = 6.57 (d, J=2, H4 and H5 **16**, 2H), 6.90 (s, H4 or H5 **1**, 1H), 7.28 (s, H4 or H5 **1**, 2H), 7.38 (s, H2 **1**, 1H), 7.53 (t, J=2, H2 **16**, 1H).

4.3.1 Raney-Nickel

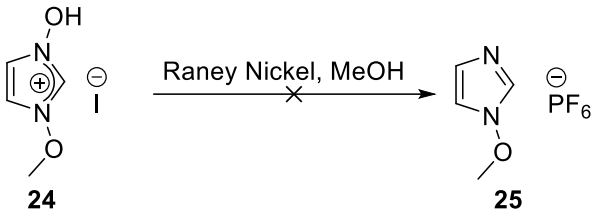

24 **25**

A sample of a 50% aqueous slurry of Raney Nickel was washed with methanol in Ar atmosphere and 2 spatulas were mixed in a Schlenk tube with 1-methoxy-3-hydroxyimidazolium hexafluorophosphate (**24**) and methanol (5 ml). The reaction was controlled with TLC plates (CD_2Cl_2+10% MeOH). After 4h the starting material was still present, hence almost 1 ml of the 50% aqueous slurry was added to the Schlenk tube and the mixing was continued overnight. Raney Nickel was filtrated, and the solvent removed under vacuum (rotary evaporator). The pale green solid was not photoactive on a TLC plate, hence it was not the product nor imidazole. ^{1}H NMR confirmed there was no species left. HRMS showed a polymerization pattern.

The residual Ni was quenched with aqueous solution of HCl 25% and hydrogen peroxide 33% to fasten the reaction. Sodium thiosulfate was added to reduce the residual H_2O_2.The formation of $NiCl_4$ leaded to a deep green solution.

4.5 Synthesis attempts

4.5.1 Asymmetrically substituted 1-hydroxyimidazolium-3-oxide

2-(bromomethyl)naphthalene

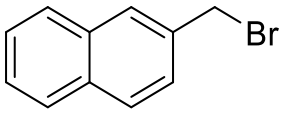

In a single-necked 250 ml round bottomed flask 2-methylnaphtalene (8.8 g, 61,9 mmol) was dissolved in chloroform (64 ml) which substituted CCl_4 because of its lower toxicity. N-

bromosuccinimide (12.9 g, 71.8 mmol) and dibenzoylperoxyl (0.50 g, 1.21 mmol) were added. The mixture was stirred under reflux (70°C) and the evolution of the reaction was followed with TLC (pure isohexeane and 1:7 EtOAc/isohexane). After 4h, when the starting material was no more visible in the TLC plate, the reaction was ice-cooled for 30 minutes and the solid succinimide was filtered. The solvent was evaporated under vacuum and the solid redissolved in ethanol with sonication. The solution was kept at 4°C for 3 days and the white solid which had precipitated was filtered. The product was dried in the Schlenk line. The ^{1}H NMR spectrum of the compound showed two peaks at 2.77 and 6.84 ppm due to the presence of starting material of the dibrominated compound. Hence, a new crystallization from hot ethanol was performed. The mixture was stirred for 24h, filtrated and the solvent evaporated.
A second batch of this reaction was performed, but dibrominated compound was detected as well.

^{1}H NMR (300 MHz, $CDCl_3$): δ (ppm) = 4.68 (s, CH_2, 2H), 6.84 (s, dibrominated compound), 7.26 ($CHCl_3$) 7.46-7.57 (m, CH_{arom}, 6H), 7.76-7.93 (m, CH_{arom}, 11H).

17.

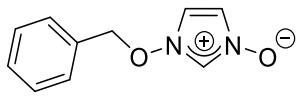

Trial 1: 1-hydroxyimidazole-3-oxide (**1**, 0.50 g, 5 mmol) in a 150 ml flask in ice-cooled methanol (5 ml) was stirred while adding KOH (85%, 0.43g, 6.5 mmol). The yellow solution became clearer after 10 minutes and benzyl bromide (0.6 ml, 5 mmol) was added slowly (2 minutes). The mixture was refluxed for 1h, filtered in vacuo and washed with methanol (2x4 ml): a white powder and a dark red solution were obtained. After filtration the methanol solution was evaporated under vacuum, the resulting red-brownish oil was redissolved in acetonitrile, filtered in a sintered glass filter to separate the solid phase (which did not contain the product, as the ^{1}H NMR showed). The solvent was evaporated under vacuum in vigorous stirring to obtain a red-brownish dense oil. Yield: 772.5 mg, 4.06 mmol, 81.2%.

^{1}H NMR (300 MHz, DMSO-d6): δ (ppm) =5.26 (s, 2H, CH_2), 7.01 (s, 1H, H4 or H5), 7.34-7.45 (m, 6H, H4 or H5 and H_{arom}), 8.58 (t, 1H, H2).

HRMS (ESI): (m/z) 213.0634 ($[M+Na]^+$), 191.0925 (M^+), 175.0869 ($[M-O+H]^+$), 157.0352 ($[M-Ph+2Na]^+$) 123.0150 ($[M-OBn+Na+H]^+$), 107.0412 ($[BnOH]^+$), 91.0549 (Bn^+), 85.0595 ($[M-OBn]^+$).

Trial 2: KOH (0.66 g, 15 mmol) was added to an ice-cooled solution of 1-hydroxyimidazole-3-oxide (**1**, 1.0 g, 10 mmol) in MeOH (10 ml) in a single neck round-bottomed flask until the solution became clear. Benzyl bromide (1.2 ml, 10 mmol) was added slowly with a syringe. The solution was refluxed for 1h and cooled down overnight. The solid was filtrated and washed with methanol. The solvent was evaporated to dryness and acetonitrile was added to the brown liquid. The precipitate was filtered and washed with acetonitrile. The solvent was evaporated to dryness. Since the ^{1}H NMR spectrum showed the presence of benzyl bromide, the product was washed with diethyl ether and sonicated. Being the by-product still present, the viscous liquid was dissolved in dichloromethane and poured dropwise in diethyl ether cooled with liquid nitrogen. The product was stirred overnight with a saturated solution of KPF_6 in water (22.0 ml, 10 mmol). Since the product was still a viscous liquid, water was removed under vacuum and the liquid was dissolved in acetonitrile. Two samples were mixed with water and tetrahydrofuran, respectively, but no solid was obtained.

18.

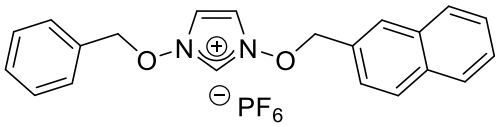

A solution of 2-bromo(methyl)naphthalene (0.9 g, 4.1 mmol) in CH_2Cl_2 was added to 1-benzyloxyimidazole-3-oxide (772.5 mg, 4.1 mmol) in a one-necked round-bottom flask in a glove box. The brown solution was stirred under reflux for 1h at 50°C.

By comparison with the ^{1}H NMR spectra of **2** and **17** the presence of the benzyl- and methylnaphtalen- monosubstituted products is detected, whereas 1,3-dibenzyloxyimiazolium bromide is not present.

The solvent is evaporated in an NMR tube and dissolved in D_2O. The liquid and solid phase were separated and dissolved in DMSO-d_6, but all the peaks of the different products were visible in both the solid and liquid phase. The product was filtered, a little amount of product

was mixed with hexane and the precipitated solid was dissolved in DMSO-d_6 and analysed by ^{1}H NMR.

^{1}H NMR (300 MHz, DMSO-d6): δ (ppm) = 5.43 (s, CH_2, 2H), 5.63 (s, CH_2 naphtalenoxyl moiety **18** and CH_2 **2**, 2H), 7.20-8.00 (m, H4+H5 and H_{arom}, 16H), 10.19 (t, H2, 1H), 10.25 (t, H2, 1H).

The zwitterionic species (1-(methyl)naphtalenoxyimidazolium-3-oxide and **17**) were removed from the mixture by dissolution in hexane. Only a di-substituted imidazole, here considered to be **2** by comparison with the respective spectrum and due to the high chemical shift of its acid proton, is present as a side product. Considering the results obtained by hexane dissolution, CH_2Cl_2 was evaporated under vacuum in a three-necked round bottom flask and the brown viscous product was stirred with hexane (15 ml). Most of the solid was sticked on the glass surface after the filtration of the hexane mixture. Hexane was evaporated under vacuum. Then water (10 ml) and a solution of NH_4PF_6 (0.67 g, 4.1 mmol) were slowly added to the mixture which was stirred overnight. A mixture of products was still visible at the ^{1}H NMR analysis and dissolution in methanol-d_4, $CDCl_3$, CD_3CN, D_2O did not lead to a separation of the products.

4.5.2 1-phenyloxy-imidazolium-3-oxides

19.

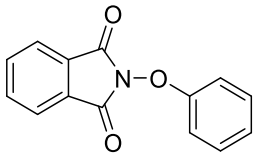

In an oven-dried 500ml one-necked round bottom flask anhydrous tetrahydrofuran (200 ml) and N-hydroxyphtalimide (8.32 g, 50 mmol) were stirred with a magnetic bar for 10 minutes, closing the opening with a septum. K^{t}OBu (5.63 g, 50 mmol) was added portionwise to the yellow solution which was stirred for 15 minutes opened to the air and became dark red. Diphenyliodonium tetrafluoroborate (18.5 g, 50 mmol) was added and the stirring was continued for 4h. The suspension was filtered through a sintered glass filter. The filtrate was

poured into a separatory funnel with ethyl acetate (100 ml) and a saturated solution of $Na_2S_2O_3$ (70.1 g, 100 ml). The mixture was shaken, and the aqueous phase was extracted with ethyl acetate (3x100 ml). The organic layer was washed with brine (200 ml, saturated aqueous solution), dried over with Na_2SO_4, filtered and the solvent removed *in vacuo*. Two crystallization trials were performed as we obtained a brown solid whereas in the literature it was described as white. The product was first solubilized in ethyl acetate (190 ml) adding n-hexane (190 ml) on top. Some colourless crystals formed overnight, but most of the solid precipitated. After filtering the solid was solubilized in 500 ml of EtOAc:n-hexane 1:1 under heating and sonication, but this attempt was unsuccessful as well. ^{1}H and ^{13}C NMR spectra showed the presence of impurities. A column chromatography using first hexane to remove the more unpolar species and then 1:2 EtOAc/isohexane leaded a white solid after the evaporation of the solvent. Yield: 2.57 g, 10.7 mmol, 21.5%.

^{1}H NMR (300 MHz, $CDCl_3$): δ (ppm) = 7.11-7.20 (m, CH_{arom}, 3H), 7.26 ($CHCl_3$), 7.30-7.39 (m, CH_{arom}, 2H), 7.79-7.85 (m, CH_{arom}, 2H), 7.89-7.96 (m, CH_{arom}, 2H).
$^{13}C\{^{1}H\}$-NMR (75.475 MHz, $CDCl_3$): δ (ppm) = 77.4 ($CDCl_3$), 114.6 (2C), 124.1 (2C), 124.8 (1C), 129.0 (1C, C_{arom}), 129.9 (2C), 135.0 (2C), 159.0 (1C, C_{arom}), 163.1 (1C, C_{arom}).
$^{13}C\{^{1}H\}$-NMR (75.475 MHz dept., $CDCl_3$): δ (ppm) = 77.4 ($CDCl_3$), 114.6 (2C), 124.1 (2C), 124.8 (1C), 129.9 (2C), 135.0 (2C).
The integrals in the ^{13}C spectrum do not correspond to the number of signals that are expected but they are the same reported by the literature.

A new batch was performed with twice the quantities of the first one. Part of the crude was purified with two columns (1:1 EtOAc/Isohexane) and the remining *via* recrystallization dissolving the crude in hot EtOAc (50 ml) and adding hexane (40 ml) until the solution became turbid. The mixed fractions were crystallized with hot ethyl acetate and isohexane after the removal of the solvent. Yield: 10.90 g, 45.6 mmol, 46.6%.

20.

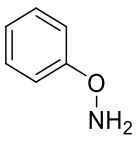

In a 250 ml single necked round bottomed flask N-phenoxyphtalimide (2.40 g, 10 mmol) was dissolved in a mixture of methanol (10 ml) and chloroform (90 ml) at room temperature open to the air. The mixture was at first yellow and it turned into white after some minutes. Hydrazine hydrate (1,5 ml, 31 mmol) was added dropwise via a syringe (it was not miscible in the solvent mixture). The solution was stirred with a stirring bar for 22 h. The white suspension was filtered with a Celite pad. The solvent was evaporated from the yellow solution. The yield was higher than 100%, hence some impurities which were not visible at the ^{1}H NMR were present.

A second batch of this reaction was performed with the same amounts of starting material of the previous. Even though ^{1}H NMR spectrum after filtering the reaction mixture with a PTFA filter proved the product to be formed, some other peaks in the aliphatic region were present. Therefore, the stirring was continued until 40 h. After filtration with a Celite pad and vacuum drying of the solvent, the solid was dissolved in hot ethyl acetate and hexane for the recrystallization. A white solid was separated by filtration and analysed with a ^{1}H NMR spectrum: no product was detected in this phase using both $CDCl_3$ and DMSO-d_6 as solvents. In the yellow liquid phase ^{1}H NMR spectrum detected the product and some impurities. Perhaps, a difference in the polarity of the solvent made it possible to dissolve some succinimide in the product mixture. The product was not soluble in isohexane and no species precipitated dissolving it in ethyl acetate. Hence a chromatographic column was necessary, as described by the literature (1:9 EtOAc/Isohexane). The product was a yellow oil. Yield: 101 mg, 0.9 mmol, 10.0%.

^{1}H NMR (300 MHz, $CDCl_3$): δ (ppm) = 5.85 (s, NH_2, 2H), 6.95 (tt, J^{I}=1.2 Hz, J^{II}=7.2 Hz, CH_{arom}, 1H), 7.10-7.18 (m, CH_{arom}, 2H), 7.21-7.34 (m, CH_{arom}+$CHCl_3$, 2H).

A third batch with twice the amount of starting material was performed. The ^{1}H NMR spectrum of the product after 10 days of storage did not correspond to the one expected because of the absence of the amine peak at 5.85 ppm and the product colour turned into red, confirming the oxidation availability of the amine compound.

21.

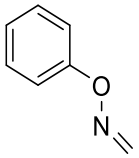

Phenoxyamine (1.09 g, 10 mmol) was dissolved in methanol (35 ml). Paraformaldehyde (0.33 g, 11 mmol) was added to the pale-yellow solution. The mixture was stirred for 1 h under reflux. The dark red solution was filtered in a sintered glass filter under vacuum and evaporated to dryness. Since the ^{1}H NMR spectrum showed peaks which were not ascribable to the product, a new crystallization was attempted dissolving the product in acetonitrile and adding diethyl ether. A tan solid precipitated and it was separated from the dark red solution through filtration. This reaction did not work, because GC-MS highlighted the product decomposed in phenol and the starting material.

GC-MS (30m x 0.25 mm): retention time (min) 5.412, 9.417.
5.412 min (m/z): 94 ($[M\text{-}NCH_2]^+$, phenol); 9.417 min (m/z): 109 ($[M\text{-}CH_2]^+$).

4.5.3 Macrocycles

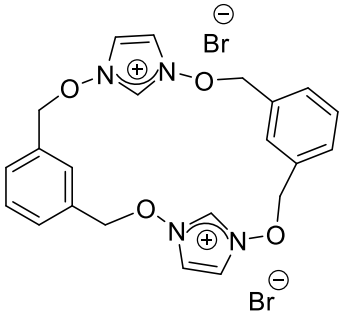

23.

Trial 1. In a 250 ml one-necked round bottomed flask KOH (0.50 g, 7.8 mmol) was added to an ice-cooled solution of 1-hydroxyimidazole-3-oxide (0.60g, 6 mmol) in methanol (70 ml). Half of the quantity of α,α'-dibromometaxylene (0.815 g, 3 mmol) was added to the mixture while stirring. The transparent solution was heated under reflux for 2 h and then cooled down to room temperature. The remining 1,3-di(methylbromo)benzene (0,816 g, 3 mmol) was slowly added to the solution. The transparent mixture was stirred overnight. A precipitate appeared. The solvent was evaporated and the ^{1}H NMR spectrum was difficult to interpret.

The solid was barely dissolved in water (50 ml) and an aqueous solution of KPF_6 (3.35 g, 18 mmol) was added dropwise with a syringe. A brown solid precipitated. It was washed with methanol, sonicated, and wash with diethyl and dried at the Schlenk line. The HRMS analysis showed a pattern at m/z higher than 650 proved that polymeric chains were formed.

Trial 2. In a 100 ml one-necked round bottomed flask 1-hydroxyimidazole-3-oxide (0.3 g, 3 mmol) was stirred in acetone (70 ml) while slowly adding α,α'-dibromometaxylene (0.41 g, 1.5 mmol). The mixture was heated under reflux overnight because a white precipitate was still present at the bottom of the flask. The mixture was cooled down to room temperature and the solvent was removed under vacuum (rotary evaporator). The yellow viscous liquid was not soluble in hexane, diethyl ether and dichloromethane. After 15 h some crystals were visible: the water which could be still present in the mixture was co-evaporated with acetonitrile, but no solid was obtained. ^{1}H NMR spectrum did not demonstrate any imidazole containing species.

HRMS (TOF, 0.5 mM NH_4OAc): (m/z) 339.1348 $[M\text{-imidazole}]^+$; 355.1655 $[M\text{-imidazole}+NH_2]^+$.

4.5.4 New synthesis of 1-hydroxyimidazolium-3-oxide

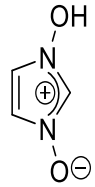

1

Trial 1. Dimethylglyoxime (0.03 mol, 3.48 g) and formaldehyde (30%, 0.03 mol, 2.25 ml) were stirred with methanol (40 ml) at room temperature for 20 h in a 250 ml single-neck round bottomed flask. NaOH (30% aqueous solution) was added to 50 ml of the solution until a good amount of white solid precipitated. After 5 minutes the white solid became yellow and then tan. ^{1}H NMR spectrum confirmed no product was formed.

Dimethylglyoxime is not soluble in methanol, but this was chosen as a solvent because it is the same used in the literature procedure. A second trial was performed with the same quantities of starting material, the same procedure and with acetone as a solvent, even

though this may cause the formation of undesired products due to its similarity with formaldehyde. ^{1}H NMR spectrum did not show the presence of any product.

Trial 2. Dimethylglyoxime (5 mmol, 0.581 g), formaldehyde (5 mmol, 0.14 ml) and concentrated HCl (1.25 mmol, 0.11 ml) were stirred in DMSO (5 ml) at room temperature for 20 h in a 25 ml single-necked round bottomed flask. NaOH (30% aqueous solution) was added to 50 ml of the until a solid precipitated. The solvent was evaporated and ^{1}H NMR spectra were performed. According to the results of the NMR spectra more than one species were present in the reaction mixture.

A second trial was performed with the same quantities of starting material, the same procedure and with DMF as a solvent. The product mixture was washed and sonicated three times with ether and a new ^{1}H NMR in $CDCl_3$ was performed, but no product was detected.

4.5.5 1-phenyl-imidazolium-3-alcoxydes

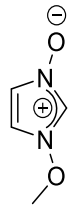

24

Trial 1: 1-hydroxyimidazole-3-oxide (1.5 g, 15 mmol) was stirred in a pressure tube with methyl iodide (0.95 ml, 15 mmol) in anhydrous THF for 4h at 65°C. The grey solid was separated by the deep red solution by filtration and washed with diethyl ether. The ^{1}H NMR of the product mixed with the starting material gave just the signal of the starting material: no product detected, the reaction did not work.

Trial 2: 1-hydroxyimidazole-3-oxide (1.5 g, 15 mmol) was stirred in a pressure tube with methyl iodide (0.95ml, 15 mmol) in HPLC grade acetonitrile for 10h at 70°C. The dark red solution was filtrated and the solid washed with acetonitrile (10 ml) and ether (10 ml). ^{1}H NMR showed no methylation occurred.

Trial 3: 1-hydroxyimidazole-3-oxide (1.5 g, 15 mmol) was stirred in a pressure tube with methyl iodide (0.95ml, 15 mmol) in dried DCM for 80 h at 30°C. The solid was filtrated and washed with dichloromethane (10 ml) and diethyl ether (10 ml).
^{1}H NMR showed no methylation occurred.

Synthesis: KOH (0.66g, 15 mmol) was added to an ice-cooled solution of 1-hydroxyimidazole-3-oxide (1.0 g, 10 mmol) in MeOH (10 ml) in a pressure tube. When the solution became clear methyl iodide (0.650 ml) was added slowly with a syringe. The solution was stirred under heating overnight. The dark red solution was evaporated to dryness. DCM (40 ml) was added and the mixture was stirred for 30 minutes. The solid was filtrated and the solution was evaporated to dryness. ^{1}H NMR confirmed the formation of the desired product. Yield: 1.89 g, 7.8 mmol, 52.1%.
In a second attempt twice the amount of starting materials were used. The product was stirred with a saturated solution of KPF_6 in water (70.5 ml, 32 mmol). The solvent was evaporated to dryness. The viscous liquid was washed with water and recrystallized from hot water in a black solid. Yield: 4.74 g, 18.2 mmol, 61%.

^{1}H NMR (300 MHz, $CDCl_3$): δ (ppm) = 4.31 (s, CH_3, 3H), 7.19-7.24 (m, C_i, 2H), 7.26 ($CHCl_3$), 9.04 (s, N(CH)N, 1H).
$^{13}C\{^{1}H\}$-NMR (75.475 MHz, $CDCl_3$): δ (ppm) = 70.1 (1C, CH_3), 77.2 (t, $CDCl_3$), 114.5 (1C, C_i), 118.6(1C, C_i), 125.8 (1C, NC(H)N).
$^{13}C\{^{1}H\}$-NMR (75.475 MHz dept., $CDCl_3$): δ (ppm) = 70.1 (1C, CH_3), 77.2 (t, $CDCl_3$), 114.5 (1C, C_i), 118.6(1C, C_i), 125.8 (1C, NC(H)N).
$^{19}F\{^{1}H\}$-NMR (282.2 MHz, $CDCl_3$): δ (ppm) = -72.9 (d, J_{P-F}=712 Hz, PF_6).
$^{31}P\{^{1}H\}$-NMR (121.5 MHz, $CDCl_3$): δ (ppm) = -144.4 (heptet, J_{P-F}=712 Hz, PF_6).
HRMS (TOF, 0.5 mM NH_4OAc): (m/z) 115.0504 $[M]^+$; 137.0326 $[M-H+Na]^+$; 144.9633 $[PF_6]^-$.

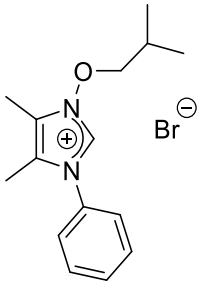

26

1-phenylimidazole-3-oxide (0.70g, 3.72 mmol) and isobutyl bromide (0.40 ml, 3.72 mmol) were dissolved in anhydrous THF (10 ml) and stirred for 80h at room temperature in a pressure tube. A TLC in MeOH/EtOAc 1:1 was performed but no product was detected. The mixture was heated at 60°C for 24h. To better dissolve the clumps, diethyl ether was added and the mixture was stirred overnight. A viscous liquid produced, so the mixture was sonicated, the solvents removed by decanting. The product was sonicated with diethyl ether, filtrated, and dried in the Schlenk line. ^{1}H NMR showed a mixture of at least 2 products. THF (10 ml) and isobutyl bromide (0.27 ml, 2.48 mmol) were added to the solid in a pressure tube and stirred with anhydrous THF (10 ml) for overnight at 100°C. The ^{1}H NMR showed the reaction did not work.

4.5.6 Phenylation

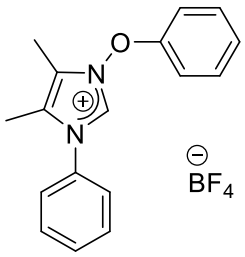

27

In a Schlenk tube anhydrous dimethylformamide (20 ml) and 1-pheny-4,5-di(methyl)imidazole-3-oxide (**8**, 0.565g, 3 mmol) were stirred with a magnetic bar for 10 minutes closing the opening with a septum. Diphenyliodonium tetrafluoroborate (1.1 g, 3 mmol) was added and the stirring was continued overnight. TLC (EtOAc:MeOH 1:1) showed the presence of starting material. Hence the mixture was heated overnight at 110°C. In TLC (EtOAc:MeOH 1:1) there was no starting material. This product was lost during the laboratory

process, but considering the analogous reaction with 1-hydroxyimidazolium-3-oxid did not work, we tried to add copper(II) as a catalyst.

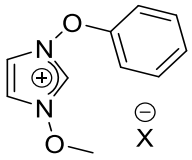

29a X=BF_4
29b X=Cl

29a, trial 1. In Schlenk tube anhydrous dimethylformamide (20 ml) and 1-metoxy-3-hydroxyimidazolium iodide (1.79 g, 7.4 mmol) were stirred with a magnetic bar for 10 minutes closing the opening of the single-neck round bottomed flask with a septum. K^tOBu (0.83 g, 7.4 mmol) was added portionwise to the solution while stirring for 15 minutes open to the air. Diphenyliodonium tetrafluoroborate (2.72 g, 7 mmol) was added and the stirring was continued overnight. TLC in 1:2 MeOH:EtOAc showed no more starting material was present. The solvent was evaporated, and the dark brown mixture extracted with CH_2Cl_2. The mixture was filtered and mixed with water (2x40ml) in a separatory funnel. A black solid was retained in the aqueous phase. $CH_2Cl_2$was evaporated to dryness. Since some impurities were detected at the ^1H NMR spectrum, the brown viscous liquid was dissolved in CH_2Cl_2, isohexane was added on top and it was stored in the fridge overnight. ^1H NMR showed no presence of the phenylated product.

29a, trial 2. In a not-dried Schlenk tube 1-metoxy-3-hydroxyimidazolium hexafluorophosphate (2.6 g, 10 mmol) and potassium carbonate (1.38g, 10 mmol) were stirred for 30 minutes in dry dimethylformamide (25ml). Diphenyliodonium tetrafluoroborate (4.42 g, 12 mmol) and copper(II) acetate monohydrate (99.8 mg, 0.5 mmol) were added. The mixture was stirred at 100 °C for 20 h and cooled down to room temperature. DMF was removed from the black mixture under vacuum (Schlenk line) under mild heating. The crude was extracted with CH_2Cl_2 and filtrated. The liquid part was concentrated under vacuum (Schlenk line) and the solid part was washed with diethyl ether and dried under vacuum. The

solid part was made of carbonate and acetate salts as it was confirmed by the absence of peaks in the ^{1}H NMR spectrum and the presence of two species in the ^{19}F NMR (PF_6^- and BF_4^-). The liquid part probably contained a phenylated species, as we can assume from the ^{1}H NMR spectrum, but TLCs in CH_2Cl_2, CH_2Cl_2+1% MeOH, CH_2Cl_2+5% MeOH, CH_2Cl_2+10% MeOH proved it difficult to separate the desired product. The product mixture was not the tetrafluoroborate species that was assumed because the ^{19}F NMR showed no peaks.

29b. Aniline (0.1 ml, 1 mmol) was dissolved in solution of sodium nitrite (0.069 g, 1 mmol) in water (0.5 ml) in a closed vial. The solution was stirred for 30 minutes at 0°C. Concentrated HCl (0,3 ml) was added and the solution was stirred at 0°C for 30 minutes. A solution of 1-methyloxyimidazole-3-oxide (0.244 g, 1 mmol) in water (3 ml) was cooled to 0°C and the diazonium salt solution was added dropwise. The mixture was stirred in a closed vial for 1 h at room temperature. ^{1}H NMR showed that the black organic phase was not the product. The water phase was dried and ^{1}H NMR spectrum did not show peaks ascribable to phenylation.

4.5.7 Pt(II) and Ag(I) NOHC complexes

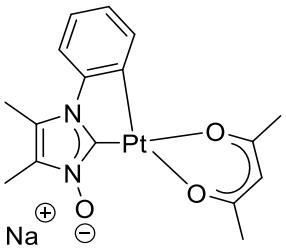

29

1-Phenylimidazole-3-oxide (90.9 mg, 0.48 mmol) and silver oxide (48.8 mg, 0.21 mmol) were added in a heated Schlenk tube. Ar atmosphere was provided and anhydrous DMF was added in counterflow. The mixture was stirred overnight at room temperature. Dichloro(1,5-cyclooctadiene)platinum(II) was added in Ar counterflow. The mixture was stirred for 24 h at room temperature, for 4 h at 120 °C and overnight at room temperature. The solvent was evaporated in high vacuum (Schlenk line) under mild heating. The black crude was extracted with dichloromethane and filtered through a Celite pad. The red-purple coloured liquid was

evaporated under vacuum (rotary evaporator). The crude was passed through a column chromatography changing the eluents: 1:4 hexane:CH_2Cl_2; pure CH_2Cl_2; 1% MeOH in CH_2Cl_2. Considering that the complex was retained by the chromatographic column, we can suppose it was charged.

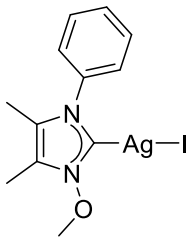

30

1-phenylimidazole-3-oxide (0.33 g, 1 mmol) and silver(I) oxide (0.116 g, 0.5 mmol) were stirred overnight in acetonitrile (15 ml) under inert atmosphere (Ar) in a non-dried Schlenk tube. The mixture was filtered with a Celite pad and the solvent evaporated from the pale yellow liquid (rotary evaporator) covering the apparatus with aluminum foil. The solid was dissolved in dichloromethane (2 ml) with an isohexane (3 ml) diffusing layer. Since no solid was obtained, the solvents were evaporated and the product was sonicated in 50 ml of isohexane for 2 times and the white powder precipitated was washed twice with diethyl ether and dried in the Schlenk line. Yield: 0.281 g, 0.6 mmol, 64.3%.

^{1}H NMR (300 MHz, DMSO-d6): δ (ppm) = 2.02 (s, 3H, CH_3), 2.43 (s, 3H, CH_3), 3.99 (s, 3H, OCH_3), 7.43-7.50 (m, 2H, CH_{arom}), 7.50-7.56 (m, 3H, CH_{arom}).

A singlet at 9.93 ppm shows the presence of non-reacted proligand. To remove it some solubility trials were performed, but the complex and the **9** are both soluble in dichloromethane and isohexane and insoluble in ethyl acetate. The product did not move in TLC using dichloromethane as an eluent. 5% methanol in dichloromethane gave smeared spots.

One equivalent of Ag_2O (0.6mmol, 0.067 g) was added to the product (0.2537 g, 0.6 mmol) and stirred overnight in acetonitrile (9 ml) under inert atmosphere in a not-dried Schlenk tube in order to complex the remaining free NOH proligand. The product was a viscous black liquid and the ^{1}H NMR spectrum showed the presence of the **9**.

4.6 Solid state structure details

Preliminary examination and data collection for single crystals of **11** and **14** were carried out on a Bruker D8 VENTURE (KAPPA goniometer, PHOTON detector) single crystal-diffractometer equipped with an Oxford Cryosystem (Cryostream 800) cooling system at the window of a sealed x-ray tube using monochromated Mo-Kα radiation (λ = 0.71073 Å) (Incoatec IμS3.0 microfocus source equipped with multilayer optics).

Idealized geometries were assigned to the hydrogen atoms. Intensity data were extracted using the APEX3 suite[82] including the SAINT software package.[83] The reflections were merged and corrected from Lorentz, polarization and decay effects and absorption correction was applied based on multiple scans.[84] The structure was solved by a combination of dual space,[85] direct methods with the aid of difference Fourier synthesis and were refined against all data using SHELXTL-XTMP.[86] Hydrogen atoms were assigned to ideal positions using the SHELXTL-XTMP riding model. All non-hydrogen atoms were refined with anisotropic displacement parameters. Full-matrix least-squares refinements were carried out by minimizing $\Sigma w(Fo^2-Fc^2)^2$ with the SHELXTL-XTMP weighting scheme. Neutral-atom scattering factors for all atoms and anomalous dispersion corrections for the non-hydrogen atoms were taken from the International Tables for Crystallography.[87] All calculations were performed with the APEX3 suite[82] including SAINT software package,[83] the SHELX program package[88] and PLATON.[89]

Complex **15** crystallographic data were collected on a Bruker D8 Venture Photon II single-crystal diffractometer working with monochromatic Mo-Kα radiation and equipped with an area detector. The structures were solved by direct methods and refined against F2 with SHELXL-2014/7 with anisotropic thermal parameters for all non-hydrogen atoms.[88,90] For the visualization Mercury[91] was used.

In Table 10 details of X-ray data collection are reported.

Table 10. X-Ray data collected.

Complex	**11**	**14**	**15**
Formula	$C_{17}H_{20}N_2O_3Pt$	$C_{39}H_{40}N_2O_3Pt$	$C_{18}H_{18}AuBrN_2O$
Formula weight	495.43	779.81	698.09
Crystal system	Triclinic	Triclinic	Monoclinic
Space group	P -1	P -1	P 2_1/n
a/Å	7.4545(9)	7.0873(4)	11.184(3)
b/Å	10.2906(12)	15.5352(10)	14.559(5)
c/Å	11.2348(13)	15.6123(10)	11.536(4)
α/°	79.217(4)	73.911(2)	90.00
β/°	84.616(4)	87.614(2)	105.929(14)
γ/°	74.004(4)	87.428(2)	90.00
Volume/Å^3	813.02(17)	1649.20(18)	1806.26
T (K)	150	150	200
Z	2	2	4
D_{calc}/g·cm^{-3}	2.024	1.570	2.042
F(000)	476.0	780.0	1048
μ(Mo-Kα)/mm^{-1}	8.645	4.294	10.362
Reflections collected	38885	234359	76346
Unique reflections	4064	8196	4522
Observed reflections	3994	7946	4021
[I > 2σ(I)]	[Rint = 0.0435]	[Rint = 0.0314]	[Rint = 0.0590,]
R [I > 2σ(I)]	*R*1 = 0.0274,	*R*1 = 0.0147,	*R*1 = 0.0324,
	*wR*2 = 0.0648	*wR*2 = 0.0410	*wR*2 = 0.0918
R [all data]	*R*1 = 0.0279,	*R*1 = 0.0156,	*R*1 = 0.0382,
	*wR*2 = 0.0651	*wR*2 = 0.0417	*wR*2 = 0.0961

Chapter 5: APPENDIX

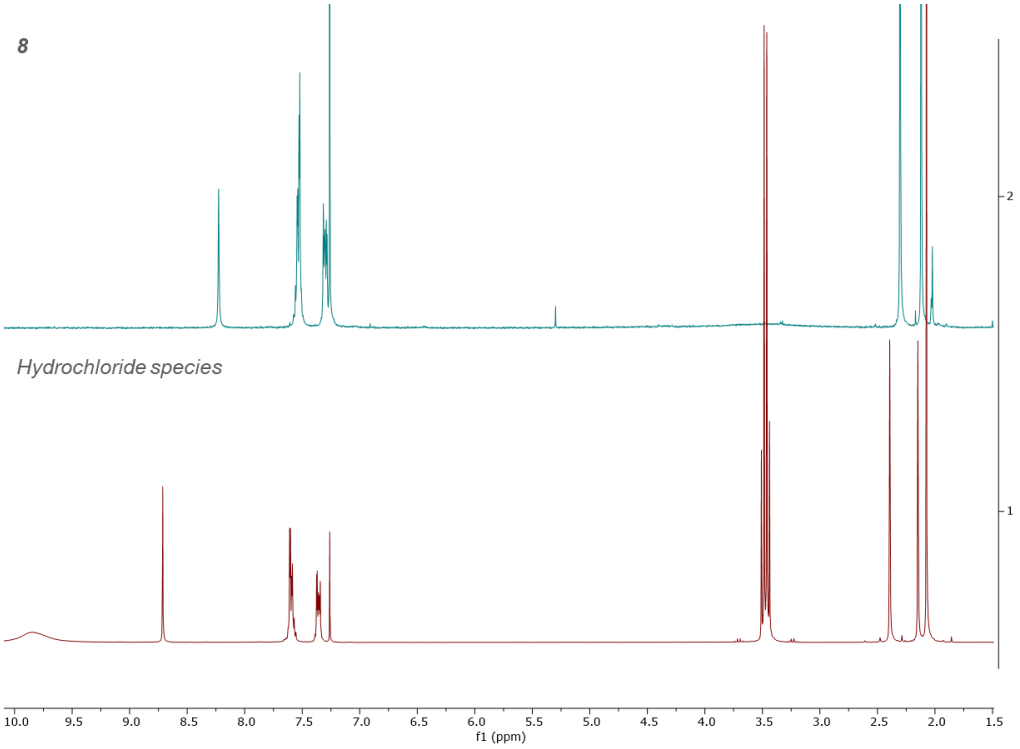

*Figure A 1 ^{1}H NMR spectra (25°C, $CDCl_3$) of compound **8** and its hydrochloride.*

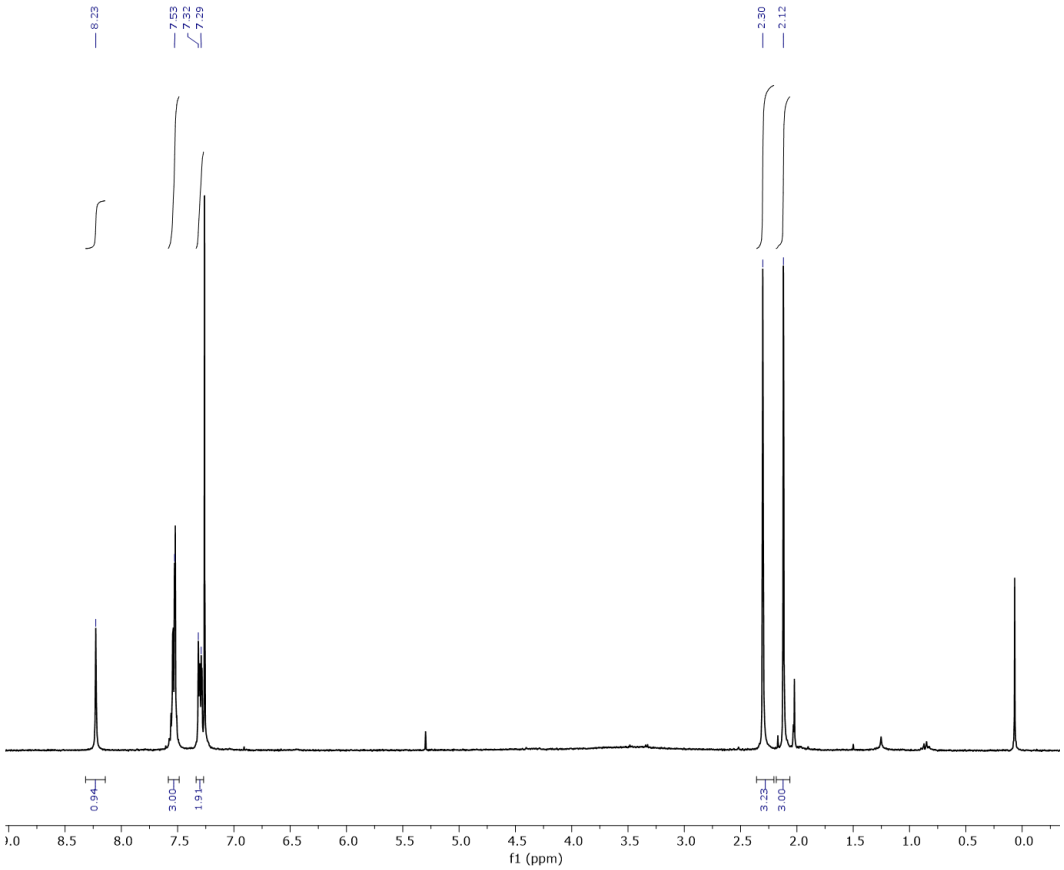

*Figure A 2. ^{1}H NMR ($CDCl_3$, 25°C) of compound **8**.*

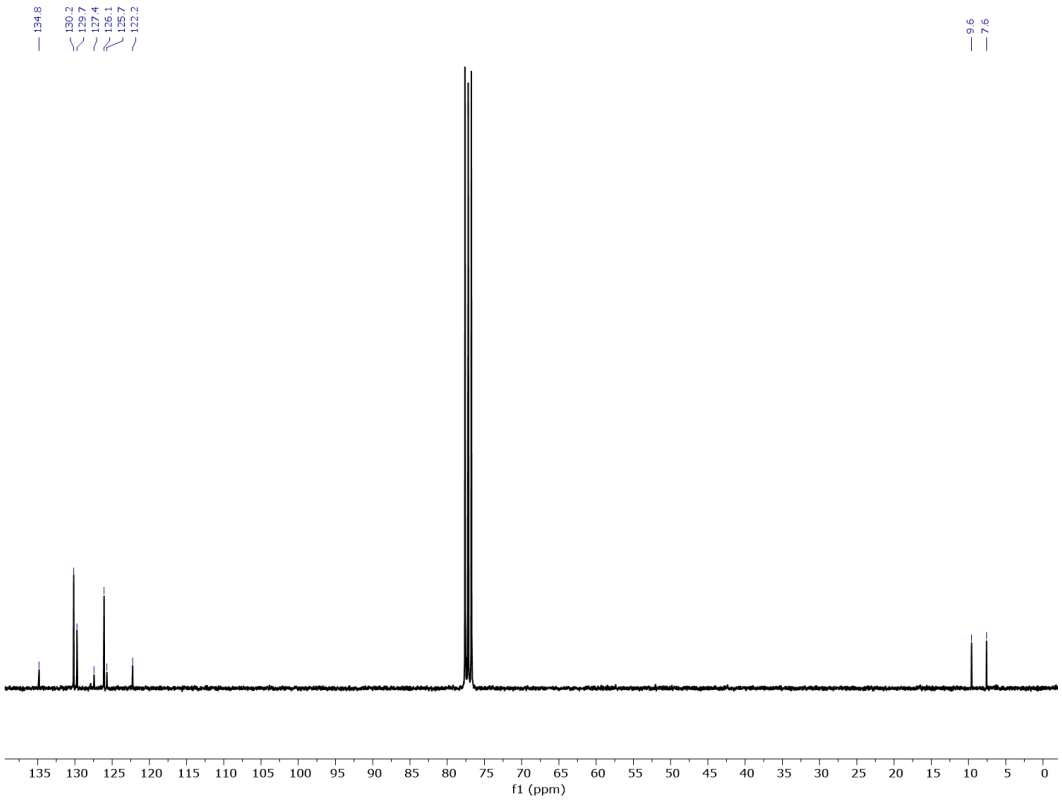

*Figure A 3. $^{13}C\{^{1}H\}$-NMR ($CDCl_3$, 25°C) of compound **8**.*

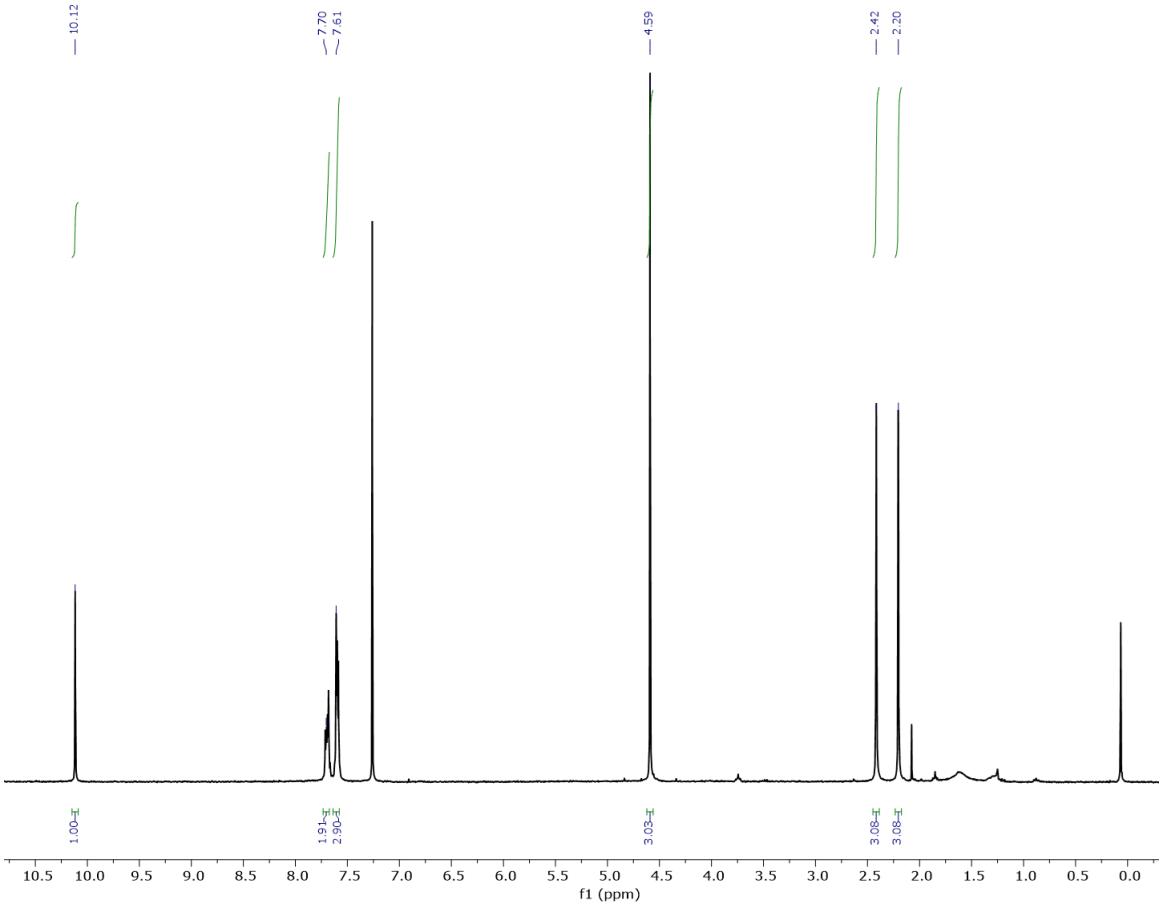

*Figure A 4. ^{1}H NMR ($CDCl_3$, 25°C) of compound **9**.*

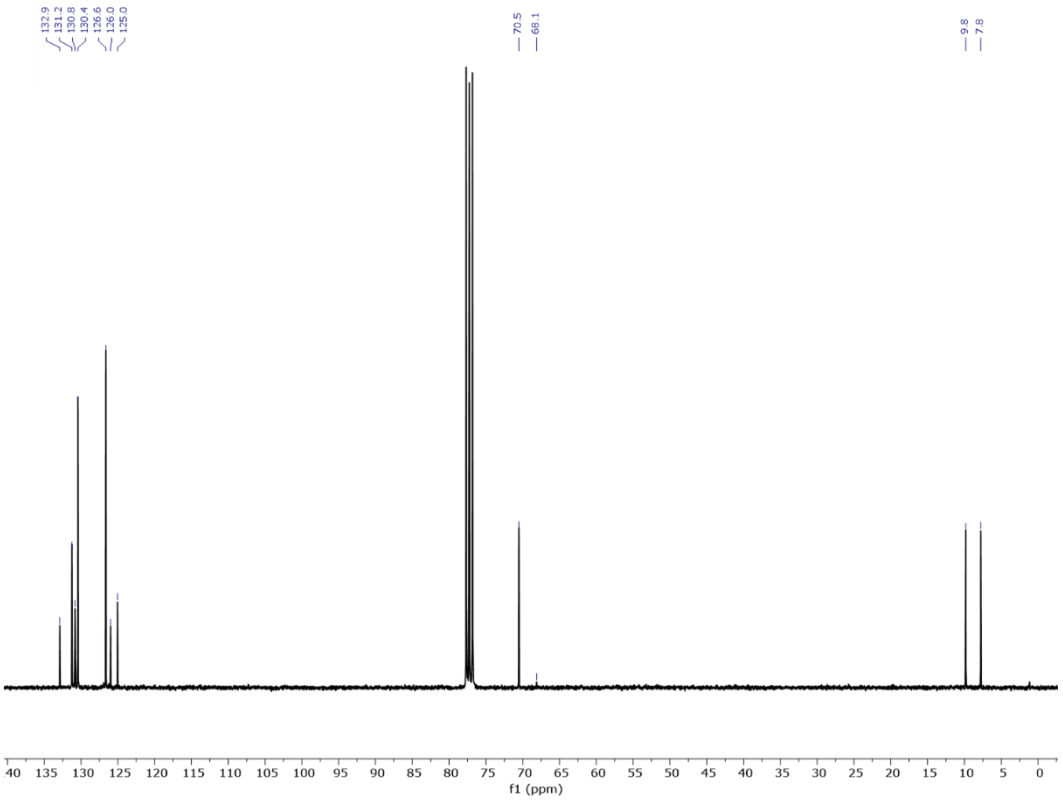

*Figure A 5. $^{13}C\{^{1}H\}$-NMR ($CDCl_3$, 25°C) of compound **9**.*

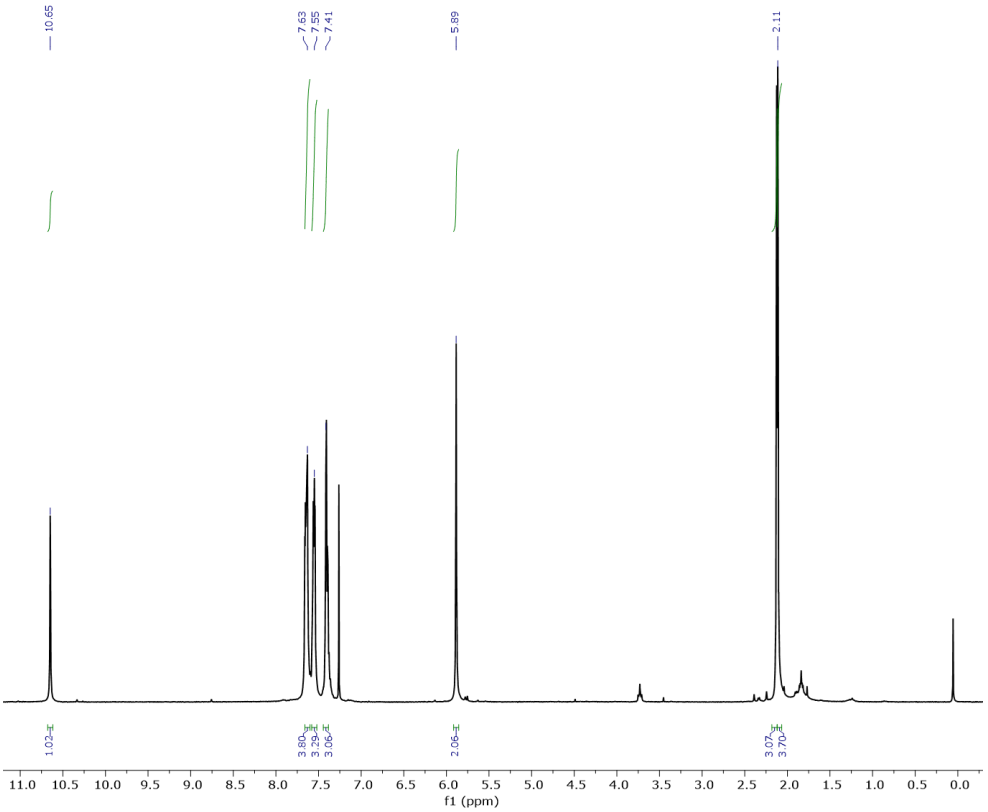

*Figure A 6. ^{1}H NMR ($CDCl_3$, 25°C) of compound **10**.*

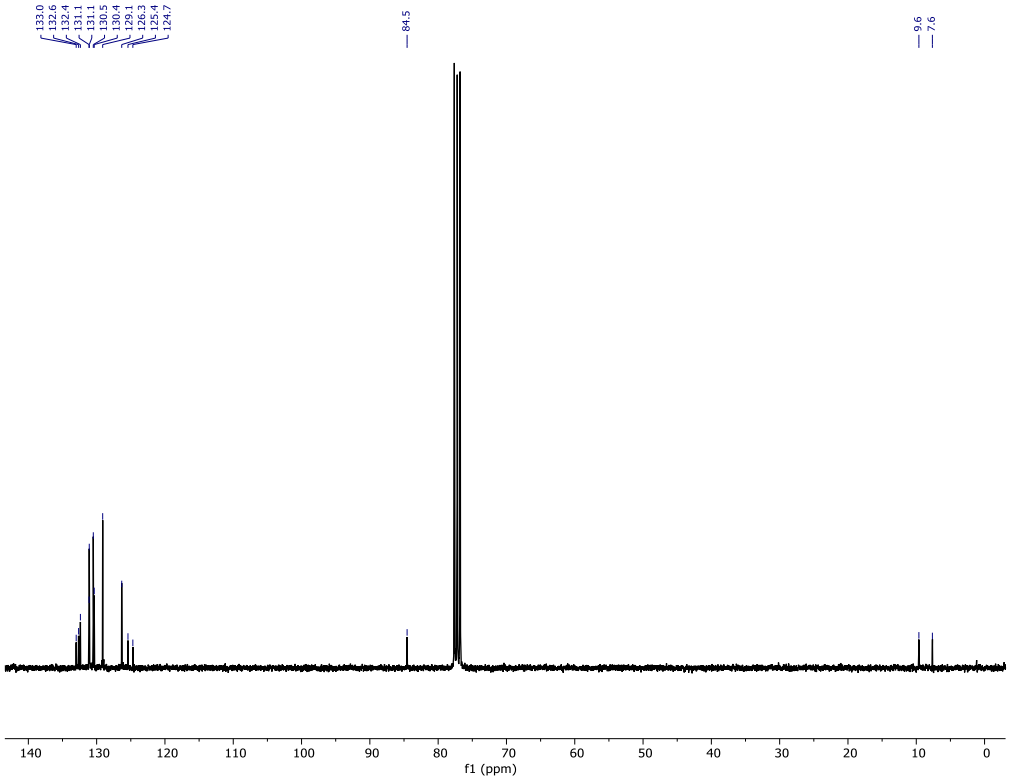

*Figure A 7. $^{13}C\{^{1}H\}$-NMR ($CDCl_3$, 25°C) of compound **10**.*

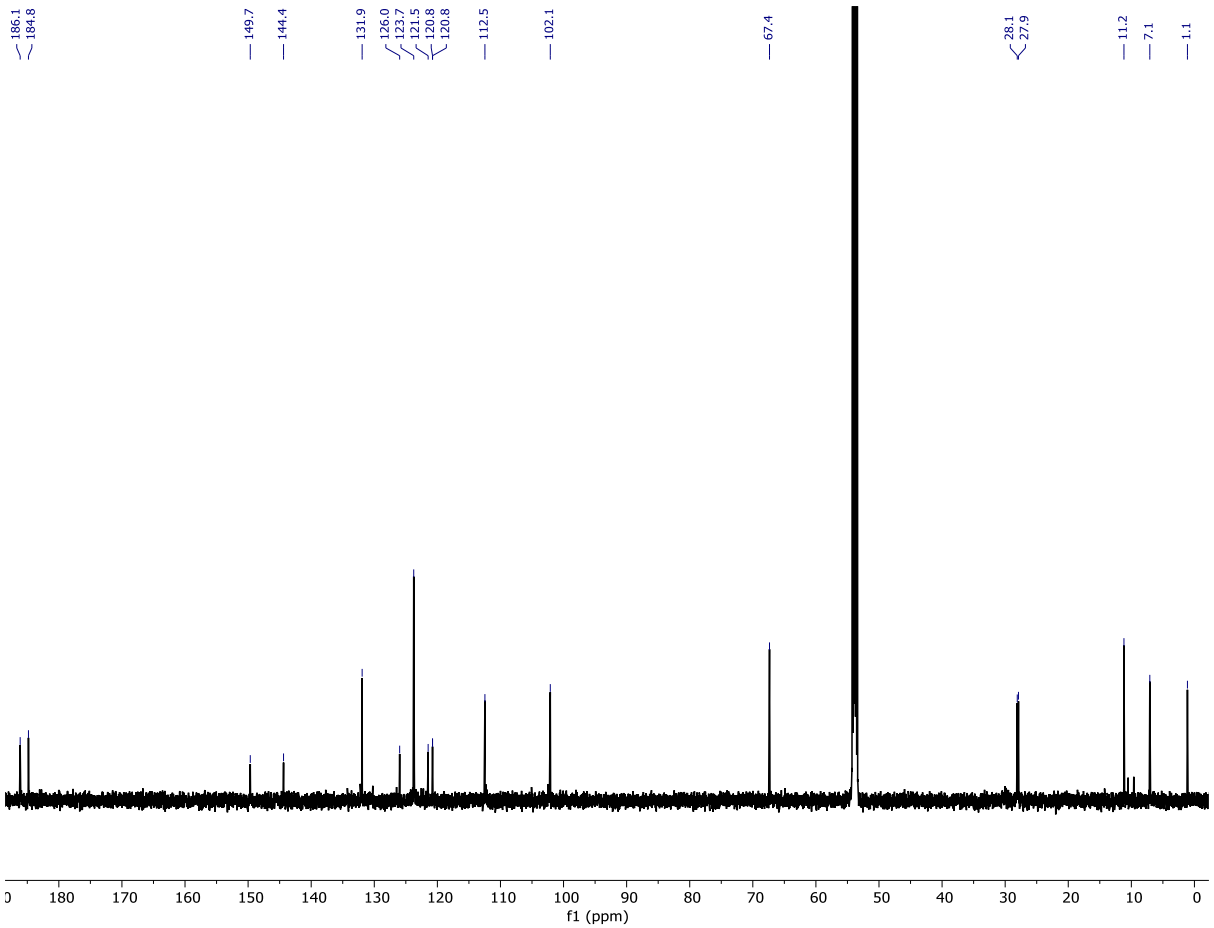

*Figure A 8. $^{13}C\{^{1}H\}$-NMR (CD_2Cl_2, 25°C) of compound **11**.*

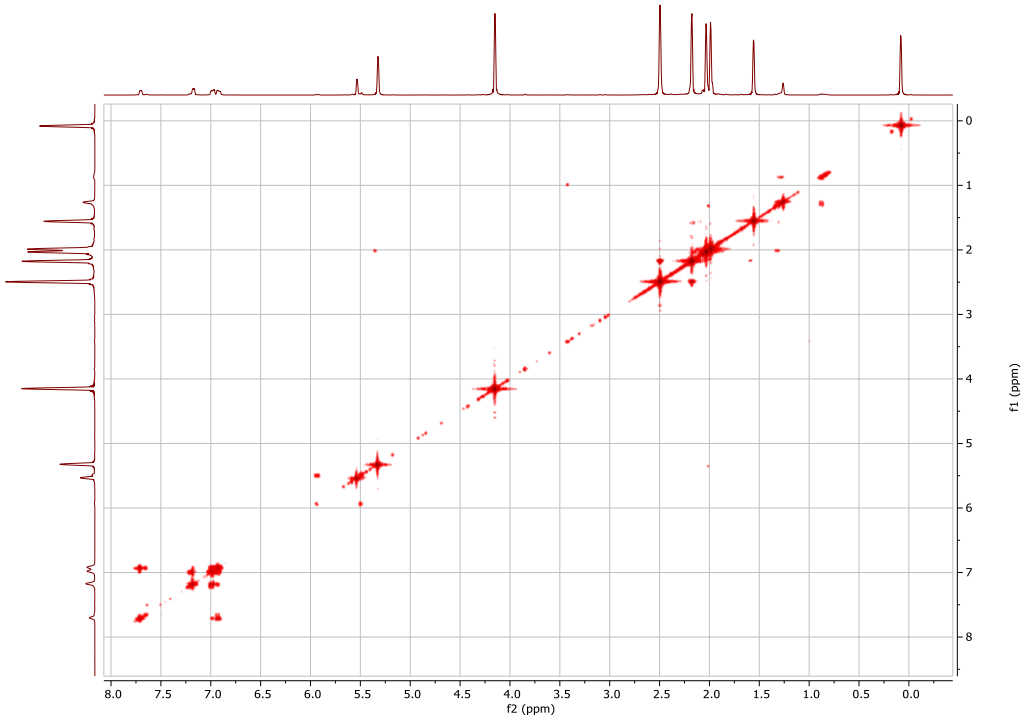

*Figure A 9. COSY spectrum of compound **11** (CD_2Cl_2, 25°C).*

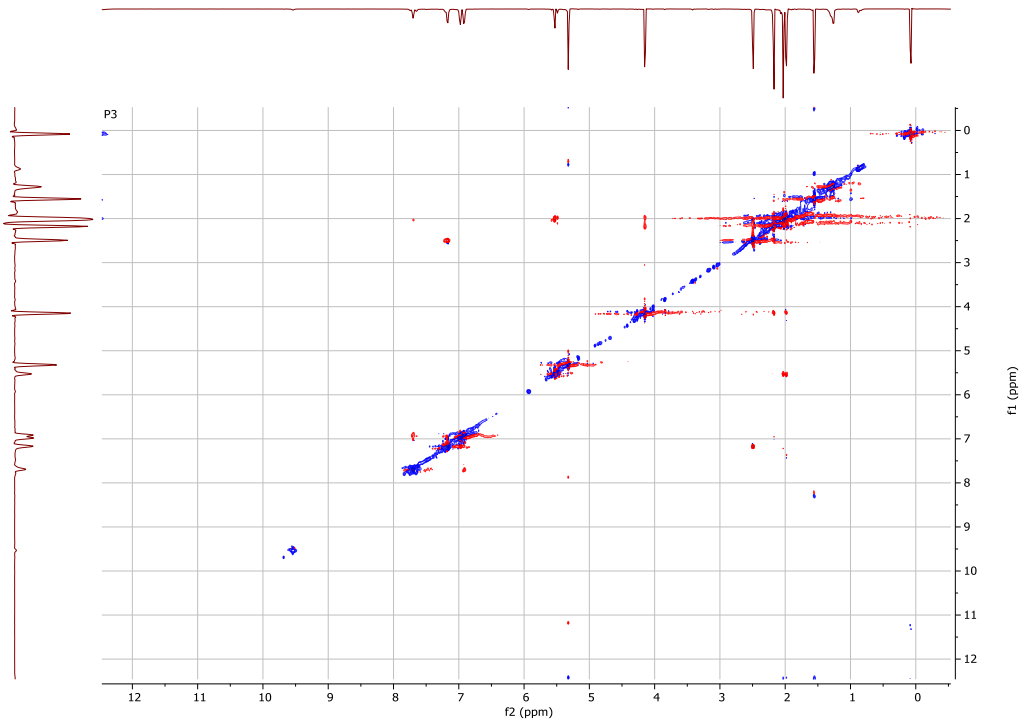

*Figure A 10. NOESY spectrum of compound **11** (CD_2Cl_2, 25°C).*

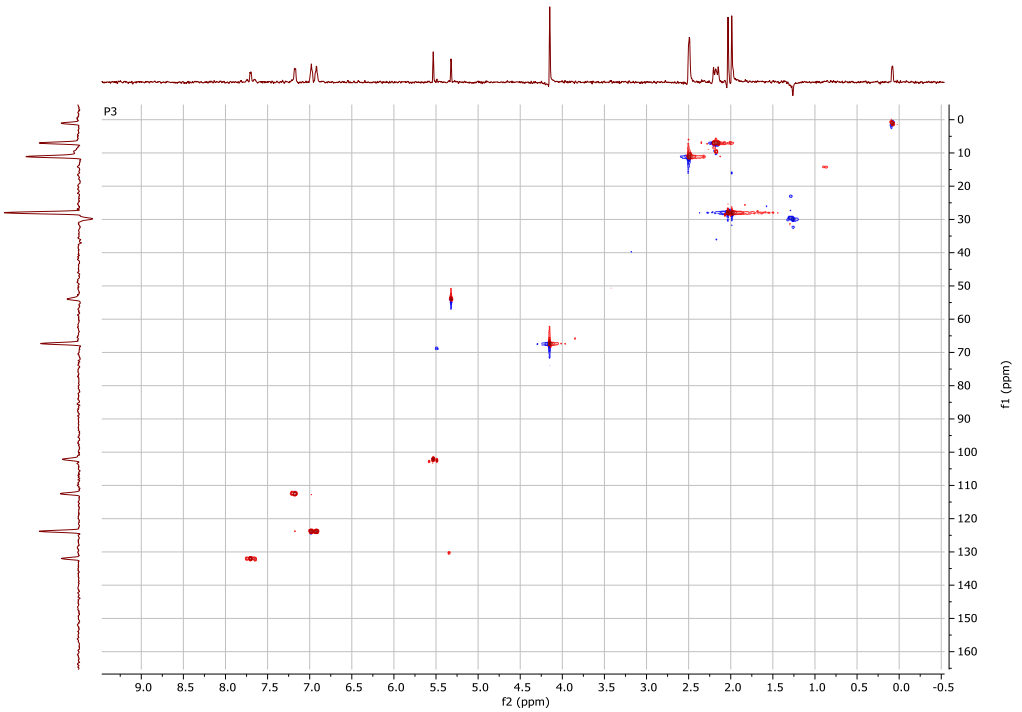

*Figure A 11. HSQC spectrum of compound **11** (CD_2Cl_2, 25°C).*

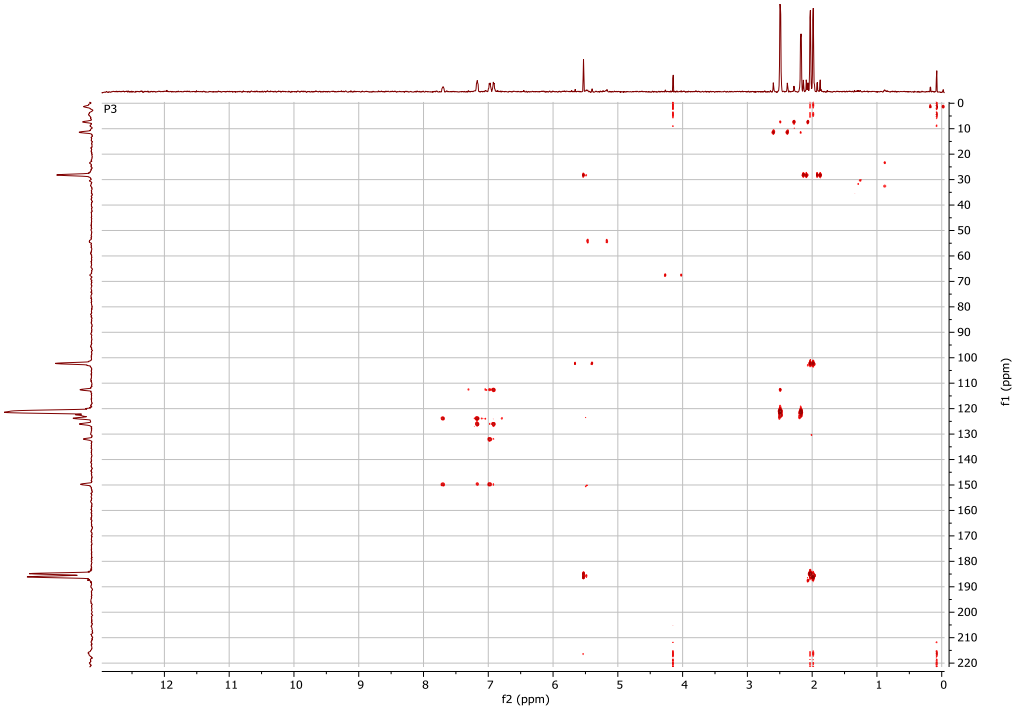

*Figure A 12. HMBC spectrum of compound **11** (CD_2Cl_2, 25°C).*

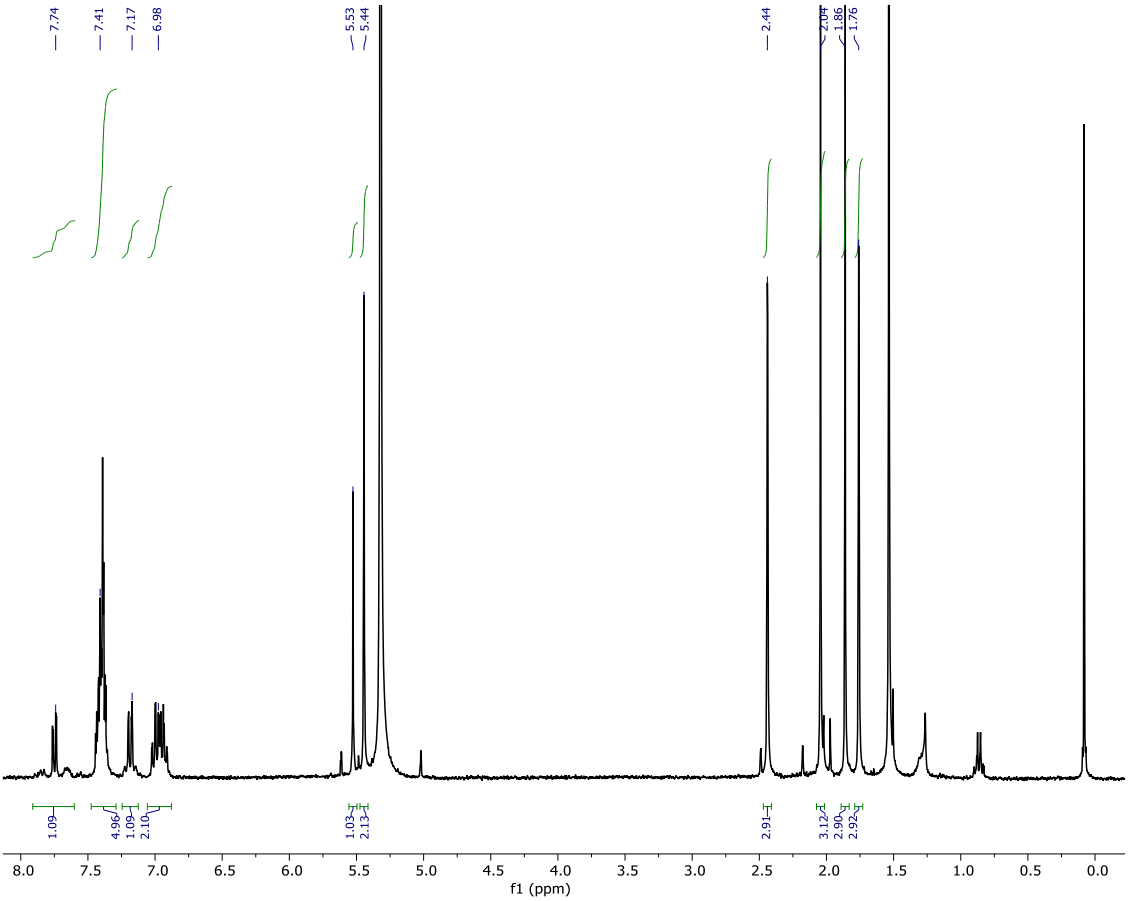

*Figure A 13. ^1H NMR (CD_2Cl_2, 25°C) of compound **12**.*

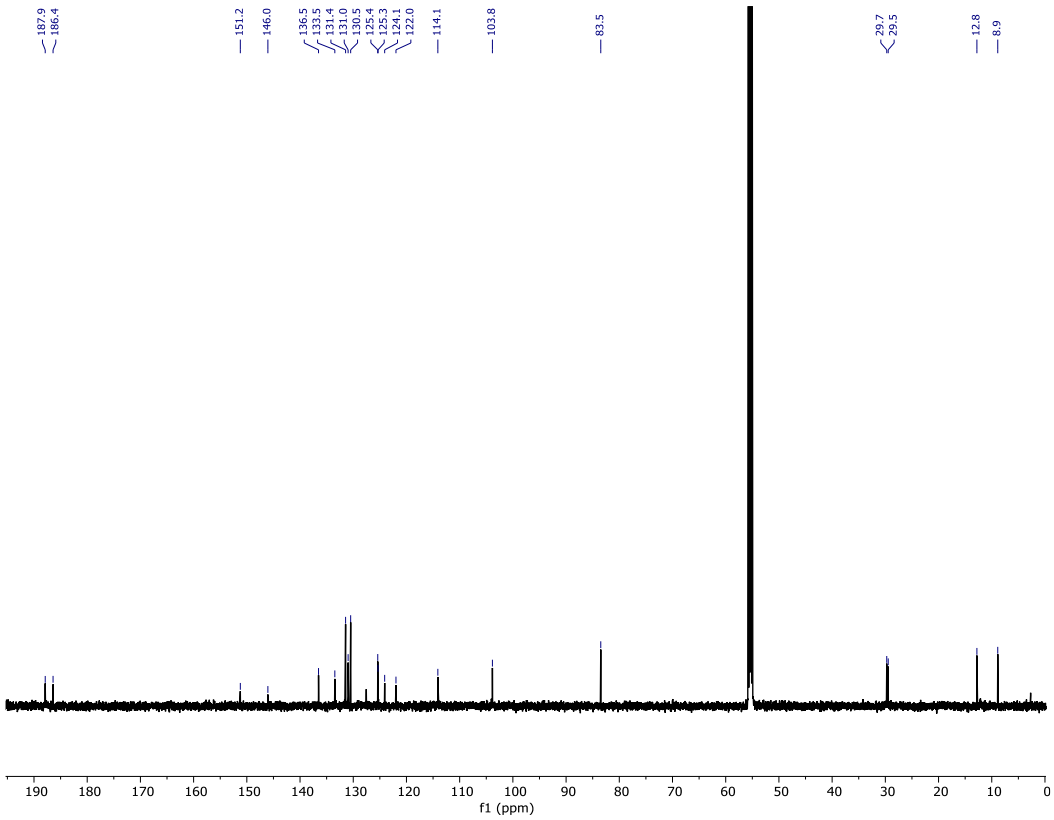

*Figure A 14. $^{13}C\{^{1}H\}$-NMR (CD_2Cl_2, 25°C) of compound **12**.*

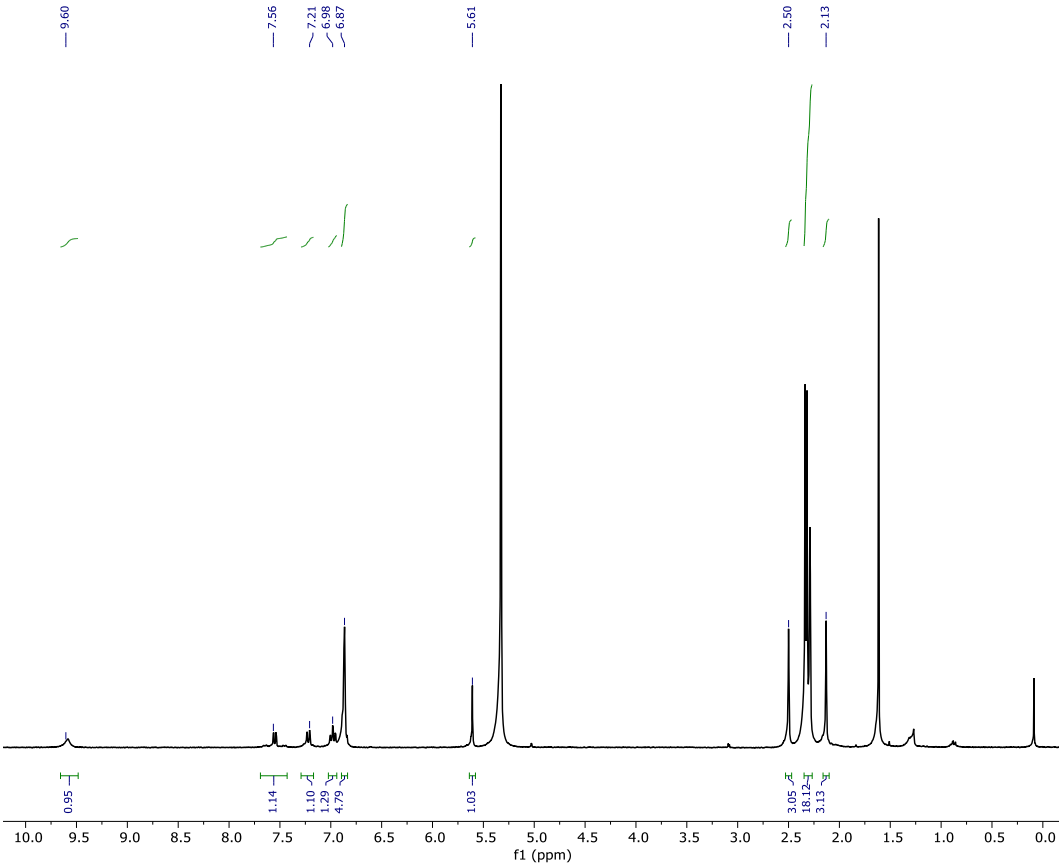

*Figure A 15. ^{1}H NMR (CD_2Cl_2, 25°C) of compound **13**.*

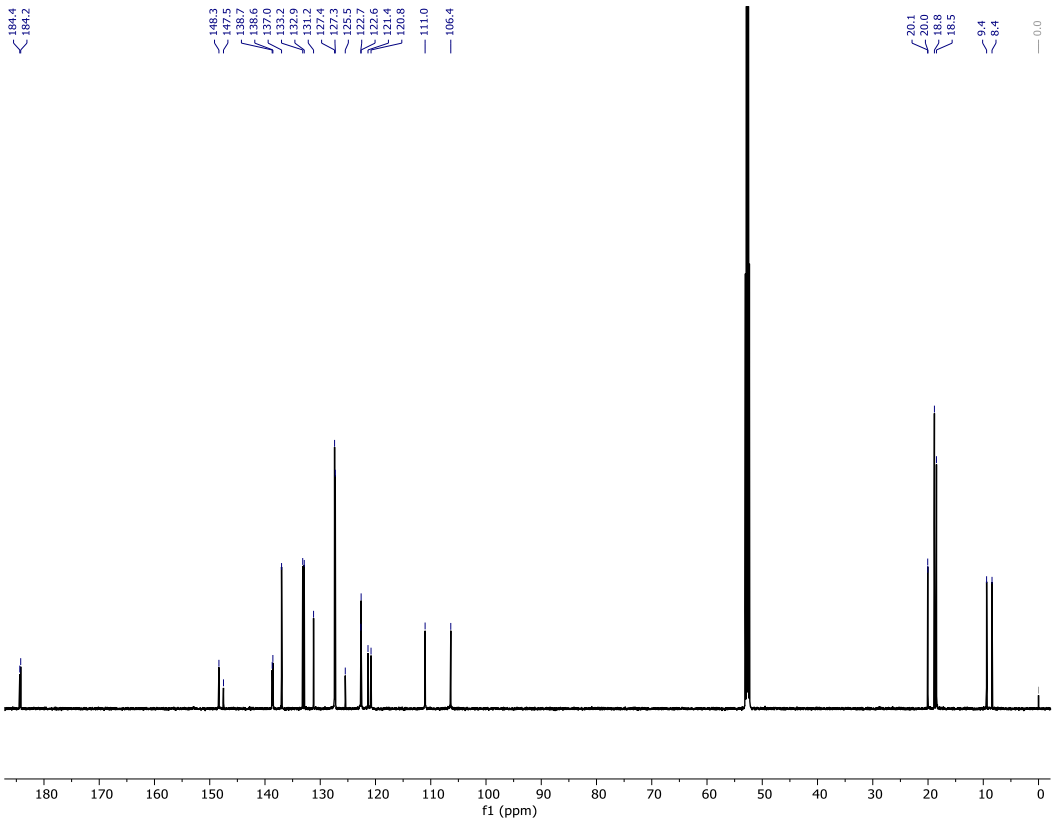

*Figure A 16. $^{13}C\{^{1}H\}$-NMR (CD_2Cl_2, 25°C) of compound **13**.*

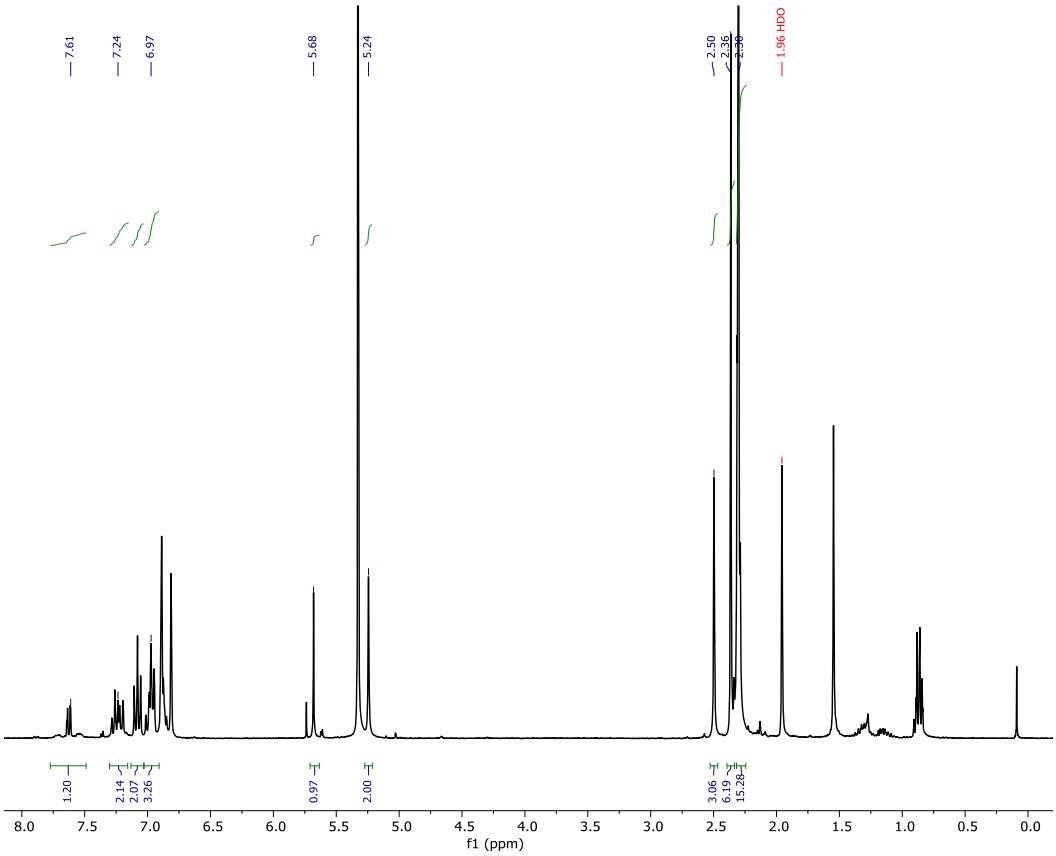

*Figure A 17. ^{1}H NMR (CD_2Cl_2, 25°C) of compound **14**.*

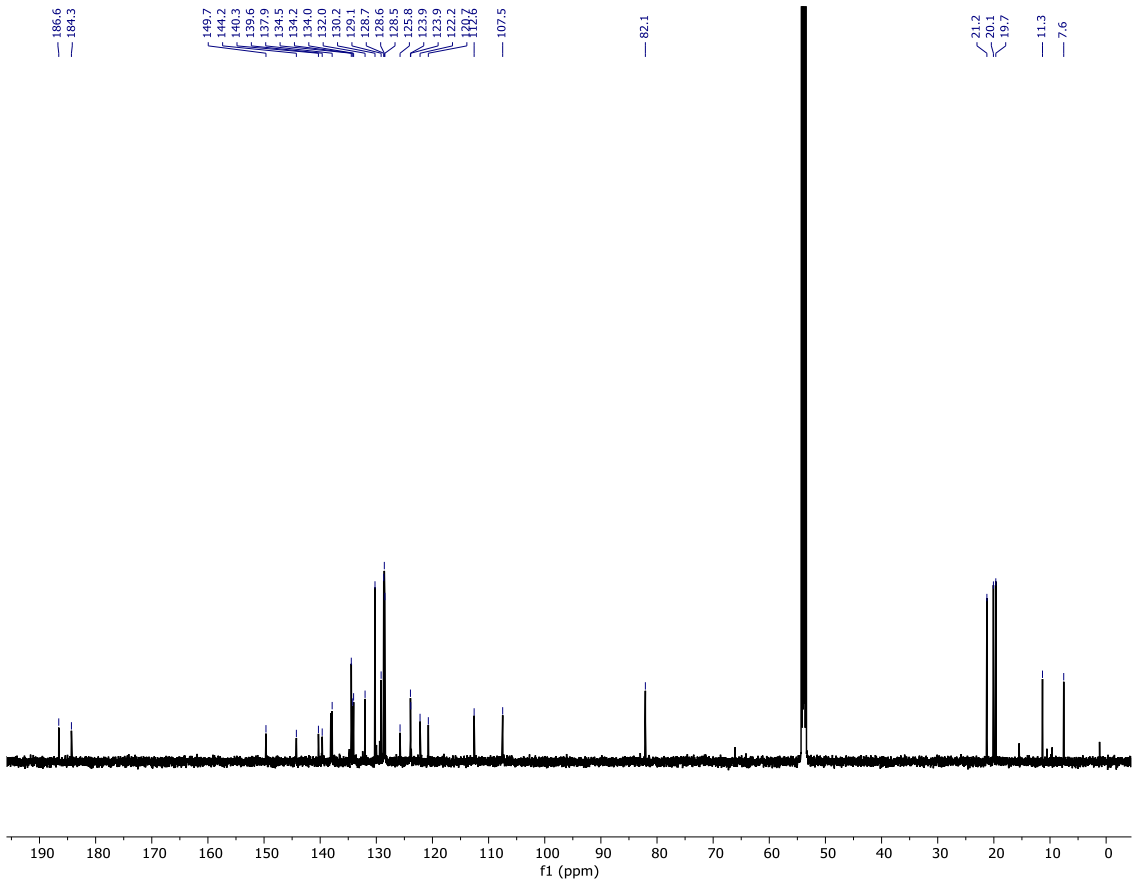

*Figure A 18. $^{13}C\{^{1}H\}$-NMR (CD_2Cl_2, 25°C) of compound **14**.*

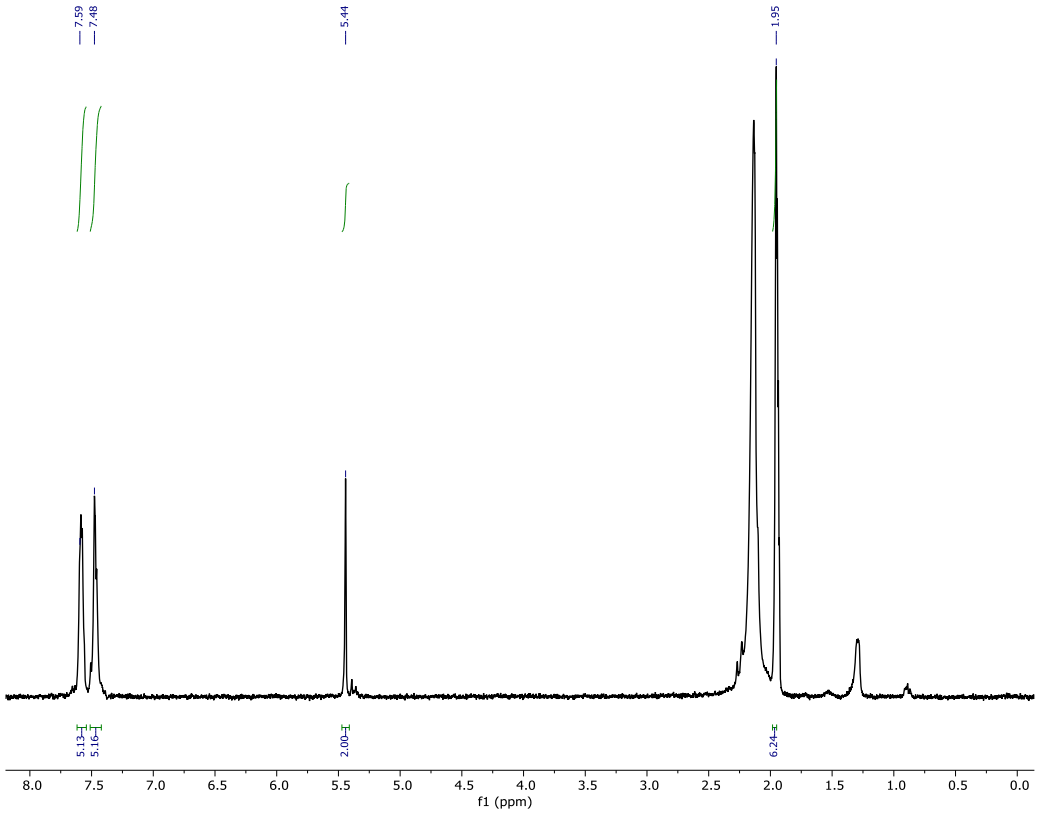

*Figure A 19. ^{1}H NMR (CD_3CN, 25°C) of compound **15**.*

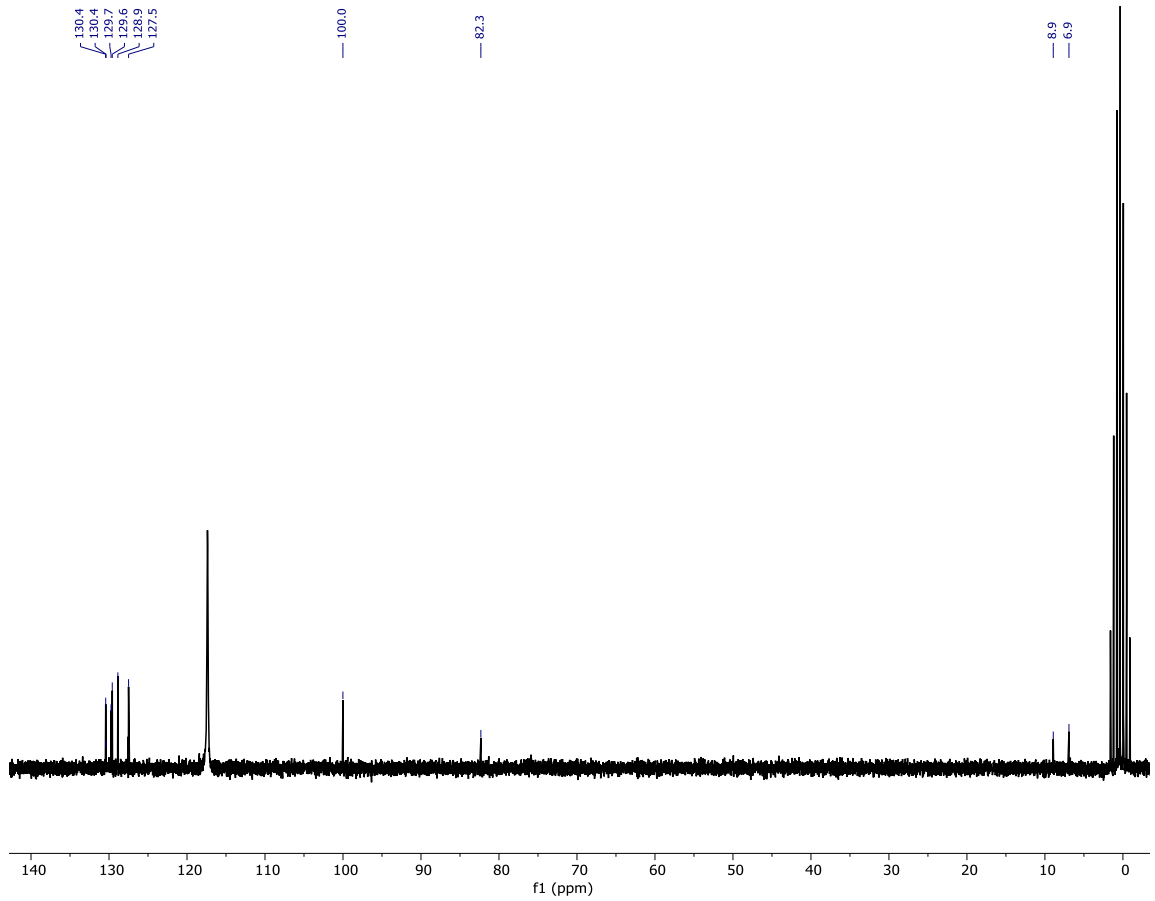

*Figure A 20. $^{13}C\{^{1}H\}$-NMR (CD_3CN, 25°C) of compound **15**.*

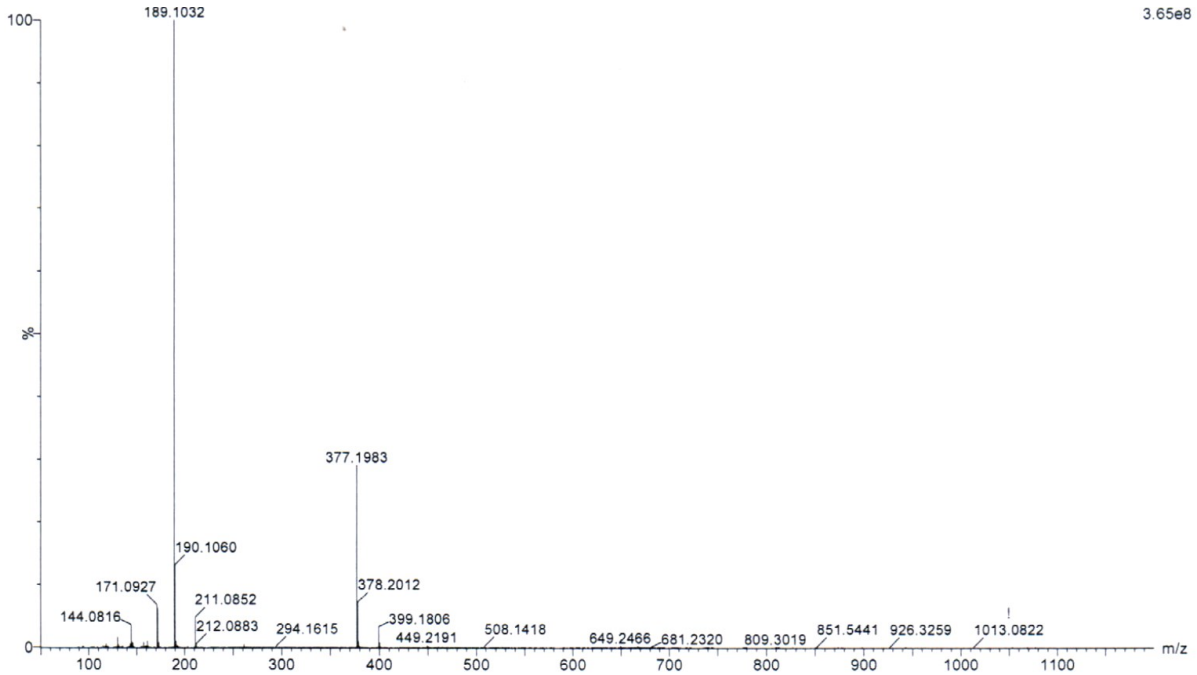

*Figure A 21. HRMS of compound **8**.*

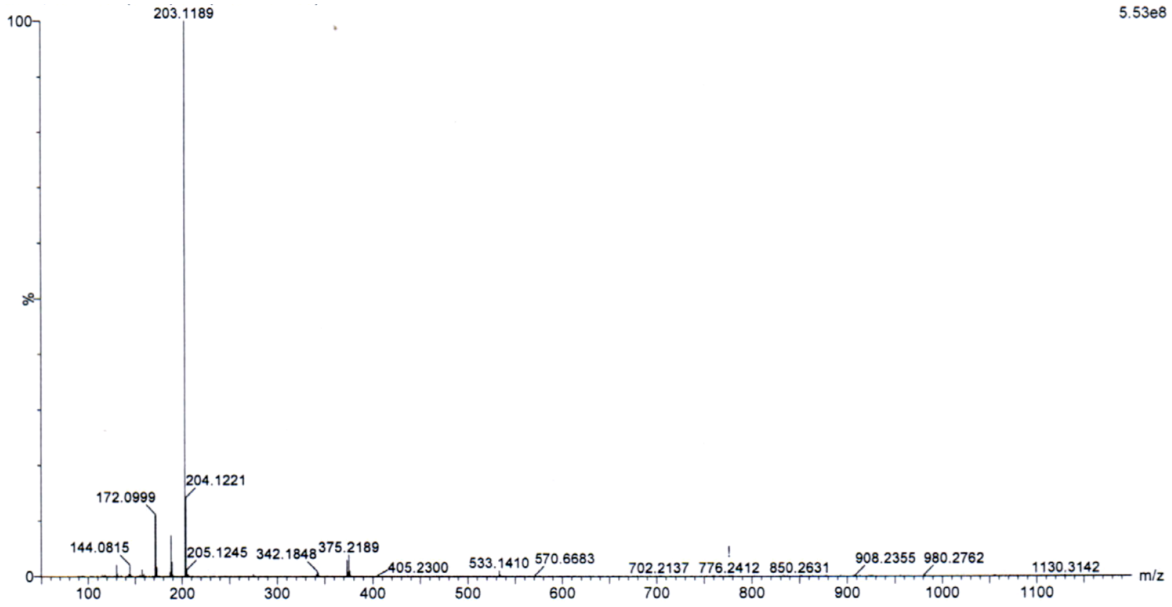

*Figure A 22. HRMS of compound **9**.*

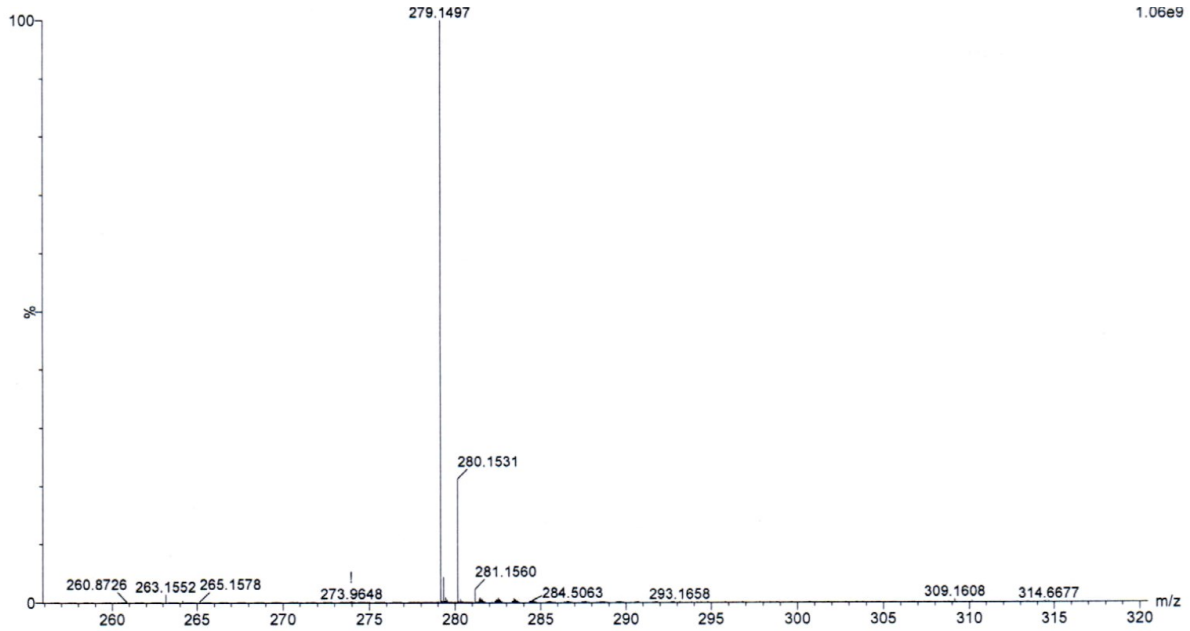

*Figure A 23. HRMS of compound **10**.*

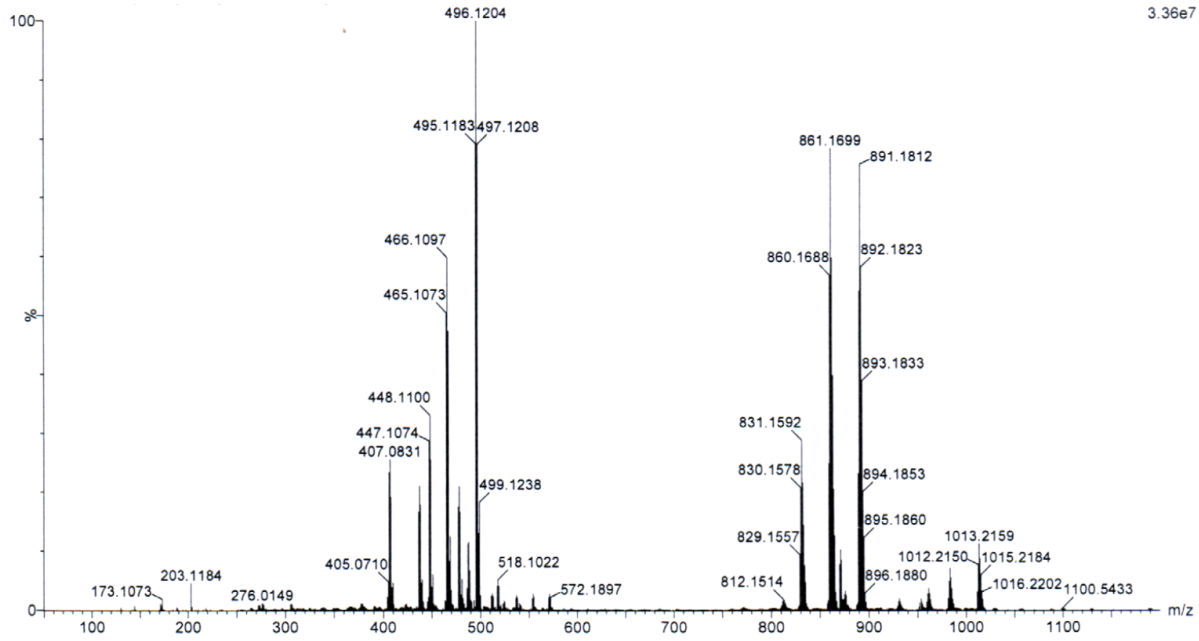

*Figure A 24. HRMS of compound **11**.*

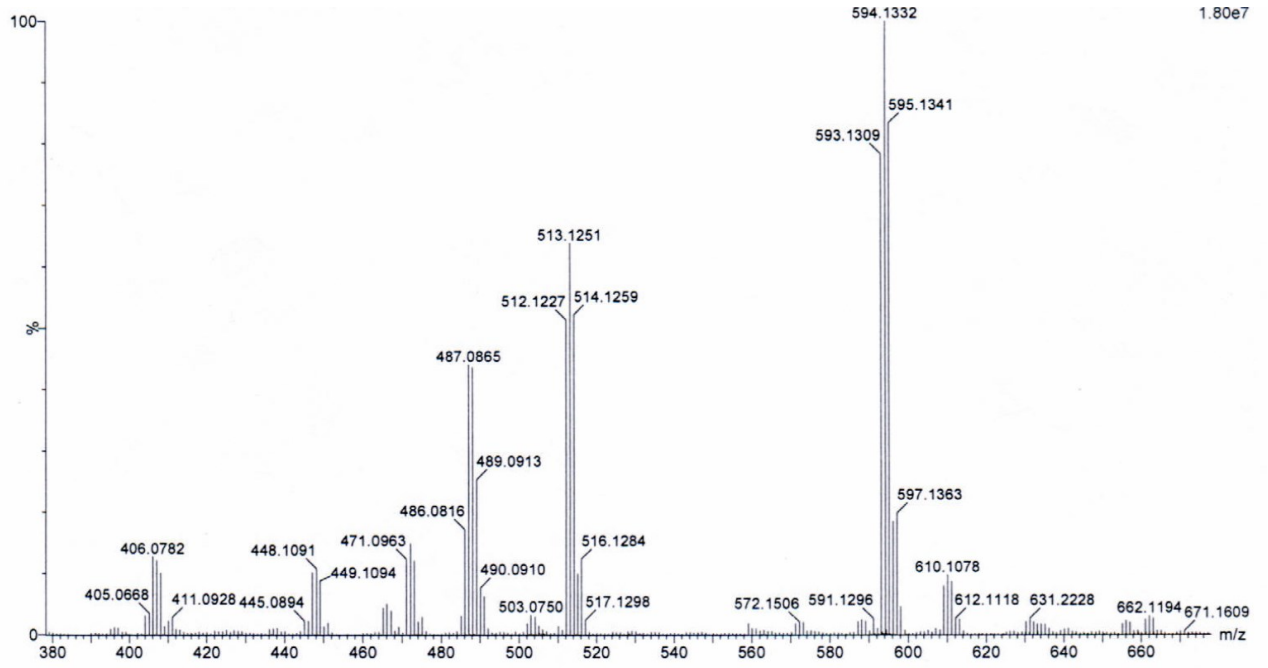

*Figure A 25. Detail of the HRMS of compound **12**.*

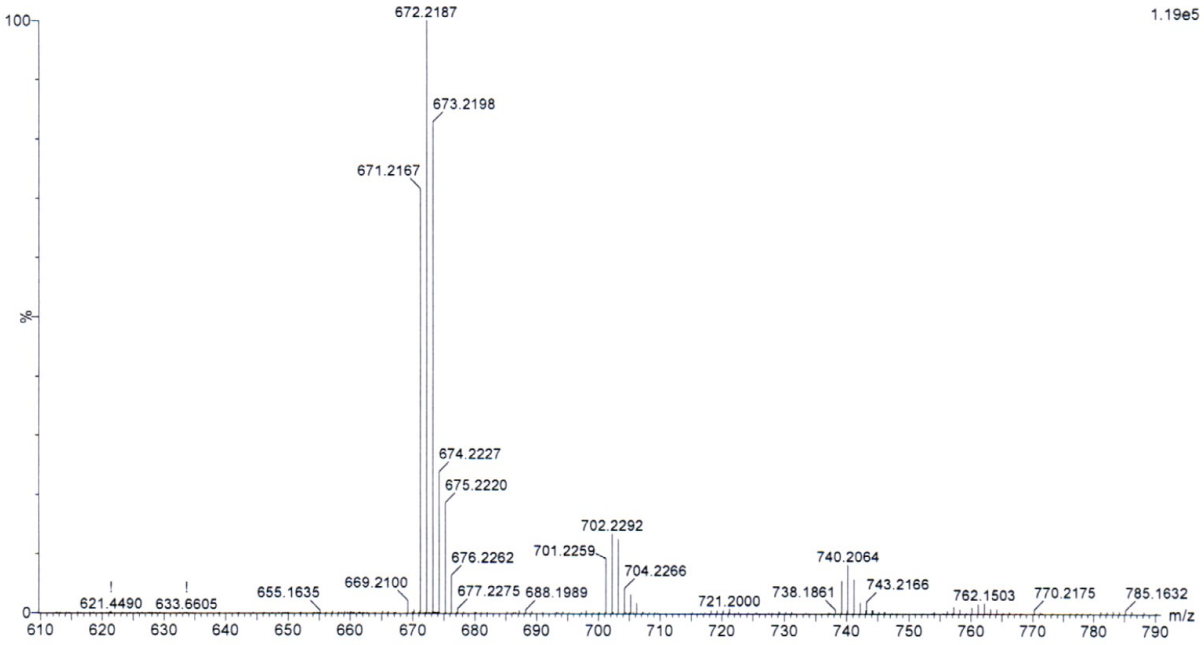

*Figure A 26. Detail of the HRMS of compound **13**.*

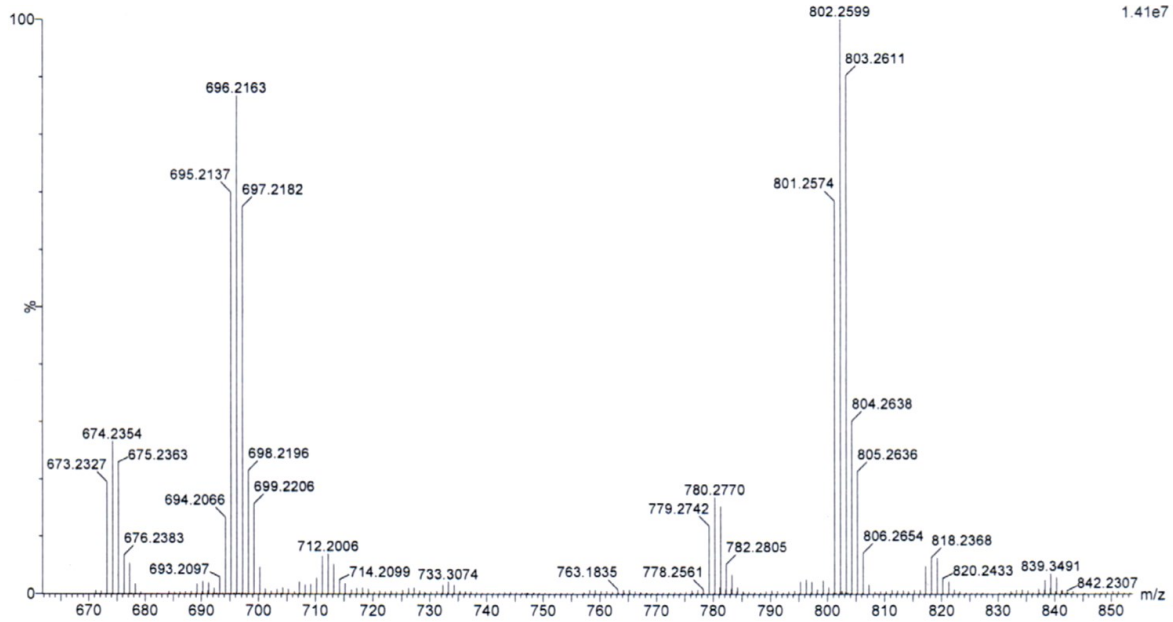

*Figure A 27. Detail of the HRMS of compound **14**.*

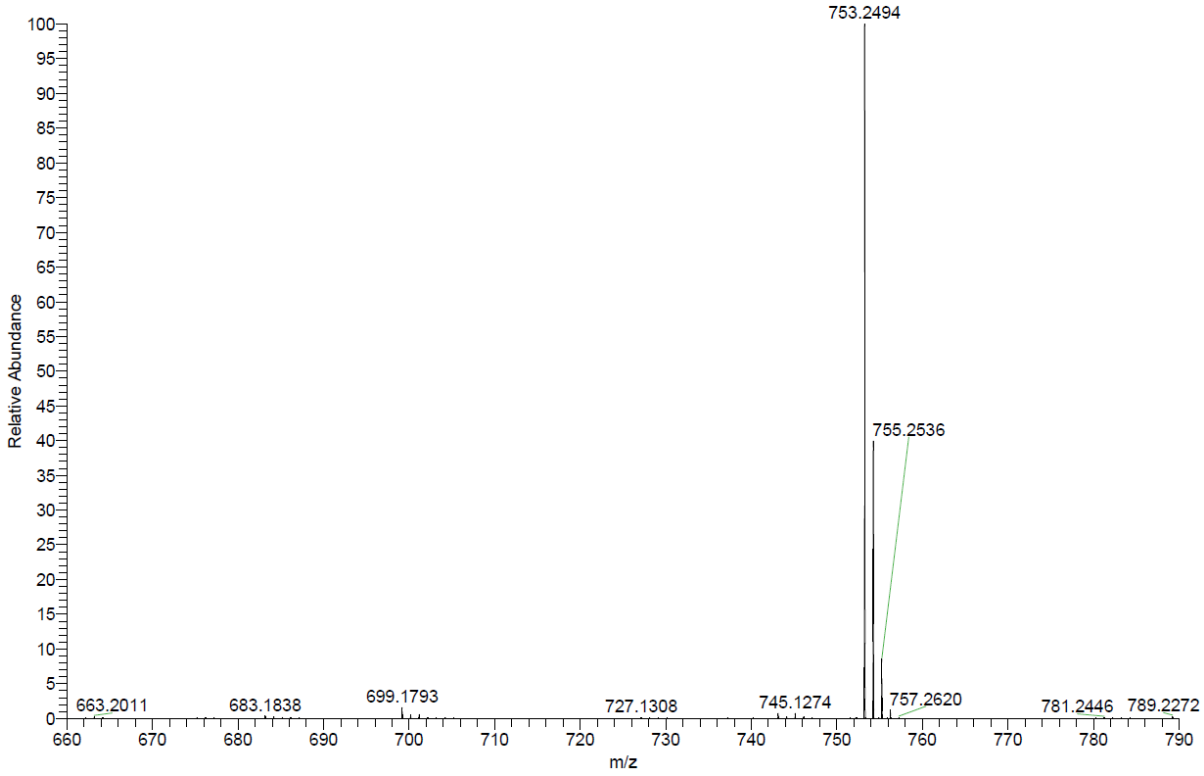

*Figure A 28. Detail of the HRMS of compound **15**.*

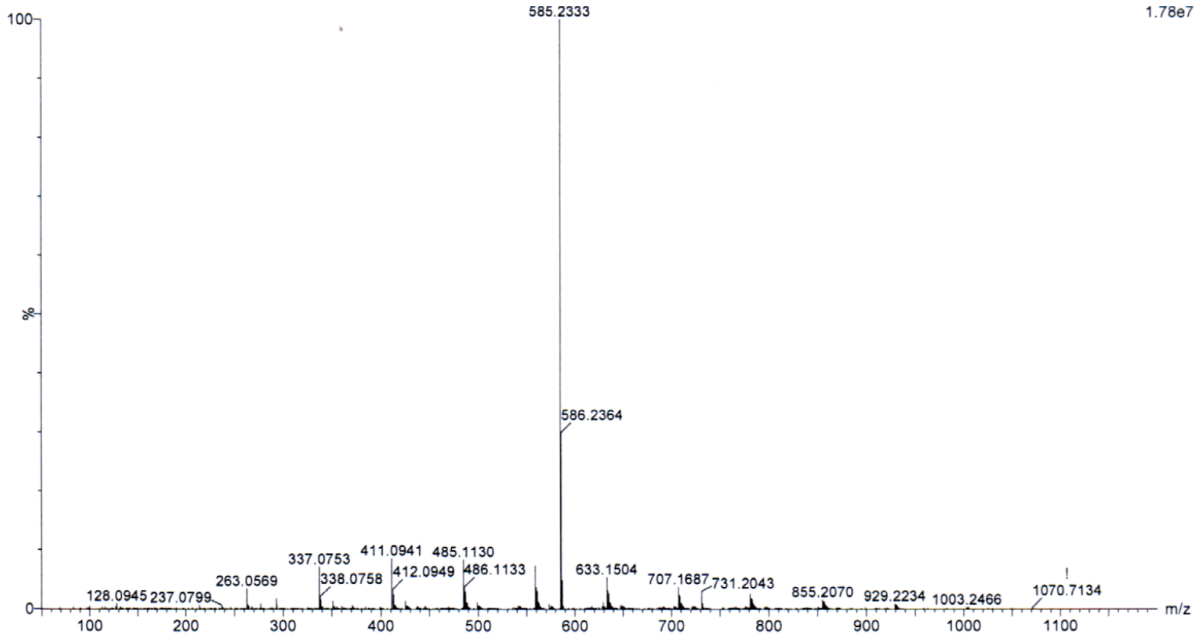

*Figure A 29. HRMS of the solid collected after deoxygenation of compound **24**.*

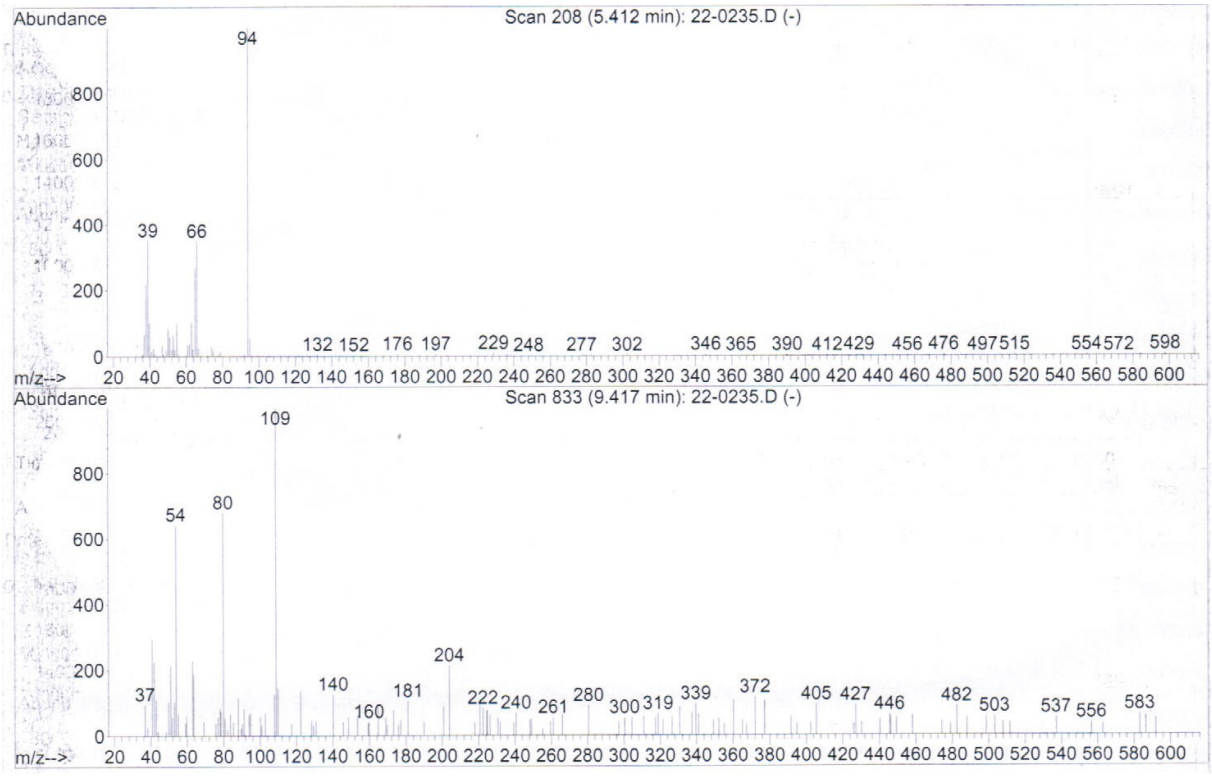

*Figure A 30. GC-MS analysis of compound **21**. The MS spectrum at retention time=5.412 min highlighted the formation of phenol, the one at 9.417 min of the starting material confirming the decomposition of the imine.*

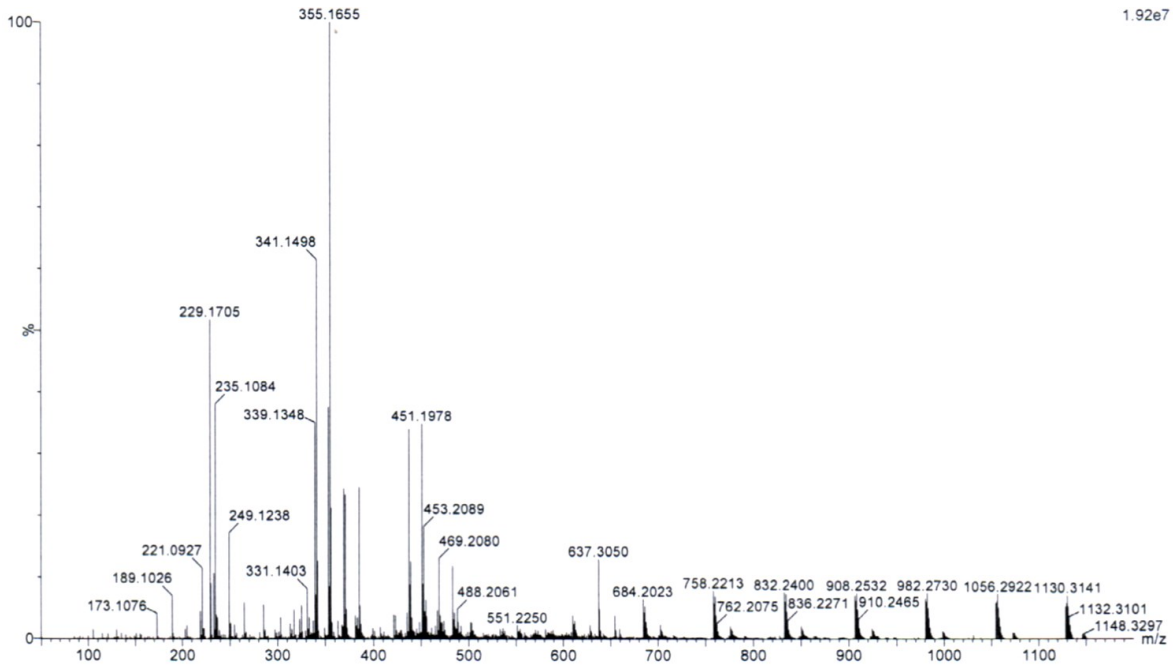

Figure A 31. Polymerization pattern displayed in the HRMS of the macrocycle synthesis attempt.

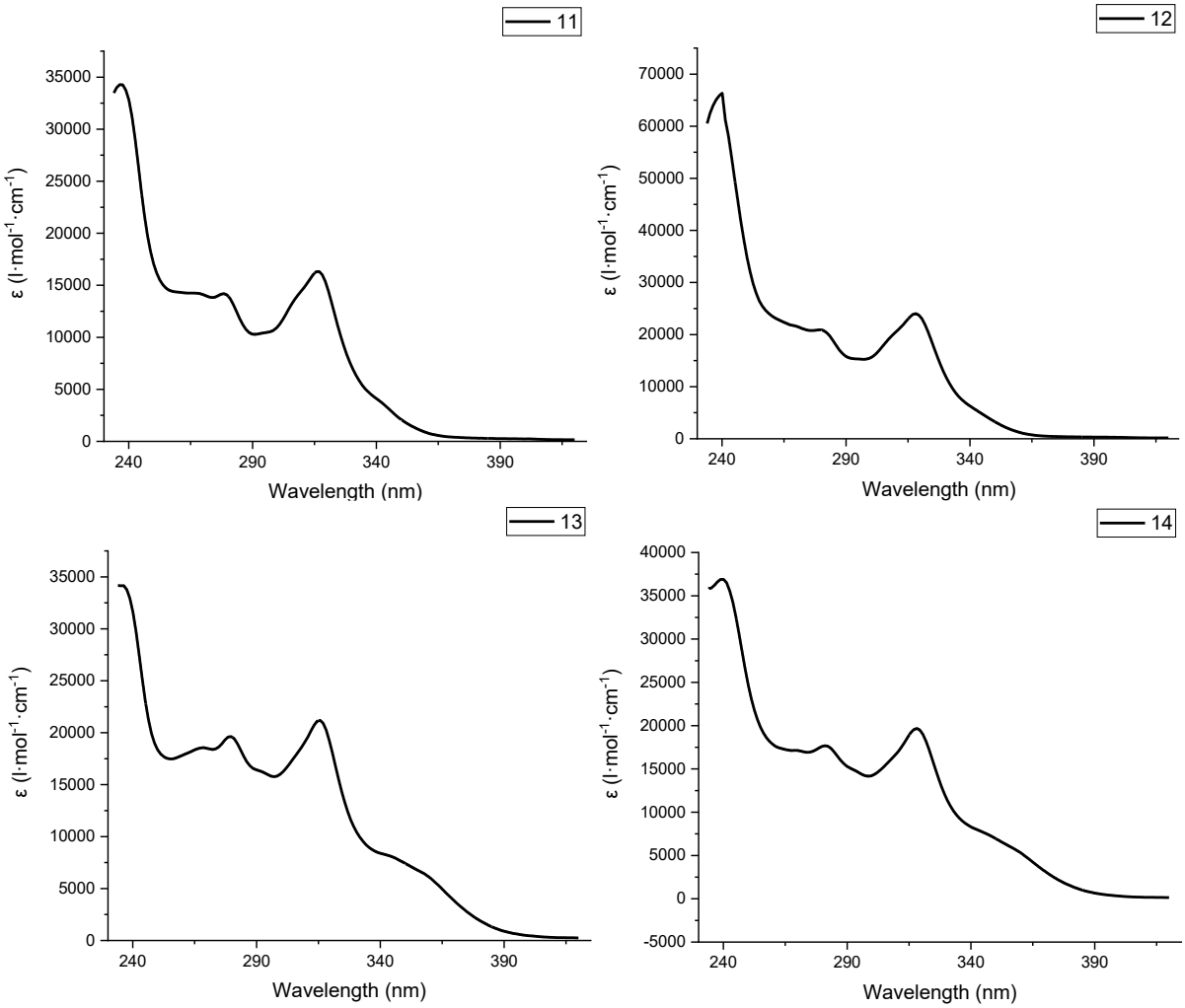

*Figure A 32. Absorption spectra of compounds **11-14** in dichloromethane solution $5 \cdot 10^{-5}$M at room temperature.*

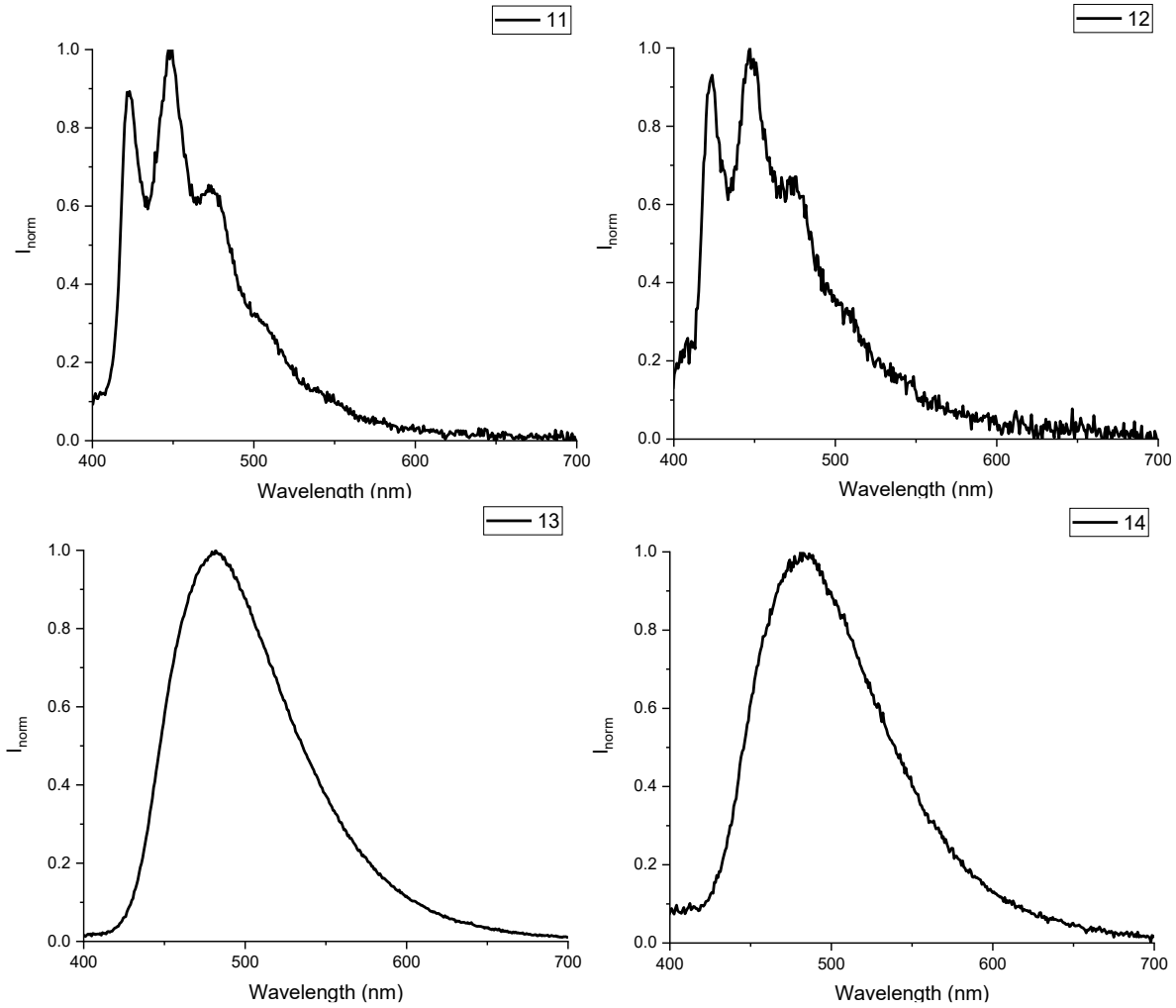

*Figure A 33. Emission spectra of compounds **11-14** in a PMMA matrix (2 wt% emitter load, λ_{exc}=320 nm) at room temperature.*

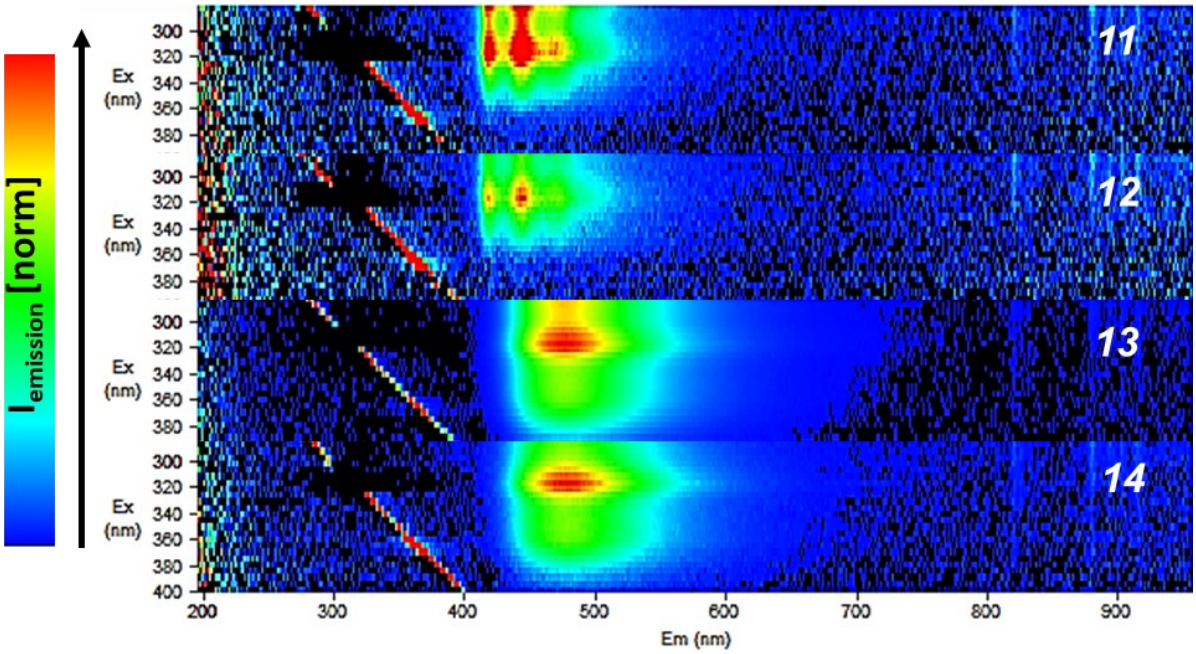

*Figure A 34. EEM of complexes **11**-**14**. A bathochromic shift can be observed in complexes **13** and **14**.*

*Table A 1. Experimental parameters for the calculation of decay time of emitters **11**-**14** on a 0.6 µm 2% wt doped PMMA matrix on a quartz glass substrate.*

	χ2	τ_1 (µs)	Rel % τ_1	τ_2 (µs)	Rel % τ_2	τ_{exp} (µs)
11	0.981	1.12	0.1054	4.26	0.8956	1.97
12	1.051	1.73	0.1519	5.46	0.8481	2.45
13	1.035	0.63	0.0542	2.21	0.9458	1.06
14	0.976	1.53	0.4749	2.72	0.5251	1.08

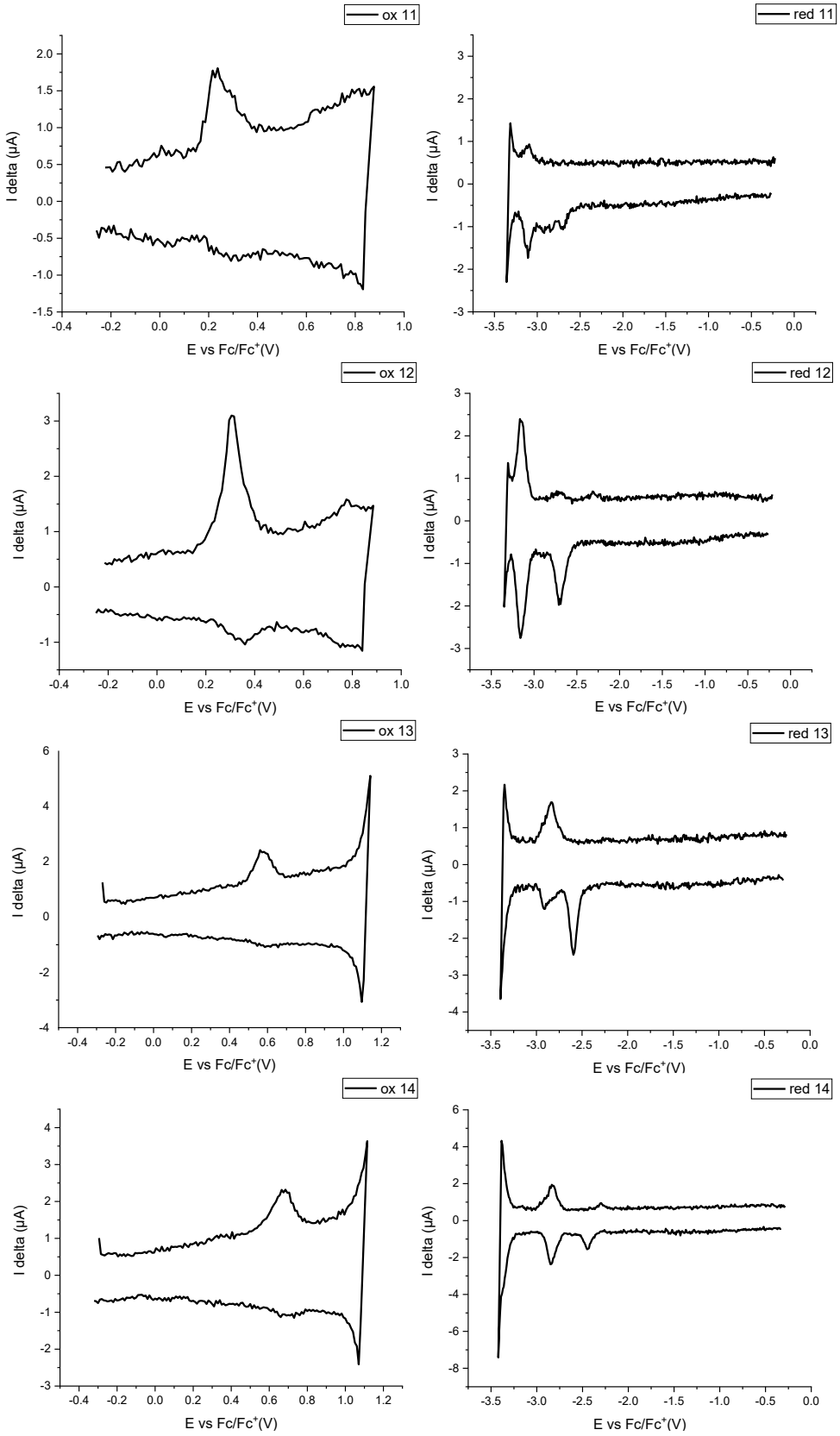

*Figure A 35. Differential pulse voltammetry measurements of compounds **11-14** in $5 \cdot 10^{-5}$ dichloromethane solution. Scanning rate 50 mV/s.*

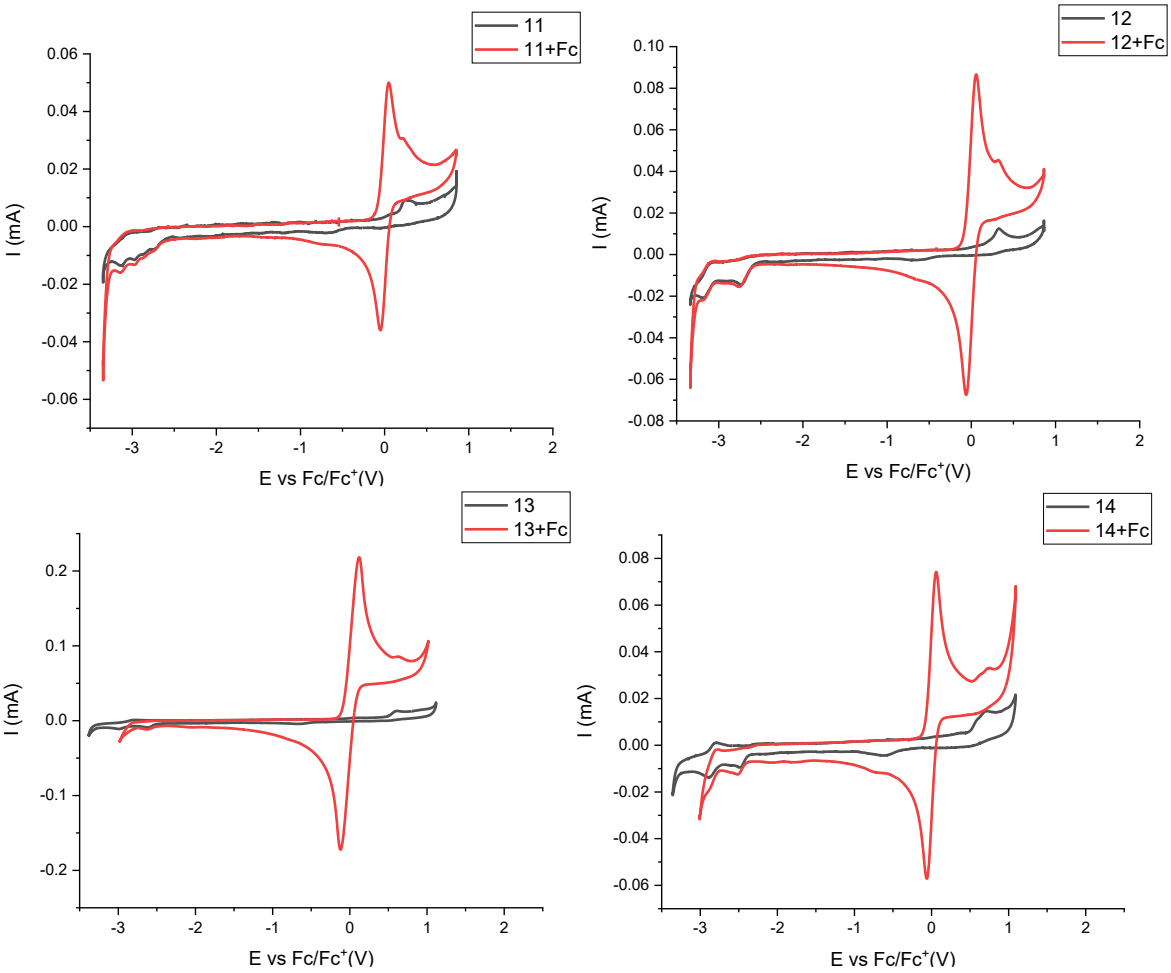

Figure A 36. Complexes CVs (black) and complexes+ferrocene CVs (red) in DMF solution, scanning rate 100 mV/s.

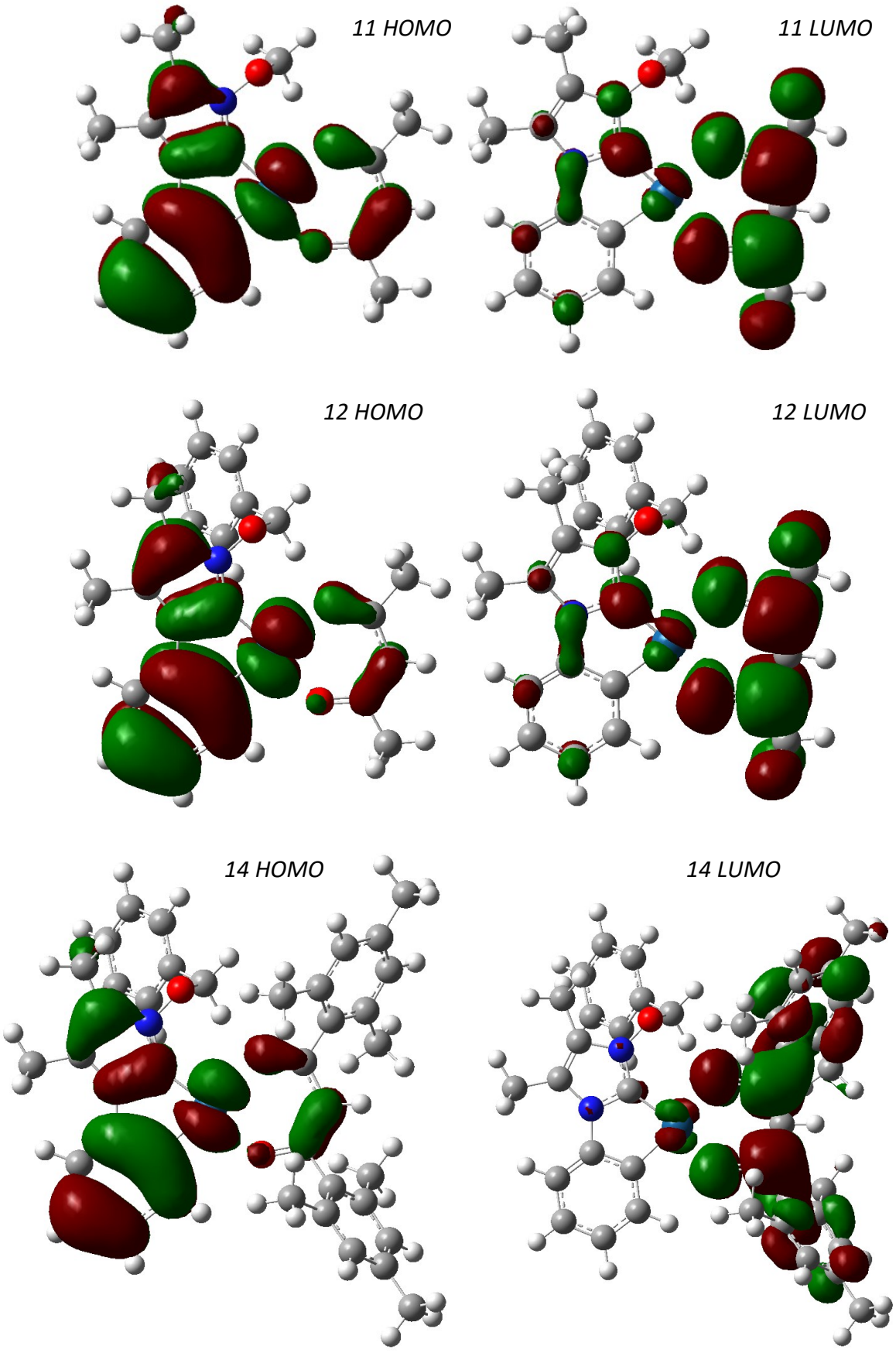

Figure A 37. Calculated frontier molecular orbitals for the ground state (isovalue=0.03). PBE/6-311G level of theory with LANL2TZ ECP for platinum and inclusion of dispersion forces as D3BJ.*

BIBLIOGRAPHY

(1) Wanzlick, H. J.; Schönherr, H. J. Direct Synthesis of a Mercury Salt-Carbene Complex. *Angew. Chem. Int. Ed.* **1968**, *7* (2), 141–142.

(2) Öfele, K. An Efficient Heterogeneous Gold(I)-Catalyzed Hydration of Haloalkynes Leading to α-Halomethyl Ketones. *J..Org. Chem.* **1968**, *12*, 42–43.

(3) Arduengo, A. J.; Kline, M. A Stable Crystalline Carbene **1991**, 361–363.

(4) Dixon, D. A. .; Arduengo, A. J. Electronic Structure of a Stable Nucleophilic Carbene. *J. Phys. Chem.* **1991**, 95, 4180–4182.

(5) Bourissou, D.; Guerret, O.; Gabbaï, F. P.; Bertrand, G. Stable Carbenes. *Chemical Reviews* **2000**, *100* (1), 39–91.

(6) Gleiter, R.; Hoffmann, R. Organic Chemistry Organic Chemistry. *J. Am. Chem. Soc.* **1968**, *90* (20), 5457–5460.

(7) Irikura, K. K.; Goddard, W. A.; Beauchamp, J. L. Singlet-Triplet Gaps in Substituted Carbenes CXY (X, Y = H, F, Cl, Br, I, SiH_3). *J. Am. Chem. Soc.* **1992**, *114* (1), 48–51.

(8) Hahn, F. E.; Jahnke, M. C. Heterocyclic Carbenes: Synthesis and Coordination Chemistry. *Angew. Chem. Int. Ed.* **2008**, *47* (17), 3122–3172.

(9) Harrison, J. F.; Liedtke, R. C.; Liebman, J. F. Carbenes and Related Molecules. *J. Am. Chem. Soc.* **1979**, 31, 7162–7168.

(10) Elschenbroich, C. *Organometallics*, Third Edit.; Wiley: Weinheim, 2016.

(11) Robert H. Crabtree. *The Organometalli Chemistry of the Transition Metals*, Seventh Ed.; Wiley, Ed.; Hoboken, NY, 2019.

(12) Lin, I. J. B.; Vasam, C. S. Preparation and Application of N-Heterocyclic Carbene Complexes of Ag(I). *Coord. Chem.Rev.* **2007**, *251* (5–6), 642–670.

(13) Mikhaylov, V. N.; Balova, I. A. Alternative Transformations of N-Heterocyclic Carbene Complexes of the Group 11 Metals in Transmetalation Reactions (A Review). *Russ. J. Gen. Chem.* **2021**, *91* (11), 2194–2248.

(14) Singh, R.; Nolan, S. P. N-Heterocyclic Carbenes: Advances in Transition Metal and Organic Catalysis. *Annual Reports on the Progress of Chemistry - Section B* **2006**, *102*, 168–196.

(15) Díez-González, S.; Marion, N.; Nolan, S. P. N-Heterocyclic Carbenes in Late Transition Metal Catalysis. *Chem. Rev.* **2009**, *109* (8), 3612–3676.

(16) Bera, S. S.; Szostak, M. Cobalt-N-Heterocyclic Carbene Complexes in Catalysis. *ACS Cat.* **2022**, *12* (5), 3111–3137.

(17) Straub, B. F. Ligand Influence on Metathesis Activity of Ruthenium Carbene Catalysts : A DFT Study. *Adv. Synth. Catal.* **2007**, *349*, 201–214.

(18) Baron, M.; Anese, D.; Miolato, A.; Cairoli, M. L. C.; Marco, V. Di; Graiff, C.; Po, A.; Tubaro, C. New Homoleptic Gold Carbene Complexes via Ag–Au Transmetalation: Synthesis and Application of $[Au(DiNHC)_2]^{3+}$ Cations as ^{1}H-NMR and UV-Vis Halide Sensors. *New J. Chem.* **2020**, 44, 5343–5353.

(19) Nayak, S.; Gaonkar, S. L. Coinage Metal N-Heterocyclic Carbene Complexes: Recent Synthetic Strategies and Medicinal Applications. *ChemMedChem* **2021**, *16* (9), 1360–1390.

(20) Yersin, H. *Highly Efficient OLEDs with Phosphorescent Materials*; 2008.

(21) Pinter, P.; Strassner, T. Prediction of the Efficiency of Phosphorescent Emitters: A Theoretical Analysis of Triplet States in Platinum Blue Emitters. *Chemistry - A European Journal* **2019**, *25* (16), 4202–4205.

(22) Aliprandi, A.; Genovese, D.; Mauro, M.; De Cola, L. Recent Advances in Phosphorescent Pt (II) Complexes Featuring Metallophilic Interactions: Properties and Applications. *Chem. Lett.* **2015**, *44* (9), 1152–1169.

(23) Maganti, T.; Venkatesan, K. The Search for Efficient True Blue and Deep Blue Emitters: An Overview of Platinum Carbene Acetylide Complexes. *ChemPlusChem* **2022**, *87* (5).

(24) Monticelli, M.; Baron, M.; Tubaro, C.; Grai, C.; Bottaro, G.; Armelao, L.; Orian, L. Structural and Luminescent Properties of Homoleptic Silver(I), Gold(I), and Palladium(II) Complexes with n NHC- Tz NHC Heteroditopic Carbene Ligands. *ACS Omega* **2019**, *4*, 4192–4205.

(25) Stoppa, V.; Scattolin, T.; Bevilacqua, M.; Baron, M.; Graiff, C.; Orian, L.; Biffis, A.; Menegazzo, I.; Roverso, M.; Bogialli, S.; Tubaro, C. Mononuclear and Dinuclear Gold(I) Complexes with a Caffeine-Based Di(N-Heterocyclic Carbene) Ligand: Synthesis, Reactivity and Structural DFT Analysis. *New J. Chem.* **2021**, *281*, 961–971.

(26) Trevisan, G.; Vitali, V.; Tubaro, C.; Marchenko, A.; Koidan, G.; Hurieva, A. N.; Kostyuk, A.; Mauceri, M.; Rizzolio, F.; Accorsi, G. Dinuclear Gold(I) Complexes with N-Phosphanyl, N-Heterocyclic Carbene Ligands: Synthetic Strategies, Luminescence Properties and Anticancer Activity. *Dalt. Trans.* **2021**, 13554–13560.

(27) Schmidbaur, H.; Schier, A. A Briefing on Aurophilicity. *Chem. Soc. Rev.* **2008**, *37* (9), 1931–1951.

(28) Elie, M.; Renaud, J. L.; Gaillard, S. N-Heterocyclic Carbene Transition Metal Complexes in Light Emitting Devices. *Polyhedron* **2018**, *140*, 158–168.

(29) Soellner, J.; Pinter, P.; Stipurin, S.; Strassner, T. Supporting Information Platinum (II) Complexes with Bis (Pyrazolyl) Borate Ligands : Increased Molecular Rigidity for Bidentate Ligand Systems. *Angew. Chem. Int. Ed.* **2021**, 60, 3556–3560

(30) Tenne, M.; Strassner, T. Neutral Platinum(II) N-Heterocyclic Carbene Complexes with Tetrazolide-Tethered Imidazolin-2-Ylidene Ligands. *J. Organomet. Chem.* **2016**, *821*, 100–105.

(31) Pinter, P.; Soellner, J.; Strassner, T. Metallophilic Interactions in Bimetallic Cyclometalated Platinum(II) N-Heterocyclic Carbene Complexes. *Eur. J. Inorg. Chem.***2021**, 30, 3104–3107.

(32) Pinter, P.; Strassner, T. Prediction of Emission Wavelengths of Phosphorescent NHC Based Emitters for OLEDs. *Tetrahedron* **2019**, *75* (35), 130431.

(33) Pinter, P.; Biffis, A.; Tubaro, C.; Tenne, M.; Kaliner, M.; Strassner, T. Palladium(II) Complexes with Electron-Poor, 4,5-Disubstituted Diimidazol-2-Ylidene Ligands: Synthesis, Characterization and Catalytic Activity. *Dalt. Trans.* **2015**, *44* (20), 9391–9399.

(34) Soellner, J.; Pinter, P.; Stipurin, S.; Strassner, T. Platinum (II) Complexes with Bis (Pyrazolyl) Borate Ligands : Increased Molecular Rigidity for Bidentate Ligand Systems. *Angew. Chem. Int. Ed.* **2021**, 3556–3560.

(35) Unger, Y.; Zeller, A.; Ahrens, S.; Strassner, T. Blue Phosphorescent Emitters : New N -

Heterocyclic Platinum (II) Tetracarbene Complexes. **2008**, 3263–3265.

(36) Pittkowski, R.; Strassner, T. Enhanced Quantum Yields by Sterically Demanding Aryl-Substituted β-Diketonate Ancillary Ligands. *Beilstein J. Org. Chem.***2018**, *14*, 664–671.

(37) Zheng, Q.; Borsley, S.; Nichol, G. S.; Duarte, F.; Cockroft, S. L. The Energetic Significance of Metallophilic Interactions. *Angew. Chem. Int. Ed.* **2019**, *131* (36), 12747–12753.

(38) Pinter, P.; Mangold, H.; Stengel, I.; Münster, I.; Strassner, T. Enhanced Photoluminescence Quantum Yields through Excimer Formation of Cyclometalated Platinum(II) N-Heterocyclic Carbene Complexes. *Organometallics* **2016**, *35* (5), 673–680.

(39) Yoshida, M.; Kato, M. Regulation of Metal–Metal Interactions and Chromic Phenomena of Multi-Decker Platinum Complexes Having π-Systems. *Coord. Chem. Rev.* **2018**, *355*, 101–115.

(40) Krogmann, K. Planar Complexes Containing Metal-Metal Bonds. *Angew. Chem. Int. Ed.* **1969**, *8* (1), 35–42.

(41) Lide, D. R. *CRC Handbook of Chemistry and Physics*, 98th ed.; CRC: Boca Raton, 2008.

(42) Jochriem, M.; Kirchler, C. G.; Laus, G.; Wurst, K.; Kopacka, H. Synthesis and Crystal Structures of Non-Symmetric 1 , 3-Di (Alkyloxy) Imidazolium Salts. **2017**, *72* (8), 617–626.

(43) Laus, G.; Schwärzler, A.; Schuster, P.; Bentivoglio, G.; Hummel, M.; Wurst, K.; Kahlenberg, V.; Lörting, T.; Schütz, J.; Peringer, P.; Bonn, G.; Nauer, G.; Schottenberger, H. N,N'-Di(Alkyloxy)Imidazolium Salts: New Patent-Free Ionic Liquids and NHC Precatalysts. *Z. Naturforsch.* **2007**, *62b*, 295–308.

(44) Laus, G.; Schwärzler, A.; Bentivoglio, G.; Hummel, M.; Kahlenberg, V.; Wurst, K.; Kristeva, E.; Schütz, J.; Kopacka, H.; Kreutz, C.; Bonn, G.; Andriyko, Y.; Nauer, G.; Schottenberger, H. Synthesis and Crystal Structures of 1-Alkoxy-3-Alkylimidazolium Salts Including Ionic Liquids, 1-Alkylimidazole 3-Oxides and 1-Alkylimidazole Perhydrates. *Z. Naturforsch. - Section B* **2008**, *63* (4), 447–464.

(45) Wróblewska, A.; Lauriol, G.; Mlostoń, G.; Bantreil, X.; Lamaty, F. Expedient Synthesis of N[Sbnd]Oxy-Heterocyclic Carbenes (NOHC) Ligands and Metal Complexes Using Mechanochemistry. *J. Organomet. Chem.* **2021**, *949*.

(46) Bakhonsky, V. V.; Becker, J.; Mloston, G.; Schreiner, P. R. N -Alkoxyimidazolylidines (NOHCs): Nucleophilic Carbenes Based on an Oxidized Imidazolium Core. *Chem. Comm.* **2022**, *58* (10), 1538–1541.

(47) Mlostoń, G.; Celeda, M.; Urbaniak, K.; Jasiński, M.; Bakhonsky, V.; Schreiner, P. R.; Heimgartner, H. Synthesis and Selected Transformations of 2-Unsubstituted 1-(Adamantyloxy)Imidazole 3-Oxides: Straightforward Access to Non-Symmetric 1,3-Dialkoxyimidazolium Salts. *Beilstein J. Org. Chem.* **2019**, *15* (1), 497–505.

(48) Eriksen, B. L.; Vedsø, P.; Morel, S.; Begtrup, M. Synthesis of 2-Substituted 1-Hydroxyhnidazoles through Directed Lithiation. *J. Org. Chem.* **1998**, *63* (1), 12–16.

(49) Laus, G.; Stadlwieser, J.; Klötzer, W. 1-Hydroxyimidazole Derivatives III. Synthesis of 1-Alkyloxy-, 1-Arylalkyloxy-, and 1-Phenoxy-1H-Imidazoles1. Laus G, Stadlwieser J, Klötzer W. 1-Hydroxyimidazole Derivatives III. Synthesis of 1-Alkyloxy-, 1-Arylalkyloxy-, and 1-Phenoxy-1H-Imidazoles. Synt. *Synthesis* **1989**, 773.

(50) Alcázar, J.; De La Hoz, A.; Begtrup, M. Carbon-13 NMR Spectra of Imidazole 1-Oxides. Comparison with the Parent Imidazoles. *Magn. Res. Chem.* **1998**, *36* (4), 296–299.

(51) Bartz, S.; Blumenroder, B.; Kern, A.; Fleckenstein, J.; Frohnapfel, S.; Schatza, J.; Wagner, A. Hydroxy-1 H -Imidazole-3-Oxides – Synthesis , Kinetic Acidity , and Application in Catalysis and Supramolecular Anion Recognition. **2009**, 1–10.

(52) Brendgen, T.; Fahlbusch, T.; Frank, M.; Schühle, D. T.; Seßler, M.; Schatz, J. Metathesis in Pure Water Mediated by Supramolecular Additives. *Adv. Synt. Cat.* **2009**, *351* (3), 303–307.

(53) Mlostoń, G.; Jasiński, M. First Synthesis of the N(1)-Bulky Substituted Imidazole 3-Oxides and Their Complexation with Hexafluoroacetone Hydrate. *Arkivoc* **2011**, *2011* (6), 162–175.

(54) Laus, G.; Wurst, K.; Kahlenberg, V.; Kopacka, H.; Kreutz, C.; Schottenberger, H. N -Heterocyclic Carbene (NHC) Derivatives of 1 , 3-Di (Benzyloxy) Imidazolium Salts. *Z. Naturforsch. B* **2010**, *65b*, 776–782.

(55) Gutiérrez, R. U.; Rebollar, A.; Bautista, R.; Pelayo, V.; Luis, J.; Montenegro, M. M.; Espinoza-Hicks, C.; Ayala, F.; Bernal, P. M.; Carrasco, C.; Zepeda, L. G.; Delgado, F.; Tamariz, J. Tetrahedron : Asymmetry Functionalized a -Oximinoketones as Building Blocks for the Construction of Imidazoline-Based Potential Chiral Auxiliaries. **2015**, *26*, 230–246.

(56) Giumanini, A.; Verrardo, G.; Zangrando, E.; Lassiani, L. 1,3,5-Triarylhexahydro-Sym-Triazines s and 1,3,5,7-Tetraaryl-l,3,5,7-Tetrazocines from Aromatic Amines and Paraformaldehyde. *J. Prakt. Chem.* **1987**, *329*, 1087–1103.

(57) Stipurin, S.; Strassner, T. Phosphorescent Cyclometalated Platinum(II) Imidazolinylidene Complexes. *Eur. J. In. Chem.* **2021**, *2021* (9), 804–813.

(58) Tronnier, A.; Heinemeyer, U.; Metz, S.; Wagenblast, G.; Muenster, I.; Strassner, T. Heteroleptic Platinum(Ii) NHC Complexes with a ɤC∗ Cyclometalated Ligand-Synthesis, Structure and Photophysics. *J. Mat. Chem. C* **2015**, *3* (8), 1680–1693.

(59) Unger, Y.; Meyer, D.; Molt, O.; Schildknecht, C.; Münster, I.; Wagenblast, G.; Strassner, T. Green – Blue Emitters : NHC-Based Cyclometalated [Pt(C^C*)(Acac)]. *Angew. Chem. Int. Ed.* **2010**, 49, 10214 –10216

(60) Stipurin, S.; Strassner, T. Phosphorescent Cyclometalated Platinum(II) Imidazolinylidene Complexes. Supporting Informations. *Eur. J. Inorg. Chem.* **2021**, 804–813

(61) Stipurin, S.; Strassner, T. C^C∗ Platinum(II) Complexes with Electron-Withdrawing Groups and Beneficial Auxiliary Ligands: Efficient Blue Phosphorescent Emission. *Eur. J. Inorg. Chem.* **2021**, *60* (15), 11200–11205.

(62) Mccaffery, A. J.; Schatz, P. N.; Stephens, P. J. Magnetic Circular Dichroism of D8 Square-Planar Complexes. *J. Am. Chem. Soc.* **1968**, 5730–5735.

(63) Unger, Y.; Meyer, D.; Molt, O.; Schildknecht, C.; Münster, I.; Wagenblast, G.; Strassner, T. Green-Blue Emitters: NHC-Based Cyclometalated [Pt(CΛC)(Acac)] Complexes. *Angew. Chem. Int. Ed.* **2010**, *49* (52), 10214–10216.

(64) D'Andrade, B. W.; Datta, S.; Forrest, S. R.; Djurovich, P.; Polikarpov, E.; Thompson, M. E. Relationship between the Ionization and Oxidation Potentials of Molecular Organic Semiconductors. *Org. Electr.* **2005**, *6* (1), 11–20.

(65) Djurovich, P. I.; Mayo, E. I.; Forrest, S. R.; Thompson, M. E. Measurement of the Lowest Unoccupied Molecular Orbital Energies of Molecular Organic Semiconductors. *Org. Electr.* **2009**, *10* (3), 515–520.

(66) Stipurin, S.; Wurl, F.; Strassner, T. CΛC∗ Platinum(II) Complexes with PtXPX Metallacycle Forming (X = N and S) Auxiliary Ligands: Synthesis, Crystal Structures, and Properties.

Organometallics **2022**, *41* (3), 313–320.

(67) Korch, K. M.; Watson, D. A. Total Synthesis of (±)-Impatien A via Aza-Heck Cyclization. *Org. Lett.* **2021**, *23* (18), 7285–7289.

(68) Sheradsky, T.; Nov, E. Studies on the Preparation of N-Alkyl-0-Phenylhydroxylamines By. *J. Chem. Soc., Perkin Trans. 1* **1980**, 1, 2781–2786.

(69) Frisch, M. J.; Trucks, G. W.; Schlegel, H. B.; Scuseria, G. E.; Robb, M. A.; Cheeseman J. R.; Scalmani, G.; Barone, V.; Petersson, G. A.; Nakatsuji, H.; Li, X.; Caricato, M.; Marenich, A. V.; Bloino, J.; Janesko, B. G.; Gomperts, R.; Mennucci, B.; Hratchi, F. . E.; F.; Goings, J.; Peng, B.; Petrone, A.; Henderson, T.; Ranasinghe, D.; Zakrzewski, V. G.; Gao, J.; Rega, N.; Zheng, G.; Liang, W.; Hada, M.; Ehara, M.; Toyota, K.; Fukuda R.; Hasegawa, J.; Ishida, M.; Nakajima, T.; Honda, Y.; Kitao, O.; Nakai, H.; Vreven, T. .; Throssell, K.; Montgomery Jr., J. A.; Peralta, J. E.; Ogliaro, F.; Bearpark, M. J.; Heyd, J.; J.; Brothers, E. N.; Kudin, K. N.; Staroverov, V. N.; Keith, T. A.; Kobayashi, R.; Normand, J.; Raghavachari, K.; Rendell, A. P.; Burant, J. C.; Iyengar, S. S.; Tomasi, J.; Cossi, M. .; Millam, J. M.; Klene, M.; Adamo, C.; Cammi, R.; Ochterski, J. W.; Martin, R. L.; Morokuma, K.; Farkas, O.; Foresman, J. B.; Fox, D. J. *Gaussian 16, Revision A.03*; Wallingford CT, 2016.

(70) Ernzerhof, M.; Scuseria, G. E. Assessment of the Perdew – Burke – Ernzerhof Exchange-Corrlation Functional. *J. Chem. Phys.* **1999**, *110*, 5029–5036.

(71) Adamo, C.; Barone, V. Toward Reliable Density Functional Methods without Adjustable Parameters: The PBE0 Model. *J. Chem. Phys.* **1999**, *110*, 6158–6170.

(72) Krishnan, R.; Binkley, J. S.; Seeger, R.; Pople, J. A. Self-Consistent Molecular Orbital Methods. XX. A Basis Set for Correlated Wave Functions. *J. Chem. Phys.* **1980**, *72*, 650–654.

(73) McLean, A. D.; Chandler, G. S. Contracted Gaussian Basis Sets for Molecular Calculations. I. Second Row Atoms, Z=11-18. *J. Chem. Phys.* **1980**, *72*, 5639–5648.

(74) Francl, M. M.; Pietro, W. J.; Hehre, W. J.; Binkley, J. S.; Gordon, M. S.; DeFrees, D. J.; Pople, J. A. Self-Consistent Molecular Orbital Methods. XXIII. A Polarization-Type Basis Set for Second-Row Elements. *J. Chem. Phys.* **1982**, *77*, 3654–3665.

(75) Hay, P. J.; Wadt, W. R. Ab Initio Effective Core Potentials for Molecular Calculations. Potentials for the Transition Metal Atoms Sc to Hg. *J. Chem. Phys.* **1985**, *82*, 270–283.

(76) Hay, P. J.; Wadt, W. R. Ab Initio Effective Core Potentials for Molecular Calculations. Potentials for K to Au Including the Outermost Core Orbitale. *J. Chem. Phys.* **1985**, *82*, 299–310.

(77) Wadt, W. R.; Hay, P. J. Ab Initio Effective Core Potentials for Molecular Calculations. Potentials for Main Group Elements Na to Bi. *J. Chem. Phys.* **1985**, *82*, 284–298.

(78) Roy, L. E.; Hay, P. J.; Martin, R. L. Revised Basis Sets for the LANL Effective Core Potentials. *J. Chem. Theory Comput.* **2008**, *4*, 1029–1031.

(79) Grimme, S.; Ehrlich, S.; Goerigk, L. Effect of the Damping Function in Dispersion Corrected Density Functional Theory. *J. Comput. Chem.* **2011**, *32*, 1456–1465.

(80) Grimme, S. Density Functional Theory with London Dispersion Corrections. *Wiley Interdiscip. Rev. Comput. Mol. Sci.* **2011**, *1*, 211–228.

(81) Dennington, R.; Keith, T. A.; Millam, J. M. *GaussView, Version 6.0*; Shawnee Mission, KS, 2016.

(82) *Bruker Crystallographic Suite APEX3, V2017.3*, Bruker AXS.; Madison, Wisconsin, USA, 2017.

(83) *Bruker Integration Engine SAINT V8.38A*, Bruker AXS.; Madison, Wisconsin, USA, 2017.

(84) Sheldrick, G. M. SADABS Multi Scan Absorption, SADABS-2016/2, University of Goettingen, Goettingen, Germany, 2016.

(85) Sheldrick, G. M. Crystal Structure Refinement with SHELXL. *cta Crystallogr. Sect. C Struct. Chem.* **2015**, *71*, 3–8.

(86) Sheldrick, G. M. SHELXT – Integrated Space-Group and Crystal-Structure Determination. *Acta Crystallogr. Sect. A Found. Adv.* **2015**, *71*, 3–8.

(87) IUCr; Wilson, A. J. C. *International Tables for Crystallography, Volume C: Mathematical, Physical and Chemical Tables International Tables for Crystallography*; Kluwer Publishers, A., Ed.; Dordrecht, Boston, London, 1992.

(88) Sheldrick, G. M. Crystal Structure Refinement with SHELXL. **2014**, No. Md, 3–8. https://doi.org/10.1107/S2053229614024218.

(89) Spek, A. L. Structure Validation in Chemical Crystallography. *Acta Crystallogr. D. Biol. Crystallogr.* **2009**, *65*, 148–155.

(90) Farrugia, L. J. WinGX and ORTEP for Windows : An Update. **2012**, 849–854. https://doi.org/10.1107/S0021889812029111.

(91) MacRae, C. F.; Sovago, I.; Cottrell, S. J.; Galek, P. T. A.; McCabe, P.; Pidcock, E.; Platings, M.; Shields, G. P.; Stevens, J. S.; Towler, M.; Wood, P. A. Mercury 4.0: From Visualization to Analysis, Design and Prediction. *J. Appl. Crystallogr.* **2020**, *53*, 226–235.